Metalorganic Vapor Phase Epitaxy and Fabrication of 1.5 µm GaN/AlN MQWs Intersubband All-Optical Switches

1.5 µm GaN/AlN 多重量子井戸サブバンド間遷移全光スイッチ
の有機金属気相エピタクシーと作製

A dissertation submitted to the Graduate School of Engineering
The University of Tokyo
in partial fulfillment of the requirements for the degree of
Doctor of Philosophy

ソダーバンル　ハッサネット

Sodabanlu Hassanet

Under the supervision of

Professor Dr. Yoshiaki Nakano

Acknowledgements

There are people I need to mention especially: Dr. Jung-Seung Yang, my research partner, who I have learned so much from him and share the enjoyable and painful time together; Dr. Wipakorn Jevasuwan who always cheerfully encourages me and strands by my side.

Last but not least, I would like to convey my heartfelt to my parents for perpetual personal support and encouragements to overcome many difficulties all along the years in Japan.

Hassanet Sodabanlu

Tokyo, March 2010

Abstract

D ramatic growth in fiber-optical network traffic demand is driving the need for new high-bandwidth optical components including optical switches. Many technologies; for example, microelectro mechanical systems (MEMS), silica-on-silicon planar lightwave circuit (PLC), polymer optical waveguide, intersubband transition (ISBT) in quantum nanostructure, optical non-linearity in semiconductor optical amplifier (SOA), have been proposed as a candidate for a solution of high optical traffic demand. Each technology possesses unique advantage and disadvantage properties. Among these competitors, intersubband transition in semiconductor multiple quantum wells (MQWs) has an outstanding merit which is the ultrafast response. In the fiber-optic communications, the conventional wavelength window, known as the C band, covers the wavelength range 1.53-1.57 µm, and the new dry fiber has a low-loss window promising an extension of that range to 1.30-1.65 µm. Hence, material systems with large enough conduction band offset to accommodate intersubband transitions at these relatively short wavelengths include InGaAs/AlAsSb, (CdS/ZnSe)/BeTe, GaInNAs/AlAs, and GaN/Al(Ga,In)N MQWs. Among these materials, GaN/AlN MQW structures are promising owing to their large conduction band offset allowing a short intersubband transition wavelength in a simple quantum well structure. Moreover, the extremely fast intersubband relaxation in the order of sub-picoseconds due to the large longitudinal optical phonon energy and the large electron effective mass promotes intersubband transition in nitrides immensely interesting for the development of ultrafast photonic devices capable for 0.1-1 Tb/s bit rate.

However, in the past few years, the number of publications of all-optical switches using intersubband transition in nitride MQWs is not as much as that of GaN-based light emitting devices and high electron mobility transistors. It has also been overwhelmed by fiber-based and phosphide-based optical switches. This is because of the growth of GaN/AlN MQWs realizing short intersubband transition wavelength is not an easy task, especially the growth by metalorganic vapor phase epitaxy (MOVPE) technique which is a large-scale fabrication system. The short intersubband transition in GaN/AlN MQWs has been long for only realized by molecular beam epitaxy (MBE) technique. Furthermore, the issue of high power consumption for operating nitride-based all-optical switches is considerably one of major obstructions. Due to

these reasons, the research of intersubband transition in GaN/AlN MQWs as well as their applications has been developed in a slow manner.

In this work, the MOVPE growth and fabrication of all-optical switches utilizing intersubband transition in GaN/AlN MQWs have been investigated. The issue of the realizing of short intersubband transition wavelength in MOVPE grown GaN/AlN MQWs has been first conducted by extracting the factors that hinder the short wavelength. A growth method called pulse injection method has been investigated and used for suppressed the problem caused by the conventional MOVPE growth. By tailoring the strain in GaN/AlN MQWs using AlGaN interlayer inserted between GaN/AlN MQWs and AlN buffer layer, 1.5-µm-range intersubband transition has been fully realized using pulse injection MOVPE. The properties of intersubband transition are excellent in terms of transition wavelength, absorption intensity and full-width at half-maximum of absorption peak.

Later in this dissertation, AlN-based waveguides with GaN/AlN MQWs grown by MOVPE have been designed and fabricated. The measurement and characterization of fabricated AlN-based waveguide has demonstrated the existence of intersubband absorption in waveguide structure which is an important step toward the fabrication of all-optical switches. The propagation loss in AlN-based waveguide has been investigated and analyzed by comparing with MBE fabricated samples. Later, the spot-size converter has also been introduced as an answer for high coupling loss issue in the plane waveguide structure. Each of AlN-based waveguides fabricated in this thesis exhibited the saturable absorption indicating the functionality of all-optical switch.

This dissertation has demonstrated the potential of all-optical switch application in MOVPE grown AlN-based waveguide with GaN/AlN MQWs absorption core. This achievement is an important milestone in the development of optical devices utilizing intersubband transition in MOVPE grown GaN/AlN MQWs. Furthermore, the succeed in the growth procedure indicates the capability of MOVPE system for the growth of high quality GaN/AlN MQWs and may renew the interest of intersubband transition in nitride semiconductors.

Table of Contents

List of Figures

List of Tables

Chapter 1 Introduction

T he basic knowledge about nitride semiconductors, crystal growth techniques and device application will be given in this chapter. Start with the general introduction in section 1.1, the concept of intersubband transition (ISBT) was adjacently explained in section 1.2. Then, in the section 1.3, principles of GaN MQWs intersubband all-optical switch was first explicated followed by the remarkably chronological record of related researches and up to date status of practical applications as well as obstacles in the development of GaN-based intersubband devices. This leads to the motivation and synopses of this work given in section 1.4 and 1.5, respectively.

1.1   General Introduction

Intersubband transitions in semiconductor multiple quantum wells (MQWs) have proven their capability for optoelectronics in the mid- and far-infrared spectral regions. In the view point of response time, sensitivity and reproducibility, intersubband photodetectors present advantages in comparison with interband devices. Moreover, intersubband quantum cascade (QC) lasers are a new and rapidly evolving technology with advantages such as their intrinsic wavelength tailorability, high-speed modulation capabilities, large output powers, operation above room temperature, and fascinating design potential. These features make them particularly promising for applications in terabit optical data communications or ultra-precision metrology and spectroscopy. The potential of QC lasers as trace gas sensors for environmental, automotive, or medical applications have already been proved in the mid- or far-infrared spectral range, using semiconductor materials such as GaAs/AlGaAs, InGaAs/AlInAs-on-InP or InAs/AlSb. The

extension of intersubband optoelectronics toward the near infrared spectral region is interesting for the development of ultrafast photonic devices for optical telecommunication networks, as well as for application in a variety of chemical forensics, biological and chemical sensors pollution detection, chemical and biological warfare, medical diagnostics, and industrial process monitoring. Semiconductor systems with large conduction band offset enough to accommodate intersubband transitions at these relatively short wavelengths include InGaAs/AlAsSb [1], (CdS/ZnSe)/BeTe [2], GaInNAs/AlAs [3], and GaN/Al(Ga,In)N QWs [4-10]. In the case of III-nitride heterostructures, their conduction band offset; around 1.8 eV for the GaN/AlN system [7-10], is large enough to develop intersubband devices operating in the fiber-optics transmission windows at 1.3 and 1.55 µm. A specific advantage of III nitrides is their extremely short intersubband absorption recovery times (~140-400 fs [11,12]) due to the strong electron-phonon interaction in these materials opening the way for devices operating in the 0.1-1 Tbit/s bit rate regime. Furthermore, the remote lateral valleys lie very high in energy (>2 eV above the Γ valley [13,14]), which is a key feature to achieve intersubband lasing. Finally, devices would benefit from other advantages of the nitride technology, such as high power handling capabilities and chemical and thermal robustness. In the last few years, various groups have reported intersubband absorption at 1.3-1.55 µm in GaN/Al(Ga)N nanostructures in the form of QWs [4-11] or quantum dots [15-16]. The first GaN/AlN photovoltaic QW infrared photodetectors (QWIP) [17-19], lateral transport quantum dot infrared photodetectors [20-21], and QC detectors [22] have been recently demonstrated. Additionally, there has been an important research effort on saturable absorbers for ultrafast all-optical switching [12,23-25]. GaN-based all-optical switches with an extinction ratio larger than 10 dB have been demonstrated [24-25]. Strong electronic coupling in double GaN/AlN QWs has been reported [26-27], which sets the basis for the fabrication of intersubband modulators and unipolar lasers. The first demonstrations of electromodulated absorption at 1.3-1.55 µm based on intersubband transitions in III-nitride nanostructures have been recently reported [28-29]. Finally, room-temperature intersubband photoluminescence from GaN/AlN QWs and quantum dots at wavelengths down to λ=1.5 µm has been observed at room temperature [30-31]. Despite several theoretical proposals [32-37], lasing action has not been achieved so far.

1.2 Intersubband Transition

1.2.1 Background

A single quantum well structure consists of a thin narrow band gap semiconductor layer (well, usually less than 10 nm) buried with two wide band gap semiconductor layers (barriers). In the thin layer, the carrier motion (both electron and hole) in the direction which normal to the layers is restricted and the kinetic energy of carrier is quantized to discrete energy levels that satisfy the Schrödinger equation. Each discrete level is called subband and can be tuned by adjusting the well thickness and depth. Both electrons and hole have their own subband energy levels, i.e. the subbands of electrons exist above the conduction band while that of holes exist below the valence band. The term "intersubband transition" is used to describe the transition of electrons or holes between their own subband energy levels. Figure 1.1 shows the intersubband and interband transition.
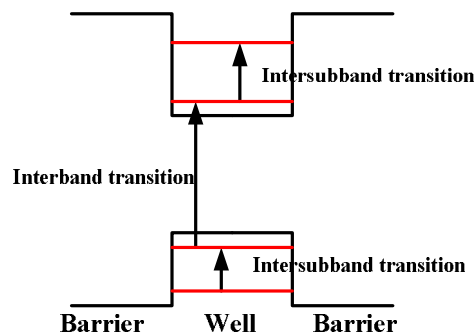
Fig. 1.1 Interband and Intersubband Transition

The interband transition is bipolar transition in which photon energy is limited by energy bandgap E_g of material. In contrast, the intersubband transition is unipolar transition in which photon energy depends on the well thickness and can be tailors. Hence, intersubband-based devices allow the transition in wavelength which is not possible in conventional interband devices.

1.2.2   Relaxation Mechanism in Intersubband

The mechanism of the intersubband relaxation is of special interest. Figure 1.2 shows the schematic of the relaxation mechanism of an excited carrier between subbands. Those relaxations relate to the scattering, for example, acoustical and optical phonon scattering. First, the excited carriers (electrons) have to be transferred with finite $k_{//}$ to the high kinetic energy region of ground subband and then followed by intrasubband cooling to the bottom region. Only electrons in this region can be re-excited by light to the upper energy level. The relaxation time is the approximately equal to the summation of the time for intersubband relaxation (T_{inter}) and intrasubband relaxation (T_{intra}). The intrasubband relaxation is much faster than that of intersubband. The fastest relaxation process is considered to be the relaxation with longitudinal optical (LO) phonon scattering [38-40].
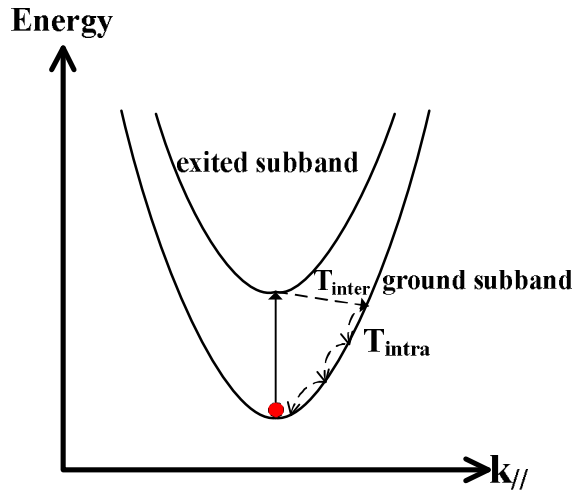
Fig. 1.2 Intersubband relaxation mechanism

Among these available materials which allow the intersubband transition at 1.55 µm, the relaxation mechanism in GaN nanostructure is considerably the fastest owing to its large LO phonon energy and large electron effective mass [11-12]. Equation 1-1 describes electron-LO phonon scattering rate.

$$W_0 = \frac{e^2}{4p\,\overline{h}}\left(\frac{2m^*w_{L0}}{\overline{h}}\right)^{\frac{1}{2}}\left(\frac{1}{e_\infty} - \frac{1}{e_0}\right) \tag{1-1}$$

4

where, W_0, m^*, w_{LO} and e are scattering rate, electron effective mass, LO phonon energy and dielectric constant, respectively.

Table 1.1 Scattering rate and related parameters of GaN compared with other semiconductors

	InGaAs	GaN	ZnSe	CdS
E_g (eV)	0.75	3.4	2.8	2.5
m^* (m_0)	0.042	0.2	0.16	0.19
e_0	14.1	9.5	9.1	10.3
e_∞	11.6	5.4	5.75	5.2
$\mathbf{h}w_{LO}$ (meV)	36	88	31	38
W_0 ($p^{-1}s^{-1}$)	6.7	121	51	90

1.3   All-Optical Switches Utilizing Intersubband Transition

1.3.1   Operating Principle

All-optical modulators and switches have been attracting much attention recently because they are expected to be realized by utilizing the ultrafast intersubband transition. Compared to other candidate technologies, for example, microelectro mechanical systems (MEMS), silica-on-silicon planar lightwave circuit (PLC), polymer optical waveguide and optical non-linearity in semiconductor optical amplifier (SOA), intersubband transition in semiconductor nanostructure have several outstanding advantages including extremely fast response time and low loss. In addition, their wide range of wavelength tunability makes these devices possible to be fabricated at wavelength around 1.55 µm, the silica-fiber-based optical communication wavelength. All-optical modulators utilizing intersubband transition have also been believed to be the key point for the development of future optical communication networks.
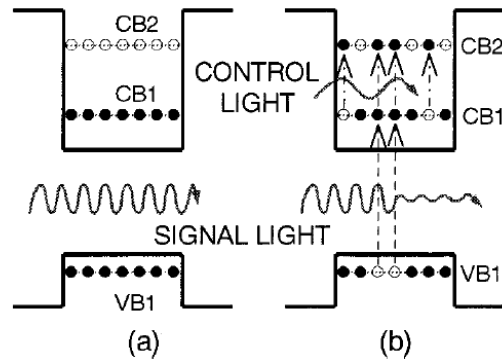
Fig. 1.3 Schematic diagram of the interband optical modulation using intersubband
transition in an *n*-doped QW (a) without and (b) with control light.

Figure 1.3 [41] shows interband optical modulation using intersubband transition. The signal light can be controlled by a control light pulse. Without the control light, the device is transparent to the signal light because electrons in valence band (VB1) cannot absorb light and excite to fully occupied conduction band (CB1). However, with the control light resonating between CB1 and CB2, some electrons are excited from CB1 to CB2, leaving empty states in CB1 which electrons excited by the signal light can fill.

However, in this modulation, the wavelength of the signal light is not applicable to the 1.55 µm optical communication networks since the wavelength resonant to the interband transition is usually much shorter than 1.55 µm. Therefore, the intersubband optical modulation using intersubband transition has been introduced. Figure 1.4 shows the modulation scheme using the cross absorption modulation technique. Both signal and control light pulses are therefore set to be around 1.55 µm with a little bit different in wavelength, while the intensity of the control light is much larger than that of the signal light. Without the control light, the signal light will be absorbed in the quantum well, thus no output signal from the device. When the large intensity control light is guided together with signal light, it will be absorbed and excites most of electrons from CB1 to CB2, causing the saturation of absorption. Therefore, the device becomes transparent to the signal light.
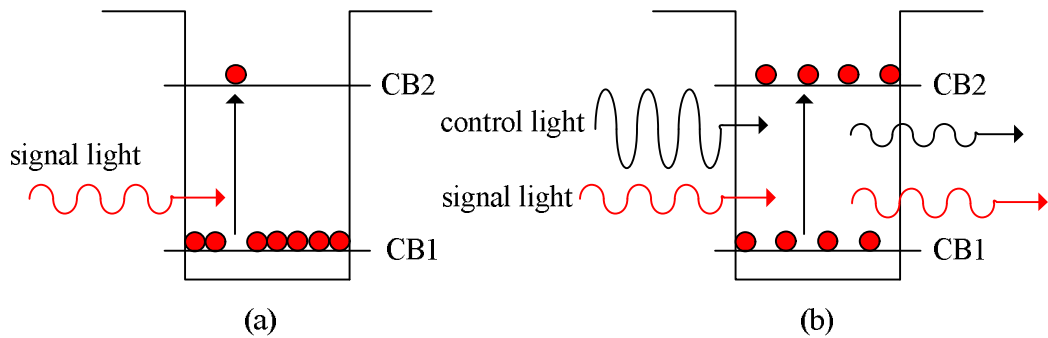
Fig. 1.4 Schematic diagram of the optical modulation using cross absorption in intersubband transition (a) without and (b) with control light.

1.3.2 A Brief History of the Progress of Nitride Intersubband All-Optical Switches

In order to clarify the current status of all-optical switches utilizing intersubband transition in GaN/Al(Ga)N MQWs, a brief explanation on related studies is chronologically given.

In 1990 S. Noda et al. has theoretically investigated and proposed the light-controlled optical modulation using n-doped quantum well structure [42]. It has been shown that the very fast modulation speed of picosecond can be expected by this device.

In 1997 N. Iizuka et al. has investigated, theoretically, the feasibility and mechanism of the intersubband transition in GaN/Al(Ga)N quantum wells for ultrafast optical switches [43]. The intersubband relaxation time at 1.55 μm is estimated about 80 fs, 30 times faster than that in InGaAs quantum well (Fig. 1.5). It showed a potential to utilize GaN intersubband optical switches operating at a bit rate higher than 1 Tb/s. This report has driven the interest of optical switches utilizing intersubband transition in GaN/Al(Ga)N quantum wells.

The intersubband optical switches using nitride multiple quantum wells have been brought close to the reality when N. Iizuka et al. has observed absorption via intersubband transition in MBE grown GaN/AlN MQWs in 2002 [11]. The intersubband transition wavelengths from 1.33 μm to 2.17 μm have been achieved. From the investigation of absorption saturation at a wavelength of 1.48 μm, a relaxation time of 400 fs was confirmed and a saturation density of 0.5 pJ/μm^2 was obtained. The dependency of the intersubband transition wavelength

on the GaN well thickness was studied and the calculation results indicated that the strain-induced electric field as large as 4-6 MV/cm exists in the wells as shown in Fig. 1.6.
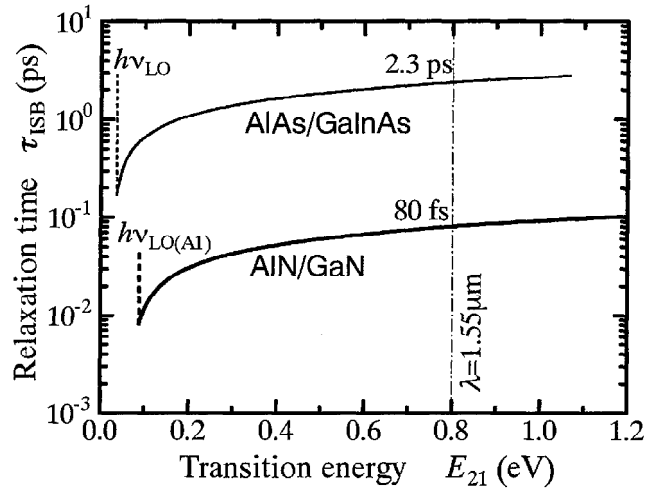
Fig. 1.5 Comparison of intersubband relaxation time in GaN and InGaAs quantum well
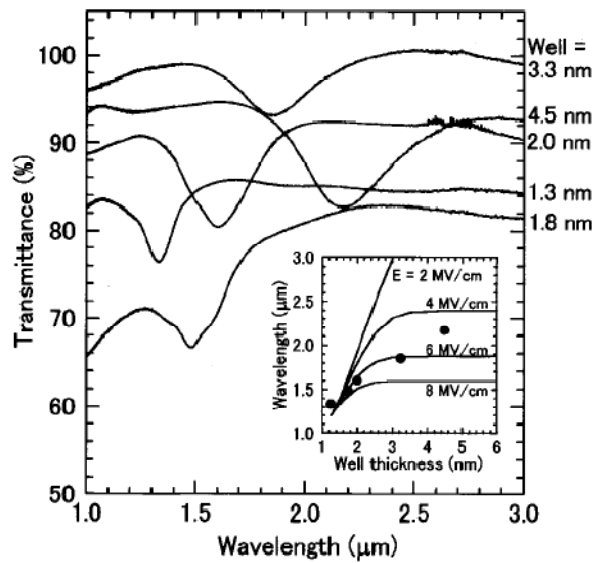
Fig. 1.6 The transmittance spectra in GaN/AlN MQWs by FTIR. The inset is the dependence of the absorption wavelength on the well thickness. The calculation results are also shown by solid lines with internal fields as a parameter.

Several achievements on optical modulation utilizing intersubband transition in MBE grown GaN/AlN MQWs have been reported by the same authors [12,23-24,44]. The noticeable improvement of intersubband absorption saturation was reported by using *MOVPE* grown GaN layer as a buffer for depositing GaN/AlN MQWs by MBE [12,24,44] as its structure is schematically shown in Fig. 1.7(a). This is because MOVPE can provide high quality with low dislocation density bulk layers which cannot be realized by MBE. An extinction ratio as high as 11.5 dB was achieved with a control pulse energy of 150 pJ in a ridge GaN waveguide (Fig. 1.7(b)).
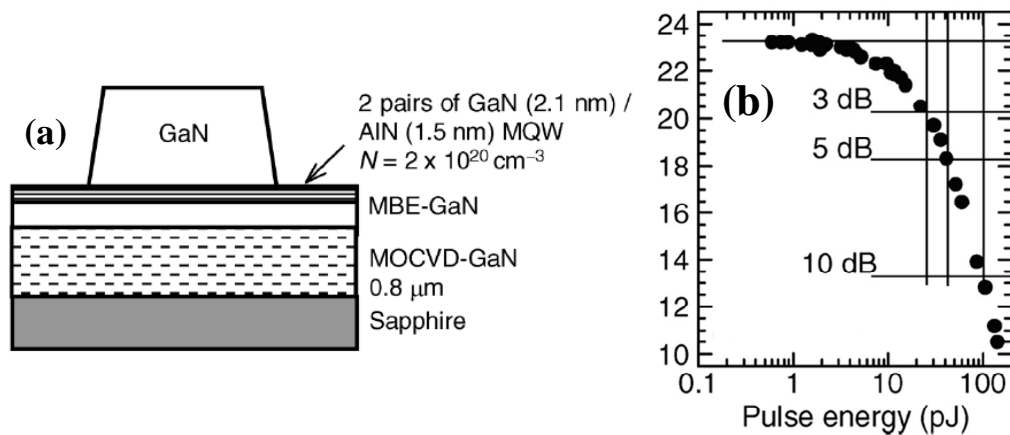
Fig. 1.7 (a) Schematic of ridge GaN-based waveguide with MBE grown GaN/AlN MQWs (b) polarization dependent loss versus input pulse energy: 3-, 5-, 10-dB saturations are indicated.

The research regime of nitride optical devices has changed in year 2007 when C. Kumtornkitikul et al. have fabricated intersubband all-optical switches using AlN waveguide with MBE grown GaN/AlN MQWs [45]. In this work MOVPE grown AlN layer was employed as a buffer for MBE grown GaN/AlN MQWs instead of GaN buffer. The author pointed out the advantages of utilizing AlN buffer layer including low background propagation loss and favorable for single mode propagation waveguide. The intersubband absorption in a high-mesa AlN-based optical waveguide has been first demonstrated in this report. A 7-dB absorption saturation at a 1.43-μm wavelength was observed using an input pulse energy of 200 pJ. The waveguide structure and intersubband absorption saturation measurement of this report are shown in Fig. 1.8 (a) and 1.8(b), respectively.
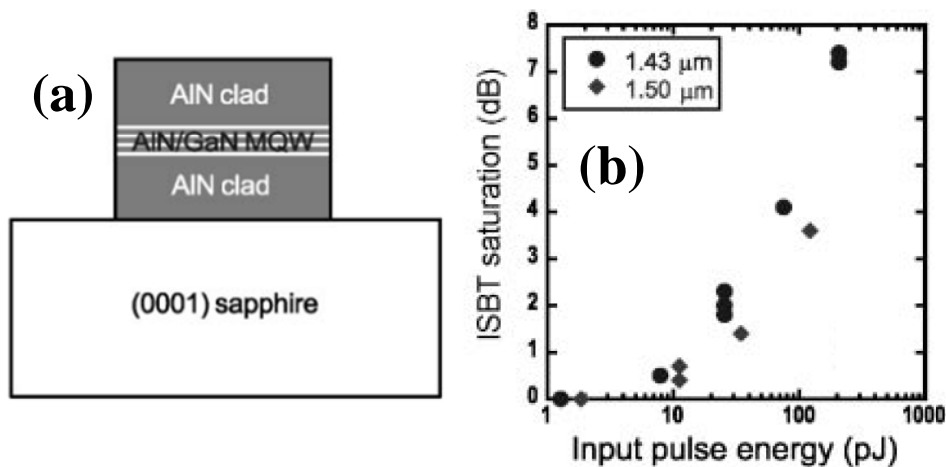
Fig. 1.8 (a) Schematic diagram of high-mesa AlN-based waveguide with MBE grown GaN/AlN MQWs (b) intersubband absorption saturation versus input pulse energy

The improvement of the above report was done in year 2007 by T. Shimizu et al [46]. The author has investigated and optimized the fabrication process of high-mesa AlN-based waveguide by inductively coupled plasma (ICP) dry etching. As a result, the background propagation loss caused by the shape and the sidewall roughness of the waveguide were dramatically decreased. Hence, an intersubband absorption saturation as large as 10 dB at 1.5 μm was observed using 100-pJ input pulse energy. The results of this study were shown in Fig. 1.9 compared with previous data (not optimized by C. Kumtornkitikul).

In 2008, the issue of high control pulse energy was again challenged by Y. Li et al. [25]. In this work, all-optical switching based on intersubband cross-absorption modulation in ridge GaN waveguides with MBE grown GaN/AlN MQWs has been demonstrated with a low values of the required control pulse energy. In particular, a signal modulation depth of 10 dB was obtained with control pulse energies as small as 38 pJ. In the mean while, the intersubband absorption fully recovers from the control-pulse-induced saturation on a picosecond time scale. Fig. 1.10(a) and 1.10(b) show transmittance of the signal pulses through a 3-μm-wide, 1-mm-long waveguide versus signal-control delay time, for different values of the control pulse energy and signal modulation depth versus control pulse energy, as determined from the traces of 1.10(a), respectively. This work was owing to the MOVPE grown AlN buffer on which high

10

quality MBE GaN/AlN MQWs were grown. The author further suggested that these nonlinear waveguide devices were suitable for all-optical switching at bit rates of several hundred Gb/s.
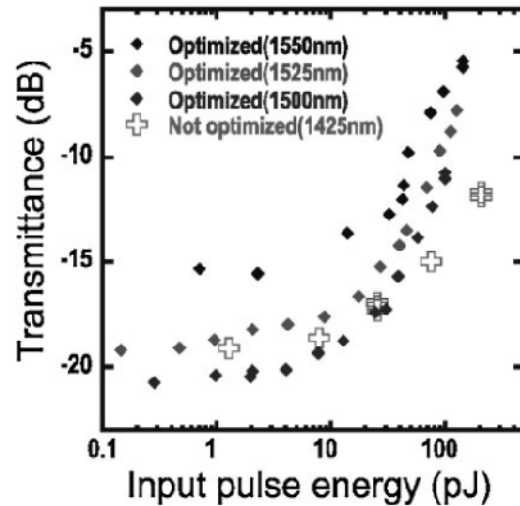
Fig. 1.9 Transmittance (intersubband absorption saturation) at wavelength of 1500, 1525 and 1550 nm as functions of input pulse energy
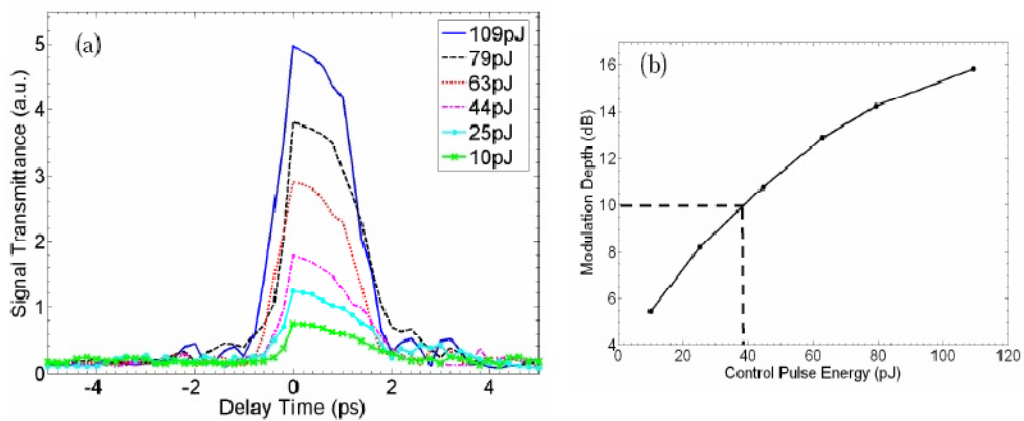
Fig. 1.10 (a) Transmittance of the signal pulses through a 3-μm-wide, 1-mm-long waveguide versus signal-control delay time, for different values of the control pulse energy. (b) signal modulation depth versus control pulse energy, as determined from the traces of Fig. 1.10(a)

Recently, N. Iizuka et al have reported the investigation of AlN-based waveguide with integrated stair-like spot-size converter [47]. The purpose of this study is to encounter the issue of high require control pulse energy for intersubband absorption saturation. The author

11

downsized the MQWs absorption core and used the spot-size converter to improve coupling efficiency of light to downscaled MQWs. The structure consisted of MOVPE grown AlN buffer and MBE grown GaN/AlN MQWs and GaN upper cladding layer. The Si_3N_4 was employed as a dielectric material for fabrication of spot-size converter. A intersubband absorption saturation by 5 dB was reported with an input pulse energy of 25 pJ which the results are shown in Fig. 1.11(a) and 1.11(b).
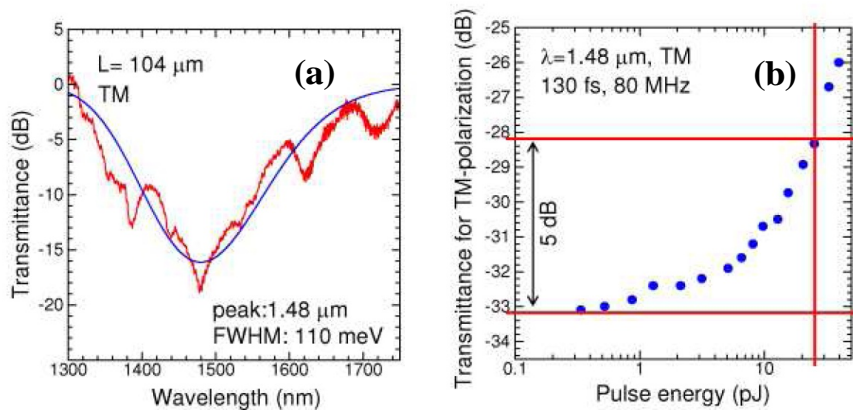
Fig. 1.11 (a) The ratio of the transmittance spectra for TM-polarization to that for TE-polarization for the sample with the length of 104 μm. The blue line represents the Gaussian fit. (b) Characteristics of the absorption saturation. Saturation by 5 dB was achieved with a pulse energy of 25 pJ.

1.3.3 Problem Issues in Current Nitride Intersubband All-Optical Switches

According to the above section which briefly introduced the progress and development of all-optical switches utilizing intersubband transition in GaN/Al(Ga)N MQWs, the issues that current nitride intersubband all-optical switches have been encountering can be pointed out as followed:

1. Until the present time, optical switches utilizing intersubband transition in GaN/Al(Ga)N MQWs have been demonstrated only in MBE grown samples. In the other hand, MOVPE grown GaN/Al(Ga)N MQWs have not been succeeded to realize 1.5-μm-range intersubband transition so far. This issue has distracted the

12

interest of intersubband transition devices in nitride MQWs as it is very difficult to be realized by MOVPE or even by MBE. Although several research groups reported the intersubband transition at 1.5-µm-range in GaN/AlN MQWs grown by MOVPE [48-50], one of major obstructions was weak ISB absorptions due to low carrier concentration in GaN well layers.

2. Although the issue of high demanded control pulse energy has been continuously improved, it still cannot compare with other material systems which have been reported very low operation energy per extinction ratio of 3.2 pJ/dB and 1.13 pJ/dB in InGaAs/AlAs/AlAsSb quantum wells [51] and in CdS/ZnSe/BeTe quantum wells [52-54], respectively.

1.4 Motivation of This Work

As pointed out in the previous section, the optical switches utilizing intersubband transition in GaN/AlN MQWs are still far from the accomplishment. However, compared with other material systems, GaN/AlN MQWs is still very promising as a solution for high optical traffic demand owing to their unique properties including fast intersubband relaxation time, simple quantum well structure and material hardness and robustness. Hence, for the first step, the achievement of 1.5-µm-range intersubband transition in GaN/AlN MQWs grown by MOVPE should renew the interest and has a big impact on this research field, not only for the all-optical switch fabrication but also for the other intersubband optical devices. This is because MOVPE is a system capable for large-scale fabrication. Furthermore, bulk nitride layers deposited by MOVPE possess good characteristics in terms of high crystal quality and low dislocation density which are promising for the fabrication of low loss optical devices.

This dissertation is focused on the MOVPE growth and fabrication of AlN-based waveguide with GaN/AlN MQWs absorption core. The objectives are to fully realize the intersubband transition 1.5-µm-range and to demonstrate the first MOVPE fabricated AlN-based all-optical switches. The achievement of this dissertation should attract the interest of nitride intersubband based optical devices and be an important milestone in this research field.

1.5 Synopses of This Thesis

In this thesis, the experiment has been started in chapter 2 with the growth of GaN/AlN MQWs on GaN buffer by conventional MOVPE method. The growth conditions are varied to clarify the original causes that hinder the achievement of short intersubband transition wavelength in MOVPE grown GaN/AlN MQWs. The deposited structures were evaluated by high resolution X-ray diffractometer (HRXRD) and atomic force microscopy (AFM). Then, the intersubband absorptions in fabricated MQWs are measured by fourier transform infrared spectrometer (FTIR) using multiple reflection method at room temperature. Chapter 3 is the details of investigation on the improvement methods for realizing short intersubband transition wavelength in GaN/AlN MQWs on AlN buffer layers. A growth method called pulse injection method is employed for the deposition of GaN/AlN MQWs at low temperature. The effects of several growth parameters on the intersubband transition characteristics are also discussed in this chapter together with the simulation in order to explicate the effects of growth parameters. After that, in chapter 4, the design and fabrication of AlN-based waveguide with GaN/AlN MQWs absorption core are carried out. The intersubband absorption characteristics in fabricated AlN-based optical waveguide were compared with that in MBE grown samples. The improvement on the issue of high required pumping pulse energy has been challenged by introducing lateral spot-size converter with integrated AlN-based optical waveguide in chapter 6. The conclusions of this thesis are discussed in chapter 7.

Chapter 2 GaN/AlN MQWs by Conventional MOVPE

T his chapter starts with the introduction in section 2.1 which describes laboratory equipments generally used in this thesis. In section 2.2, the experiment procedures are given in detail. The GaN/AlN MQWs varied GaN well width grown by conventional MOVPE and the resultant intersubband transitions have been investigated in section 2.3. Therefore, the MQWs grown by varying growth temperatures using conventional MOVPE has been studied in section 2.4. After that, the effects of growth temperature on the carrier concentration and surface morphologies of GaN and AlN layers are explained in section 2.5. The conclusions have been discussed in section 2.6.

2.1 Introduction

2.1.1 Metal Organic Vapor Phase Epitaxy

Metal organic vapor phase epitaxy (MOVPE) is a chemical vapor deposition method of epitaxial growth of materials, especially compound semiconductors from the surface reaction of organic compounds or metalorganics and metal hydrides containing the required chemical elements. For example, gallium nitride could be grown in a reactor on a substrate by introducing trimethylgallium ($(CH_3)_3Ga$) and ammonia (NH_3) which their chemical reaction is [55]:

$$Ga(CH_3)_3(l) + NH_3(g) + H_2(g) \rightarrow GaN(s) + 3CH_4(g) + H_2(g) \qquad (2\text{-}1)$$

Alternative names for this process include organometallic vapor phase epitaxy (OMVPE), metalorganic chemical vapor deposition (MOCVD) and organometallic chemical vapor

deposition (OMCVD). Formation of the epitaxial layer occurs by final pyrolysis of the constituent chemicals at the substrate surface. In contrast to molecular beam epitaxy (MBE) the growth of crystals is by chemical reaction and not physical deposition. This takes place not in a vacuum, but from the gas phase at moderate pressures. As such this technique is preferred for the formation of devices incorporating thermodynamically metalstable alloys. It has become the dominant process for the manufacture of laser diodes, solar cells, and LEDs.
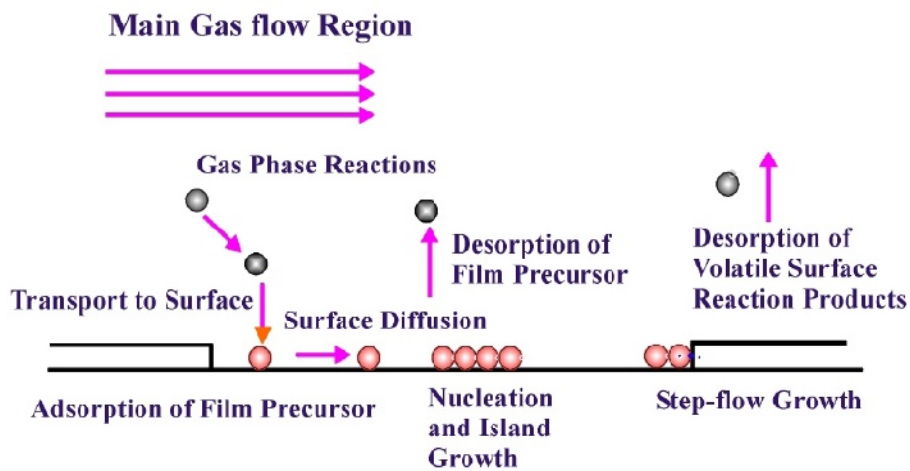
Fig. 2.1 Schematic of epitaxy growth on atomic level
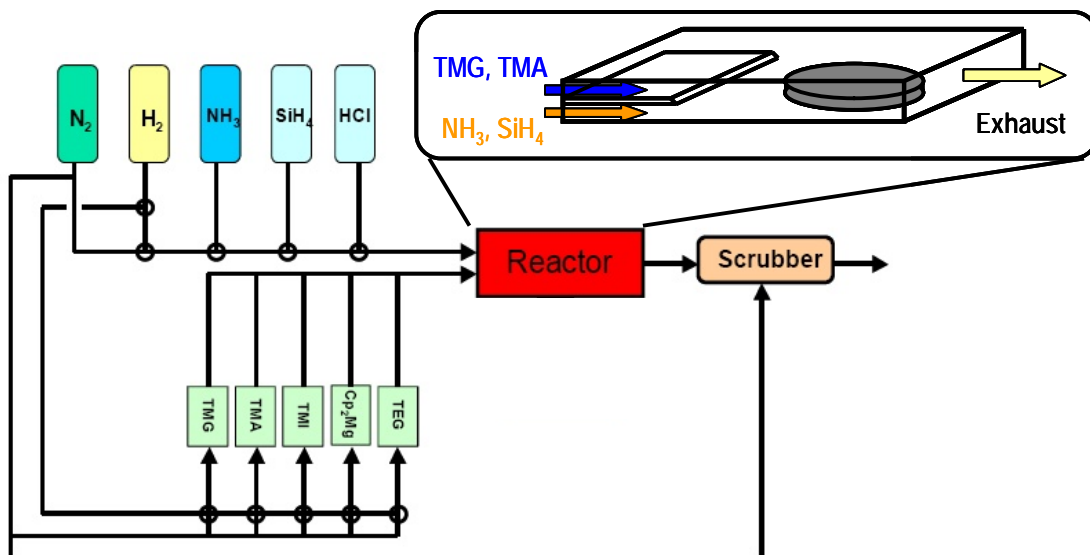
Fig. 2.2 Schematic of MOVPE system equipment for nitride semiconductors

2.1.2 High-resolution X-ray Diffractometer

X-ray diffraction (XRD) is a powerful and commonly available technique for identifying the presence of crystalline phase. The quantitative, high-accuracy measurements of interatomic spacings provided by XRD have motivated some detailed studies. The XRD patterns also provide information on strain, grain size, preferential orientation and epitaxy. In addition, XRD is non-destructive and can sometimes be used *in situ*.

X-rays with wavelength, λ, between 0.5 and 2Å are impinged upon a sample. The diffracted X-rays are measured at $2q$, the angel between X-ray source and detector. Diffracted waves from different atoms can interfere with each other and the resultant intensity distribution is strongly modulated by this interaction. If the atoms are arranged in a periodic fashion, as in crystals, the diffracted waves will consist of sharp interference maxima (peaks) with the same symmetry as in the distribution of atoms. Measuring the diffraction pattern therefore allows us to deduce the distribution of atoms in a material. The peaks in an x-ray diffraction pattern are directly related to the atomic distances. Let us consider an incident x-ray beam interacting with the atoms arranged in a periodic manner as shown in 2 dimensions in Fig. 2.3. The atoms, represented as green spheres in the graph, can be viewed as forming different sets of planes in the crystal (colored lines in graph on left). For a given set of lattice planes with an inter-plane distance of d, the condition for a diffraction (peak) to occur can be simply written as:

$$2d \sin q = nl \tag{2-2}$$

which is known as the Bragg's law. In the equation, l is the wavelength of the x-ray, q the scattering angle, and n an integer representing the order of the diffraction peak. The Bragg's Law is one of most important laws used for interpreting x-ray diffraction data.
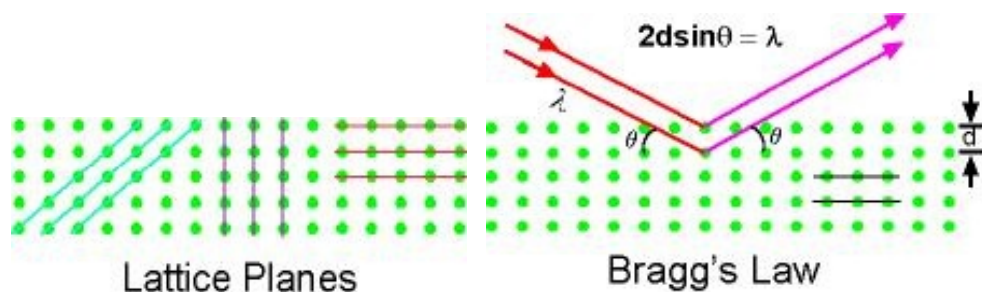
Fig. 2.3 Lattice planes and Bragg's law

2.1.3 Atomic Force Microscope

The atomic force microscope (AFM) is a very high-resolution type of scanning probe microscope, with demonstrated resolution of fractions of a nanometer. The AFM consists of a microscale cantilever with a sharp tip (probe) at its end that is utilized to scan the surface. The cantilever is typically silicon or silicon nitride with a tip radius of curvature in the order of nanometers. When the tip is brought into proximity of a sample surface, forces between the tip and the sample lead to a deflection of the cantilever. Typically, the deflection is measured using a laser spot reflected from the top of the cantilever into an array of photodiodes. The sample is mounted on a piezoelectric tube, which can move the sample in the z direction for maintaining a constant force, and the x and y directions for scanning the sample. A schematic and mode of AFM measurement are shown in Fig. 2.4 and 2.5 respectively.
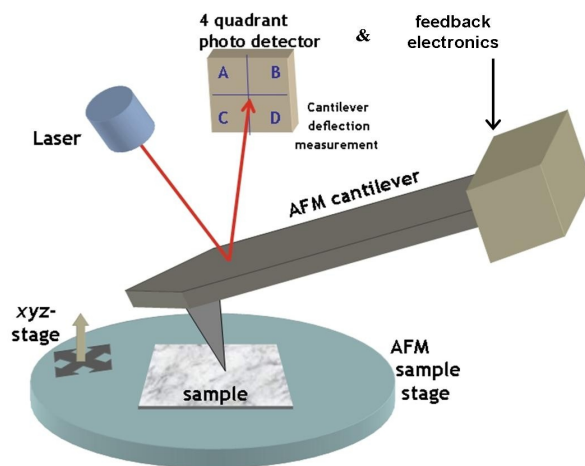
Fig. 2.4 A schematic of AFM measurement
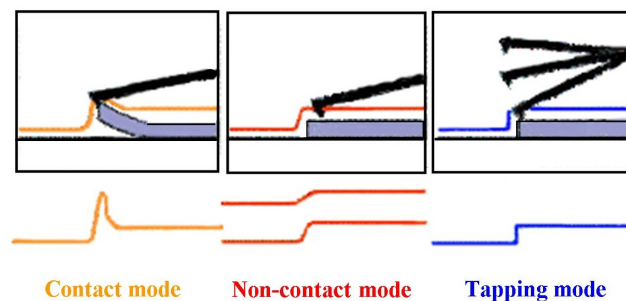
Fig. 2.5 Modes of AFM measurement

2.1.4   Fourier Transform Infrared Spectroscopy

The fourier transform infrared spectroscopy (FTIR) is typically based on a Michelson interferometer as shown in Fig. 2.6. In FTIR spectroscopy, light from an infrared light source is collimated and incident on a beam splitter. An ideal beam splitter creates two separate optical paths by reflecting 50% of the incident light and transmitting the remaining 50%. In one path the beam is reflected by a fixed-position mirror back to the beam splitter where it is partially reflected to the source and partially transmitted to the detector. In the other arm of the interferometer, the beam is reflected by the movable mirror that is translated back and forth and maintained parallel to itself. The interference of two beams of light waves propagated through two separate optical path lengths is thus produced when they are combined. For different positions of the movable mirror the two partial waves obtain different phase shift with respect to each other. Therefore, on the detector, the radiation field is superimposed with a time-delayed copy of itself. Hence, what is basically measured when the detector signal is recorded while the mirror moves is the autocorrelation function of the radiation field, which is called the interferogram in the FTIR spectroscopy. The Fourier transform of this autocorrelation function is the desired power spectrum in a frequency domain. In the FTIR spectroscopy, there are three important components that determine the wavelength range of the measurement, which are light source, beam splitter, and detector.
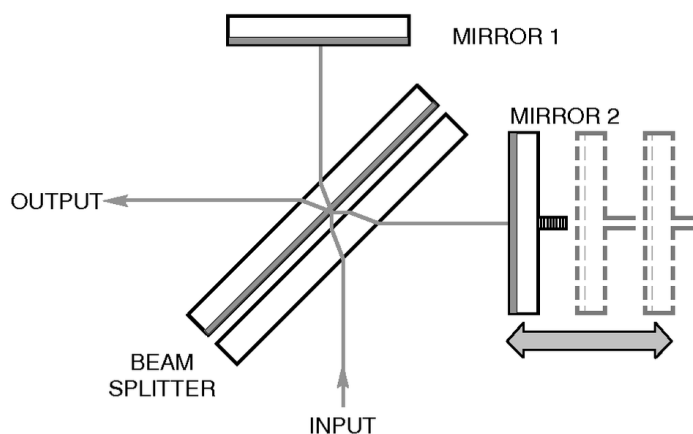
Fig. 2.6 Schematic of a generic Michelson interferometer

2.2 Experimental Details

The experiment has been started with the growth of GaN/AlN MQWs on GaN buffer layer by using conventional MOVPE method. The reasons of choosing GaN layers as buffers rather than AlN for the first experiment are:

1. GaN is the most common used and famous for growing nitride epitaxial layers for devices fabrication including light emitting diodes (LED) [56-58], laser diodes (LD) [59,60], high power electronic devices [61,62], photodetectors [63,64], and high electron mobility transistors (HEMT) [65,66].

2. High quality GaN bulk layers can be grown easier than AlN bulk layer by the MOVPE machine used in this work.

3. Growth rate of GaN is generally much faster than that of AlN, thus the experiment can be progress faster [67-69].

4. There are lots of references and published papers relate to intersubband transition in GaN/AlN MQWs using GaN buffer layers [44,48,70].

All of samples were grown on 2-side polished c-plane sapphire by low pressure MOVPE (AIXTRON 200/4 RF-S) using trimethylgallium (TMG), trimethylaluminium (TMA) and NH_3 with H_2 carrier gas as precursors. SiH_4 was used as a dopant gas for Si-doped GaN layers (n-doped). The MQWs structures in this work was stacks of GaN wells berried between AlN barriers. The intersubband transition occurs in GaN well which is the transition of electrons from ground state to higher energy levels particularly the first excite level. It is commonly known that the thickness of GaN well affects the quantized energies in QW. Therefore, the effects of well width would be first investigated. After that, the effects of growth temperature would be next studied. The investigated MQWs structure is shown in Fig. 2.7.

The fabricated samples were then evaluated the quality and structure by XRD. The information taken from (0002) 2θ-ω scan was used to estimate the thicknesses of well and barrier by the angular distances of satellite peaks. To measure intersubband transition, the samples were polished 45° at two facets to allow 15 total reflections as shown in Fig. 2.8. The measurement was carried out by FTIR at room temperature. It should be commented here that, due to the selection rule in MQWs, only light that is perpendicular to the MQWs plain, i.e. p-polarized light or TM-mode light, will be absorbed by the intersubband transition. Therefore,

only transmittance spectra of p-polarized light containing the information of intersubband characteristics evaluated by FTIR are given in plotting graphs. The intersubband absorption can be directly determined by the transmittance spectra of p-polarized light since the summation of transmittance and absorbance should be equal 1. In the other hand, the absorption peaks are the transmission valley and vice versa.
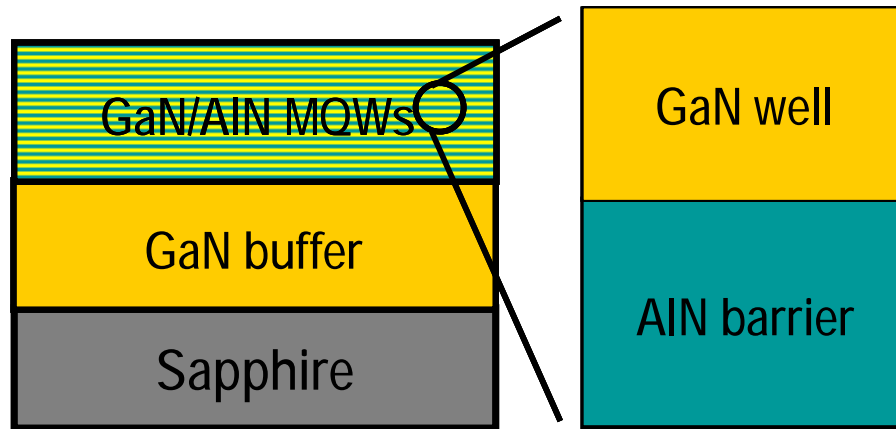
Fig. 2.7 Schematic of Investigated MQWs on GaN buffer
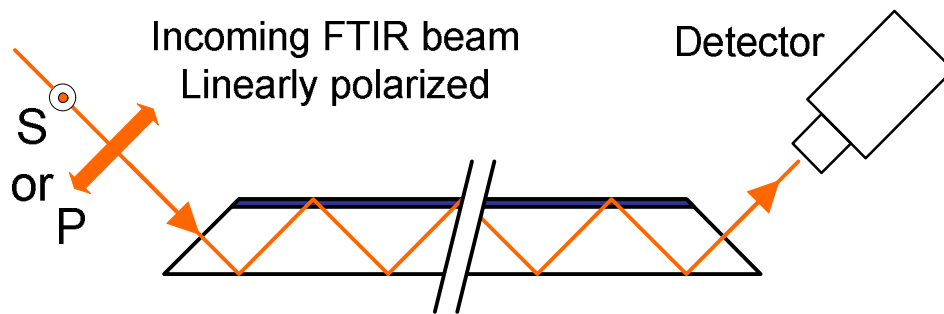
Fig. 2.8 Schematic of multiple reflection method

2.3 Effects of GaN Well Width on Intersubband Transition in GaN/AlN MQWs

There are many reports on the intersubband transition wavelength tailoring by changing GaN well thickness [6,11,70]. However, in order to confirm the results acquired by the MOVPE used in this study, investigate other effects and determine the short intersubband transition

wavelength which can be achieved by conventional MOVPE growth method, the intersubband transition in GaN/AlN MQWs was studied by varying the GaN well thickness. The depositions of 100-period GaN/AlN MQWs were done at a temperature of 1130 ℃ on high quality 3-µm-thick GaN buffer layers grown at high temperature. During the growth of GaN buffers and MQWS, the reactor pressure was 200 and 100 mbar, respectively. The AlN barrier thickness was controlled to be around 1.60 nm for all sample. The V/III ratio is calculated from the amount of group V and group III gases supplied into reactor. Thus, V/III ratio during the growth of GaN buffer, GaN well and AlN barrier could be determined as 420, 1000 and 10200, respectively.

Figure 2.9 shows the XRD (0002) 2θ-ω scans of MQWs grown at 1130 ℃ varied GaN well thickness. It is clear that, with thick GaN layer, the MQWs show high order and sharp satellite peaks. It can be explained that the thicker GaN wells resulting in thicker total MQWs thickness. The resultant intensities of XRD peaks corresponding to GaN/AlN MQWs therefore became stronger in thick GaN well sample. The other reason is the high temperature during the growth of MQWs leads to the interdiffusion between Ga and Al atoms and results in non-abrupt GaN/AlN interfaces. Hence, with the same growth temperature at 1130 ℃, the degree of non-abruptness should be approximately same for all samples. This can be interpreted that the effect of non-abrupt GaN/AlN interface becomes greater in the sample with thin GaN well since the thickness of this non-abrupt region becomes relatively large compared to that of GaN well. In addition to the well width, the abruptness of GaN/AlN interface plays a crucial role to determine the intersubband transition wavelength. This fact will be discussed and proved by the simulation in chapter 3. Figure 2.10 shows the transmittance spectra of p-polarized light measured by FTIR. Agreeing with the quantum theory, the decrease of GaN well thickness results in blue-shift of intersubband transition wavelengths as shown in Fig. 2.11. However, the samples with too thin GaN well did not show any intersubband transition peaks. Considering the XRD (0002) 2θ-ω scans together with FTIR result, it is clear that the sample which could not observed any intersubband transition had poor satellite peaks of GaN/AlN MQWs. It can be simply state that the sample with poor abrupt interface did not show any intersubband activity. In the contrast with MBE grown GaN/AlN in many literatures, the degree of abruptness of GaN/AlN is generally low and the interdiffusion effect is typically negligible. Besides the difference of crystal deposition mechanisms between MBE and MOVPE, the growth temperatures in MBE and MOVPE

chamber are quite different. Since the growth temperature seems to have a great effect on the abruptness of MQWs, this growth parameter would be investigated in next section.
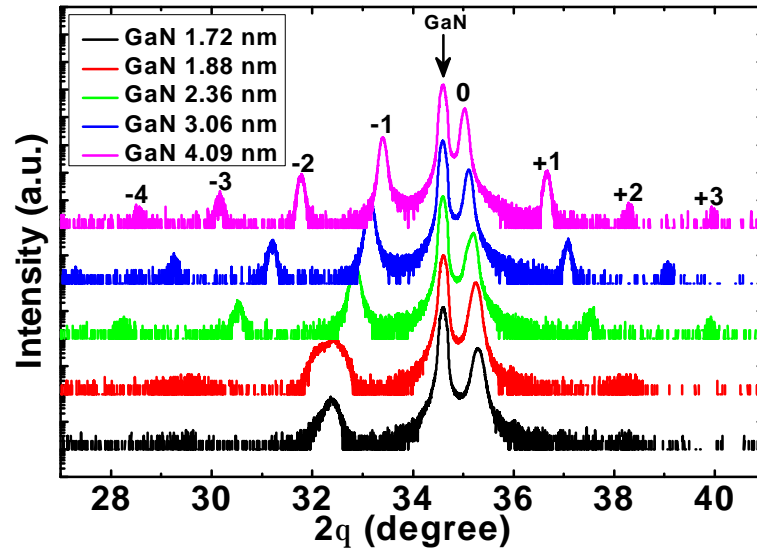
Fig. 2.9 XRD (0002) 2θ-ω scans of the conventional MOVPE grown GaN/AlN MQWs at 1130 ℃ varied GaN well thickness
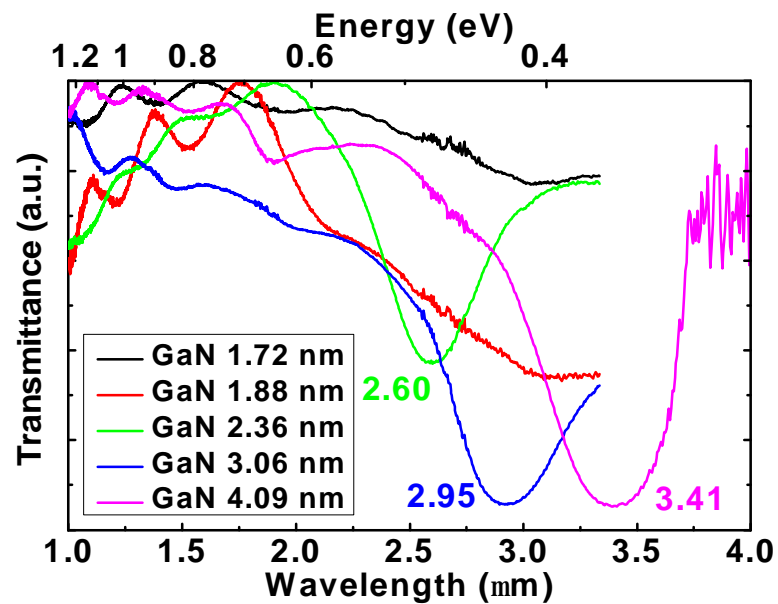
Fig. 2.10 Transmittance spectra of p-polarized light in the conventional MOVPE grown at 1130 ℃ GaN/AlN MQWs varied GaN well width
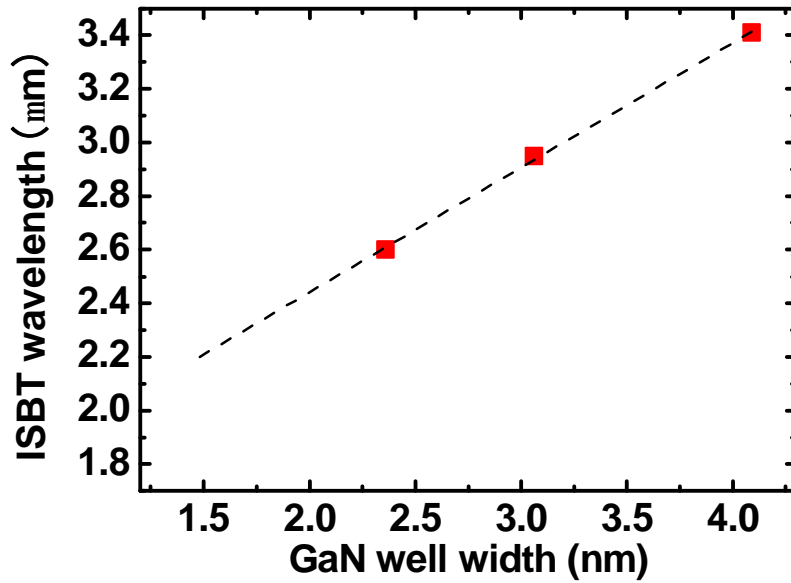
Fig. 2.11 Dependency of intersubband transition wavelength in GaN/AlN MQWs
grown by conventional MOVPE at 1130˚C as a function of GaN well width

2.4 Effects of Growth Temperature on Intersubband Transition in GaN/AlN MQWs

The studied MQWs structures in the experiment were similar with the previous section as shown in Fig. 2.7. The GaN (2.50 nm)/AlN (1.60 nm) MQWs were grown at the growth temperatures of 900, 950, 1000, 1050, 1100 and 1130 ℃. The samples were investigated in the same manner with the previous experiment. Figure 2.12 displays the XRD (0002) 2θ-ω scans of MQWs grown at different temperatures. Obviously, the samples grown at lower temperature had relatively sharper and higher satellite peaks. This indicates that the MQWs grown at lower temperature had better abrupt GaN/AlN interface. The reason is, at lower temperature, the interdiffusion between Ga and Al atoms was limited by the thermal energy and the thickness of non-abrupt region becomes thinner as a result. From the simulation in chapter 3, it can be expected the blue-shift of intersubband transition wavelengths resulted by better abruptness on MQWs. Nevertheless, the intersubband transition measurement results did not completely agree with this assumption. As shown in Fig. 2.13, we can observe the blue-shift of intersubband transition wavelength from 2.60 μm to 2.41 μm when the growth temperature was decreased from 1130 to 1100 ℃. However, the intersubband absorption became weak and disappeared

when the temperature was lower than 1100 ℃. This can implied that, although the interface between GaN/AlN can be improved by low temperature growth, the intersubband transition become weaker and weaker as a function of temperature. Some of the possible reasons of this phenomenon are:

1. The growth temperature changes the strain in MQWs and thus changes the built-in electric field over the wells and barriers. As a result of this, the oscillation strength becomes weaker. The weak oscillation strength, therefore, results in weak intersubband absorption [71,72] since these two parameters are quantitatively proportional to each other.

2. It is widely acknowledge that the conventional nitride MOVPE requires high growth temperature for effective chemical reactions since NH_3 is barely deformed at low temperature. As a result, the nitride epilayers are suffered from incomplete chemical reaction and the crystal quality is dramatically degraded at low growth temperature.

3. It can be considered that, at low growth temperature, the electron population in ground energy level becomes insufficient. Hence, the transition rate and absorption intensity which are proportional to the carrier concentration becomes weaker at a result.

Therefore, there are two distinguish investigation in order to clarify the above assumptions. One is theoretical and numerical study on the conduction band line-up and wave functions of electrons in quantum wells. The other is experimental study on the nitride epitaxial layers deposited at different temperature. Choosing the simplest experiment, the effects of the growth temperature on the carrier concentration in n-doped GaN wells and the surface morphologies of GaN and AlN layers are investigated in the next chapter rather than the numerical study of oscillation strength.
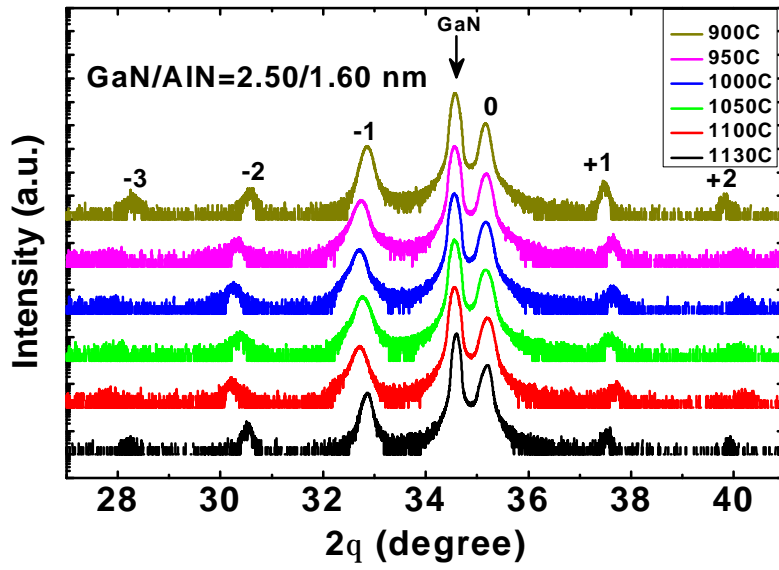
Fig. 2.12 XRD (0002) 2θ-ω scans of GaN (2.50nm)/ AlN (1.60 nm) GaN/AlN

MQWs grown at different temperature by conventional MOVPE
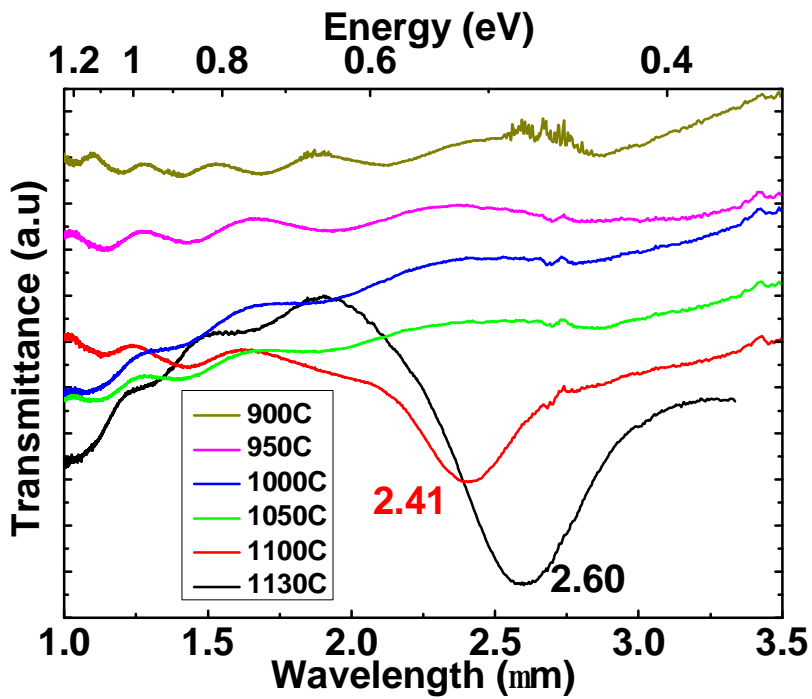
Fig. 2.13 Transmittance spectra of p-polarized light in the GaN/AlN MQWs grown

by conventional MOVPE at different growth temperatures

2.5 Effects of Growth Temperature on Carrier Concentration in n-doped GaN and Surface Morphologies of GaN and AlN Layers

First, in order to clarify the dependency of carrier concentration in n-doped GaN on the growth temperature, the n-type Si-doped GaN layers were deposited on AlN templates at different temperature. After the growth, the samples were cut and Ti/Au contacts were evaporated on the 4 corners of each samples using electron-beam (EB) evaporator. Thicknesses of Ti and Au layers were 50 and 200 nm, respectively. To form the ohmic contacts, GaN samples with Ti/Au contacts were annealed at 400º C, 5 min under N_2 ambient to prevent the oxidization of Ti/Au contacts. Therefore, the carrier concentration in GaN layers was evaluated by Hall-effect measurement. Figure 2.14 displays the dependency of concentration and mobility of electron in n-doped GaN layers as functions of growth temperature. We can clearly observe that the carrier concentration intensively decreased at the growth temperature lower than 1050 ºC as well as the electron mobility. So that, the n-doped GaN layers grown at 900, 950 and 1000 ºC could not be evaluated by Hall-effect measurement. The possible reasons of the decrease of carrier concentration could be:

1. The degradation of crystal quality and the increasing of defects and dislocations due to ineffective chemical reaction and the deposition of undesired abduct compounds at low temperature.

2. Trapping of electrons by carbon atoms which are products of incomplete chemical reaction and abduct compounds due to ineffective NH_3 decomposition at low temperature.

3. Ineffective incorporation of Si atoms (donor atoms) into GaN layers at low temperature.

In order to point out the cause of this problem, first, the surface morphologies of thin GaN and AlN layers grown at different temperatures were investigated by atomic force microscope (AFM). The AFM images from this experiment were shown in Fig. 2.15 with a resolution of 1×1 µm^2. Clearly, even at low temperature, the thin GaN layers show step-flow growth mode which can be also observed from the excellent quality bulk GaN grown at high temperature. This can be implied that the crystal quality of GaN thin layers is tolerance to the growth temperature. In the case of AlN layers, we can observe the transition of surface

morphologies from smooth and homogeneous at high growth temperature to grain-like surface at low temperature. This indicates that the AlN quality drops with decreasing the growth temperature. It should be marked here that, later in the chapter 5, quality of AlN layers can affect on the background propagation loss in AlN waveguide with GaN/AlN MQWs core.
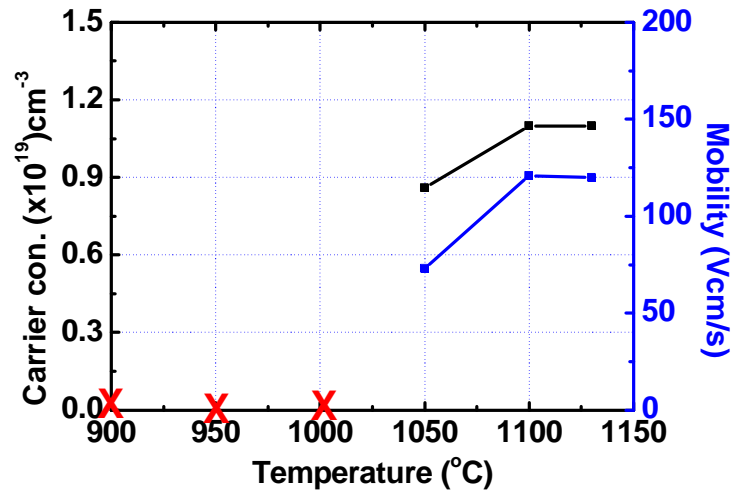
Fig. 2.14 Carrier concentration and electron mobility of n-doped
GaN grown at different temperature
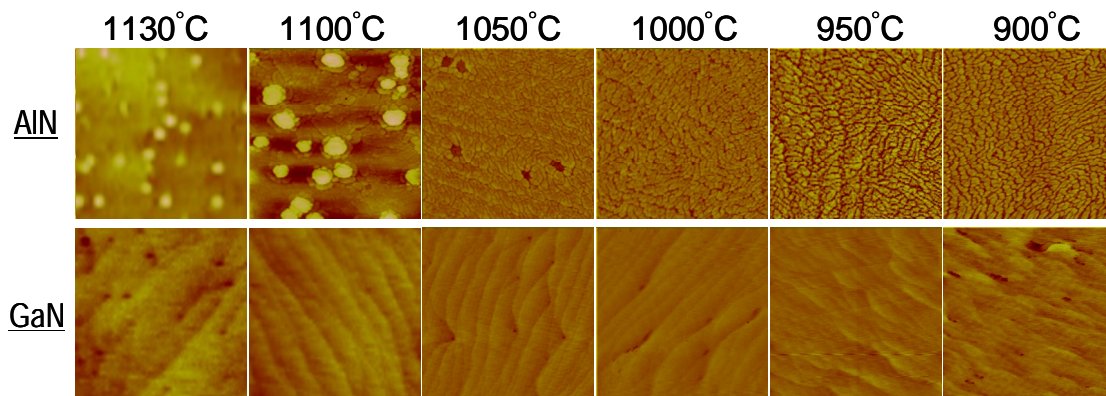
Fig. 2.15 Surface morphologies of thin GaN and AlN layers grown at different temperature evaluated by AFM in 1×1 μm^2 resolution

Next, the concentrations of each element in Si-doped GaN layers have been investigated by secondary ion mass spectrometry (SIMS). Of the most interesting elements, the concentration of C and Si are plotted as functions of depositing temperature which are shown in Fig. 2.16. We can see that Si concentration changed very slightly compared to that of C when the growth temperature was varied. It is clear that, at low temperature, the overwhelming amount of C over Si results in the low carrier concentration. This can be explained that electron from Si-dopant are trapped and nullified by C atoms [73-74]. Hence, the problem of disappearance of intersubband transition at low temperature growth has been extracted which the crystal quality of AlN barriers and the low carrier concentration in GaN wells are concerned as the causes.
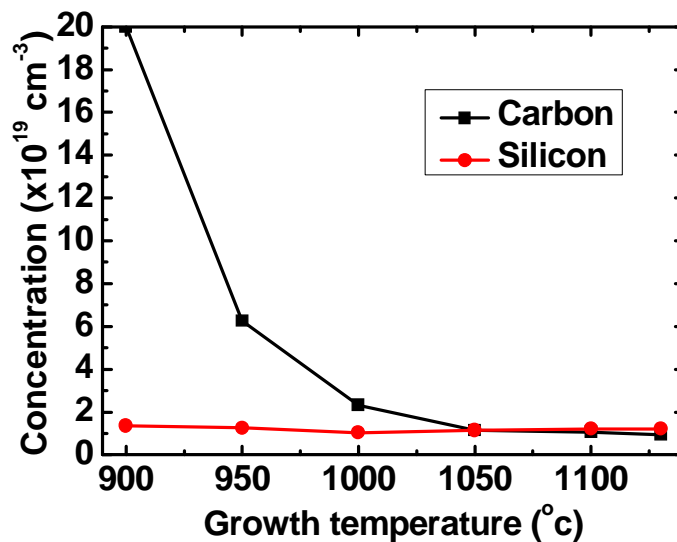
Fig. 2.16 Concentration of C and Si atoms in GaN layers grown at different temperature

2.6 Related Reports on Intersubband Transition in MOVPE Grown GaN/AlN MQWs

It has been obviously shown here that the short intersubband transition wavelength is very difficult to realize in MOVPE grown GaN/AlN MQWs using conventional growth method. Hence, several researches groups have put much effort to investigate the effective growth method for short intersubband transition in MOVPE grown GaN/AlN MQWs. Some examples of these reports are shown as listed:

1. Our group reported the strain-managed GaN/AlN super lattices for intersubband transition in 2003. The GaN interlayers were used to tailor strain which resulted in the crack-free 200-period GaN/AlN super lattices on GaN layer [75].

2. In 2006, Nicolay et al. reported the 2-µm intersubband transition with 64-meV full-width at half-maximum of absorption peak in GaN/AlN MQWs grown at 935°C using indium surfactant to improve the surface morphologies of AlN layer and the abruptness of MQWs [48]. However, in this report, the intersubband transition measurement was done by photoinduced infrared absorption (PIA) spectroscopy under excitation by a frequency-doubled argon laser at λ=244 nm. It can be intimated that the carrier concentration in GaN wells was very low and needed a laser to excite carriers from valence band to conduction band for evaluating the intersubband transition characteristics.

3. Further report from the same group demonstrated the transition wavelength at 1.59 µm by using AlN buffer which manages the strain in AlN barrier [49]. This is because the strain in AlN barrier induces the surface instability and causes the non-abrupt GaN/AlN interface. However, in their report, the absorption measurement was also performed using photoinduced absorption (PIA) technique indicating that insufficient carrier concentration in GaN wells was still an obstacle.

4. Recently, Bayram et al. reported the intersubband transition at 1.53 µm in GaN/AlN MQWs grown at 1035°C using indium surfactant and pulsed MOVPE [50]. However, the absorption intensity measure by slab waveguide method was weak.

5. Our group has investigated the effect of growth temperature on the physical properties of GaN/AlN MQWs using conventional MOVPE method and concluded that the low temperature is favorable for abrupt interface between GaN and AlN and is one of mandatory factors toward the achievement of short intersubband transition wavelengths in MOVPE grown GaN/AlN MQWs [76,77].

From the above reports, it is clear that although the abruptness of GaN/AlN MQWs can be improved and 1.5-µm-range intersubband transition wavelength were realized by several techniques, including indium surfactant, low temperature growth, AlN buffer layer and pulse MOVPE, the absorption intensity was suffered from the issue of low carrier concentration in GaN wells. This is due to the exceed carbon incorporating into n-doped GaN layers which has

been described in the last section. Of the most important, the issue of doping and carrier concentration needs a close investigation which is carrier out in the next chapter.

2.7   Conclusion

1. GaN/AlN MQWs were fabricated by conventional MOVPE. The intersubband transition wavelengths are blue-shifted with decreasing GaN well width. However, the shortest transition wavelength achieved by this method was only 2.6 μm. The problem is non-abrupt interface between GaN and AlN by high growth temperature particularly in samples with thin GaN wells.

2. By lowering the growth temperature, the abruptness of GaN/AlN MQWs was improved. Although the intersubband transition wavelength was blue-shifted due to the better GaN/AlN abruptness, at the growth temperature lower than 1100˚C, the intersubband absorption disappeared.

3. The reasons of no intersubband transition at low growth temperature were analyzed as the crystal quality of AlN barriers and the low carrier concentration in GaN wells.

4. Several groups have successfully demonstrated the short intersubband transition wavelength particularly at 1.5-μm-range by improving the growth method of GaN/AlN MQWs. The growth temperature was lowered as it was considered as a cause of non-abrupt interface. Nevertheless, the intersubband absorption intensities were very weak due to low carrier concentration in GaN wells.

Since the low temperature growth has been proved to be necessary for abrupt GaN/AlN interface and was promising for short intersubband transition wavelength, the improvement of carrier concentration in GaN wells grown at low temperature will be investigated in next chapter.

Chapter 3 GaN/AlN MQWs Grown by Pulse Injection Method on AlN Buffer

From the last chapter, the GaN/AlN MQWs grown by conventional MOVPE did not demonstrate any good intersubband properties although the MQWs structure itself was greatly improved by low temperature growth. One of the possible explanations is that the GaN wells in the MQWs had not enough carriers in the first subband to be excited to higher subbands and exhibit an intersubband transition. Therefore, at the beginning of this chapter, an improvement called pulse injection method is explained in section 3.1 as a promising technique for n-doped GaN layer grown at low temperature. In section 3.2, the GaN/AlN MQWs grown by pulse injection method on AlN buffers have been investigated. The effects of growth temperature and AlGaN interlayer on intersubband characteristics in GaN/AlN MQWs grown by pulse injection method have been studied and explained in section 3.3 and 3.4. The simulation of intersubband transition wavelength in GaN/AlN MQWs has been conducted to explain the experiment results. This simulation model is based on a self-consistent Schrödinger-Poisson equation implemented with effects of piezoelectric field, band non-parabolicity and non-abrupt interface (graded interface) between GaN and AlN. The solution of self-consistent Schrödinger-Poisson equation is determined using 3-point finite different method. Section 3.5 is an improvement of intersubband absorption intensity by changing the reactor pressure during the growth of MQWs to prepare samples for the fabrication of AlN-based waveguide with GaN/AlN MQWs core. The conclusion, therefore, is given in the last part, section 3.6.

3.1   Pulse Injection Method for Low Temperature GaN/AlN MQWs

As described in the previous chapter that one of the obstructions hindering the low temperature grown GaN/AlN MQWs to exhibit intersubband transition, even though the interface was much improved, is the low carrier concentration in GaN layers. The origin of this problem corresponds to the exceed carbon concentration due to ineffective carbon reduction at low temperature. Recently, J. S. Yang et al. has reported the GaN/AlN MQWs grown at low temperature and significantly blue shifted of intersubband transition wavelength [78]. This achievement was owing to the pulse injection (PI) growth method which enhances the carbon reduction and promotes surface migration. As a result, GaN layers can be sufficiently doped at relatively low temperature compared with conventional MOVPE growth [79-81]. Figure 3.1 shows gas flow sequence during the GaN/AlN MQWs growth in Yang's work. As its literature, in pulse injection method, TMG and SiH_4 were pulse supplied with the constant flow of NH_3 during the growth of n-doped GaN. 1 cycle of pulse injection method consists of 12 seconds of group III and SiH_4 supplying time and 7 seconds of only NH_3 flow. The desired GaN thickness can be achieved by adding the number of cycles and changing the partial pressure of TMG. Although it is possible to adjust the deposition rate of pulse injection grown GaN layer by changing supply time, it was not recommended here since the carrier concentration in GaN layer can change dramatically with the changing of supply time. As illustrated in Fig. 3.1, AlN layers were grown by conventional method instead of pulse injection method which has been report in Ref. 82-84. This is based on an assumption that poor surface morphologies of low-temperature AlN layers shown in Fig. 2.14 did not obstruct the intersubband transition as much as the issue of low electron concentration in GaN wells. Hence, in this chapter, the pulse injection method and the structure of GaN/AlN MQWs in Yang's work have been adopted to grow MQWs on AlN buffer layers. Here, AlN bulk layers were chosen as buffers for MQWs growth since:

1. There are several publications report that the intersubband transition wavelengths of MQWs grown on AlN was noticeably shorter than that of MQWs grown on GaN buffer using the same structure [49,85].

2. S. Nicoley et al. has reported that strain in AlN layers in GaN/AlN MQWs system leads to non-abrupt interface between GaN and AlN [49]. Therefore, by changing the buffer layer from GaN to AlN, the strain in AlN barrier can be greatly decreased.

Consequently, the better abruptness of MQWs as well as the short intersubband transition wavelength can be possibly achieved.

3. AlN bulk layer is more favorable than GaN in the view point of low background loss in waveguide-based optical devices [25,47,85,86].
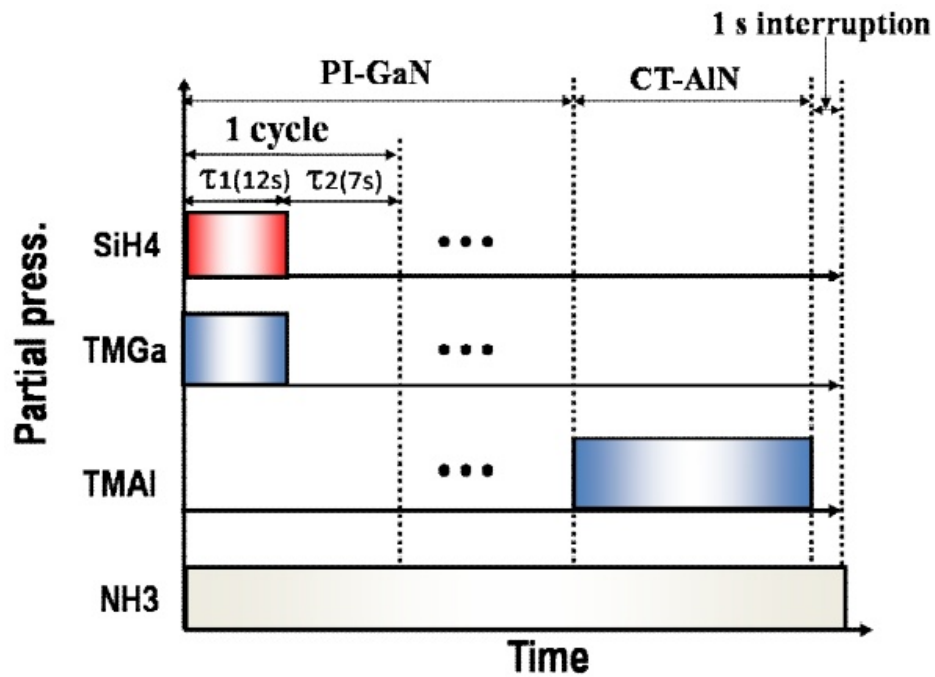
Fig. 3.1 Schematic of gas flow sequence during 1 period of GaN/AlN MQWs grown by pulse injection method [78]

3.2 Pulse Injection Grown GaN/AlN MQWs on AlN Buffers

In this chapter, 0.5-µm thick AlN bulk layers grown at 50 mbar, 1175 ℃ were used as buffer layers for depositing GaN/AlN MQWs layers. The MQWs structure and the gas flow sequences were adopted from Yang's work. However, in early state of this experiment all of GaN/AlN MQWs grown by pulse injection method on AlN buffers exhibited terribly poor characteristics in the view point of crystal quality, uniformity and abruptness. Therefore, there was no intersubband transition observed from these samples but only absorption from defects and dislocation in crystal structure. Fig. 3.2(a) and 3.2(b) display the XRD (0002) 2θ-ω scan and

p-polarization transmittance of a MQWs grown by pulse injection method on an AlN buffer. The XRD (0002) 2θ-ω scan revealed an extremely poor MQWs quality evidenced by lacking of satellite peaks and low MQWs peak intensity. One of possible explanations which cause the difference between MQWs in this experiment and Yang's samples is the buffer layers; i.e. AlN in this work and GaN Yang's work, leads to dissimilarity of strain level in GaN/AlN MQWs. Hence, in order to imitate the strain in MQWs as in Yang's work, 0.1-µm-thick GaN interlayer was deposited on AlN buffer prior to the growth of MQWs as shown in Fig. 3.3. This was followed by the growth of GaN/AlN MQWs by pulse injection method as similar as the previous study. The samples grown with GaN interlayers showed a marvelous improvement not only the abruptness of MQWs but also the intersubband transition properties confirmed by XRD and FTIR. This improvement satisfied the assumption of strain in GaN/AlN MQWs. Thereafter, a series of GaN/AlN MQWs with varied GaN well thickness have been deposited on GaN-interlayer/AlN-buffer to study the intersubband characteristics. The AlN thickness was controlled at 2.0 nm and the growth temperature of MQWs was fixed at 950 ℃ for all samples. The p-polarized transmittance spectra of polished samples are shown in Fig. 3.4.
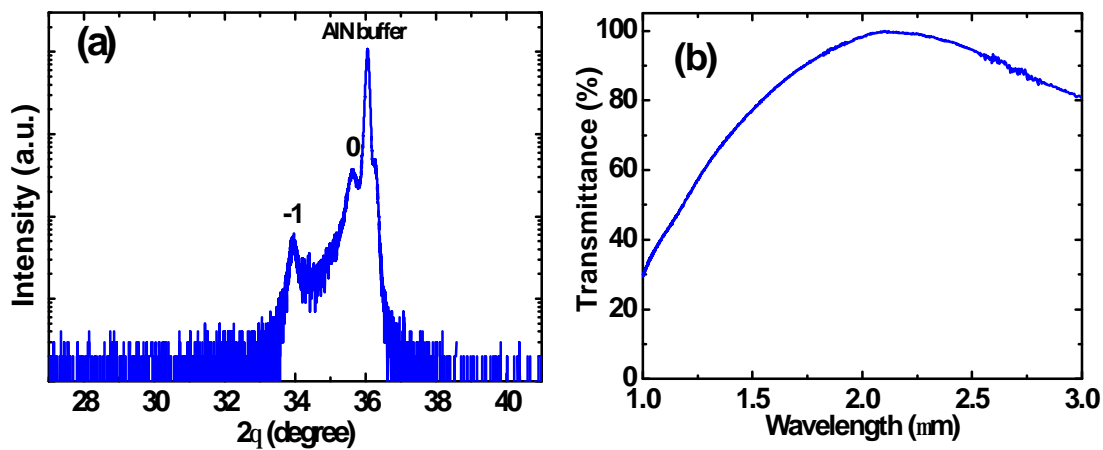
Fig. 3.2 (a) XRD (0002) 2θ-ω scan and (b) transmittance of p-polarized light in a MQWs grown by pulse injection method on an AlN buffer
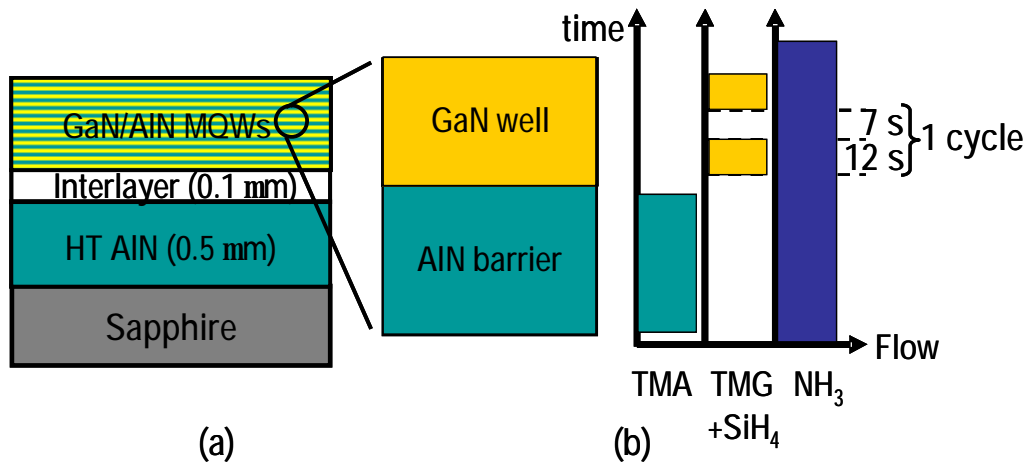
Fig. 3.3 (a) GaN/AlN MQWs structure on an AlN buffer using an interlayer to manage strain and (b) gas flow sequence during GaN/AlN MQWs growth
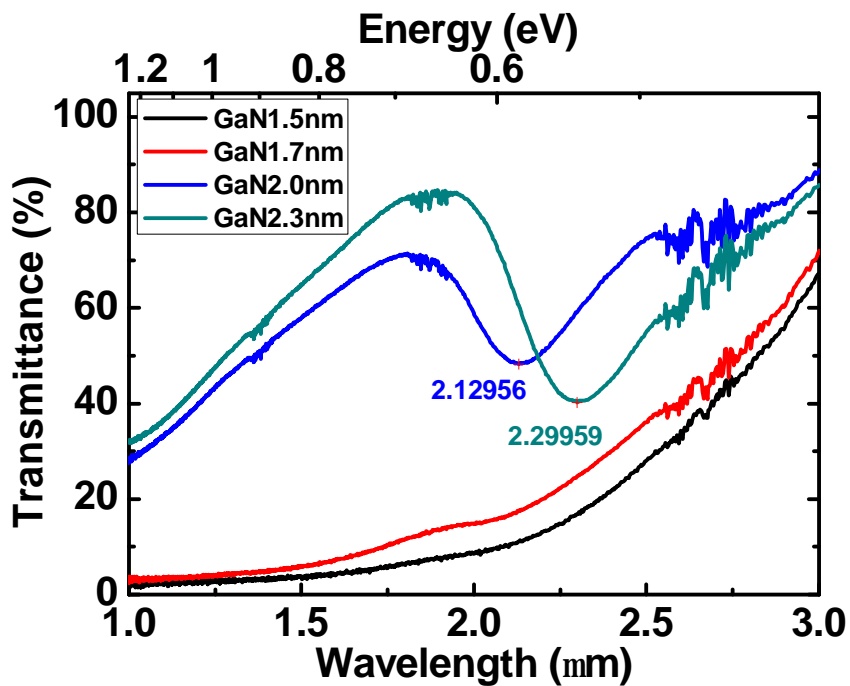
Fig. 3.4 Transmittances of p-polarized light in GaN/AlN MQWs grown at 950 ℃ on AlN buffers using GaN interlayer. The thickness of AlN barrier was 2.0 nm and varied GaN well thickness

There are some remarkable points from the above figure including:

- Compared with the conventional MOVPE grown sample which had similar MQWs structure, the intersubband transition of pulse injection grown MQWs were noticeably shifted to shorter wavelengths. This is due to the improvement of GaN/AlN abruptness and the resultant thinner graded interface layer by low temperature growth (950 ℃ in this experiment).

- Pulse injection method has been proved to be an effective method for growing good n-doped GaN for MQWs at low temperature.

- The shortest intersubband transition wavelength in the experiment was 2.1 μm and could not be further shifted to a shorter wavelength by only changing the GaN well width.

- Interlayer showed a potential to adjust the strain in GaN/AlN MQWs which the intersubband transition properties were remarkably improved compared with the sample without interlayer.

With the above discussions, it seems that two key factors for realizing 1.5-μm-range intersubband transition are (1) the growth temperature which can be lowered than 950 ℃ to obtain more abrupt interface (thin graded interface layer) and (2) the strain in GaN/AlN which can be tailored by an interlayer. By considering these two parameters, a MQWs sample was fabricated at 920 ℃ using AlGaN interlayer with Al-content about 0.3. Figure 3.5(a) show XRD (0002) 2θ-ω scan of this sample. Obviously, the quality of GaN/AlN MQWs was very tremendous. XRD scan showed not only high order and sharp satellite peaks from -5th to +3rd order but also strong MQWs peaks intensity comparable with that of AlN buffer. Moreover, in Fig. 3.5(b), this sample demonstrated an intersubband transition wavelength at 1.64-μm which is the first one that can break through the limitation at 2.0 μm. This intersubband absorption peak can be fitted with 3 Lorentz curves indicating effective grade layer thickness of approximately 3 monolayers (ML) [71]. Hence, of the most interesting factors, the growth temperature and AlGaN interlayer have been intensively studied. Before that, in the next section, some essential calculation methods and useful equations for analyzing MQWs structure are first given in details.
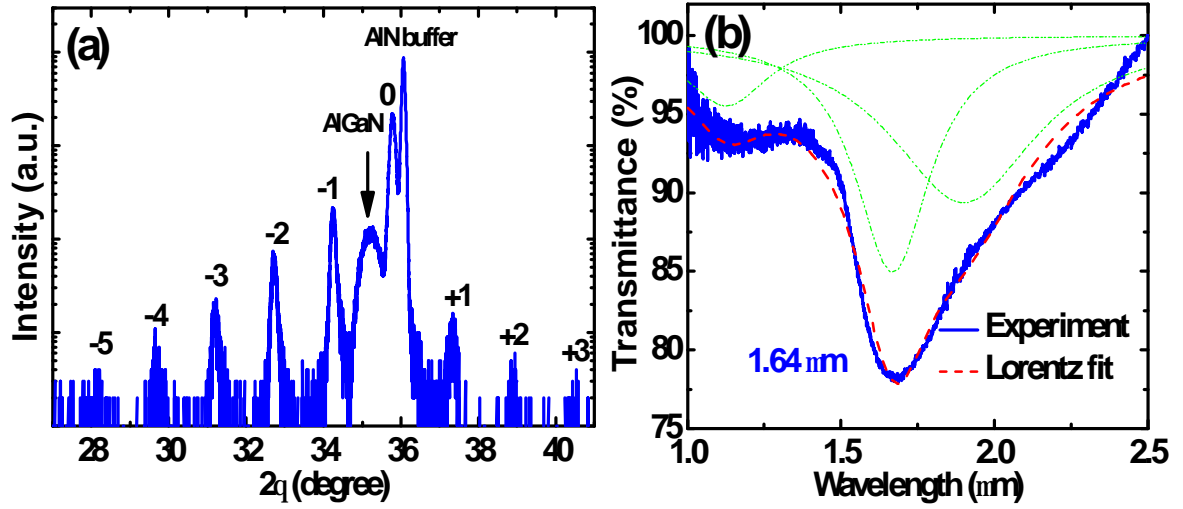
Fig. 3.5 (a) (0002) 2θ-ω XRD pattern of 40-period GaN (1.4 nm)/AlN (4.3 nm) MQWs on AlN buffer with an AlGaN interlayer and (b) transmittance of p-polarized light and Lorentz fitting

3.3   Calculation of Al-content in AlGaN and Strain in GaN/AlN MQWs

In this section, the essential equations and calculation method for determining Al-contents as well as strains in AlGaN interlayer and MQWs are given in details. 2θ-ω symmetrical scans and a reciprocal space mapping by high-resolution XRD (Philips X'pert, CuKa₁ radiation, l =0.1514 nm) were used to study the structure properties. A 2θ-ω symmetrical scan (0002) for a 40-period MQWs sample is shown in Fig. 3.6(a). One diffraction peak, between the AlN buffer (2θ= 36.067) and Al$_x$Ga$_{1-x}$N (2θ=34.951) peaks, due to the MQWs structure, is marked as the zero-order (0th) superlattice peak. The fifth-order (-1th) to third-order (+3rd) satellite peaks are also clearly found in the figure. The average thickness, t , for one period in the MQWs is obtained by [87]:

$$t = \frac{(m-n)\,l\,/2}{\sin q_m - \sin q_n} \qquad (3\text{-}1)$$

where l , m (n) and q_m (q_n) are the wavelength of CuKa₁ radiation, the satellite peak order and the satellite peak angle position, respectively. Thus, the average thickness of 1-period GaN/AlN MQWs, $t_{AlN} + t_{GaN}$, is calculated to be 5.70 nm. In order to gain more information, especially

about the in-plain crystal lattice a and compositions of the grown layers, a reciprocal space mapping around the AlN (10-15) plane was obtained by XRD. The result for the 40-period sample, after converting to reciprocal lattice units, is shown in Fig. 3.6(b). The strained lattice parameters, of both MQWs and interlayers, can be calculated from [88]:

$$Q_x = \frac{\sqrt{\frac{4}{3}\left(h^2 + hk + k^2\right)}}{a} = \frac{\left[\cos w_{10\bar{1}5} - \cos(2q_{10\bar{1}5} - w_{10\bar{1}5})\right] - \left[\cos w_{0002} - \cos(2q_{0002} - w_{0002})\right]}{l} \tag{3-2}$$

$$Q_y = \frac{l}{c} = \frac{\sin w_{0002} + \sin(2q_{0002} - w_{0002})}{l} \tag{3-3}$$

where Q_x and Q_y are the in-plane and out-of-plane components of the reciprocal lattice vector given in r.l.u. (reciprocal lattice unit), respectively. Therefore, the strained lattice parameters for $Al_xGa_{1-x}N$ are a_{AlGaN} = 0.3115 nm and c_{AlGaN} = 0.5140 nm. The Al-content, x_{Al}, can be determined by:

$$\frac{c_x - c_0}{c_0} = -2u\frac{a_x - a_0}{a_0} \tag{3-4}$$

where a_0, c_0 and u are the unstrained $Al_xGa_{1-x}N$ lattice parameters. Poisson's ratio, u, for $Al_xGa_{1-x}N$ is linearly interpolated between u_{GaN} =0.19 and u_{AlN} =0.3 [89,90]. Therefore, the Al-composition of $Al_xGa_{1-x}N$ layer is calculated to be 37.8%. By representing the MQWs structure with one $Al_xGa_{1-x}N$ layer, the average lattice parameters for the MQWs are calculated to be a_{MQW} =0.3129 nm and c_{MQW} =0.5011 nm from Eq. 3-2 and 3-3. Therefore, again using Eq. 3-4, the average Al-content for the MQWs is 82.2%. From Eq. 3-1, the average period thickness is known to be 5.70 nm, and then the GaN and AlN layer thicknesses could be calculated to be 1.01 and 4.69 nm, respectively. In addition, the layer strain values, S, defined by:

$$S = \frac{a - a_0}{a_0} \tag{3-5}$$

where a is the strained layer lattice parameter, a_0 is the bulk lattice parameter of layer, gives S_{GaN} =-1.88% and S_{AlN} =0.55% for the MQW layers. The sign plus (+) and minus (-) denote tensile and compressive strain, respectively.
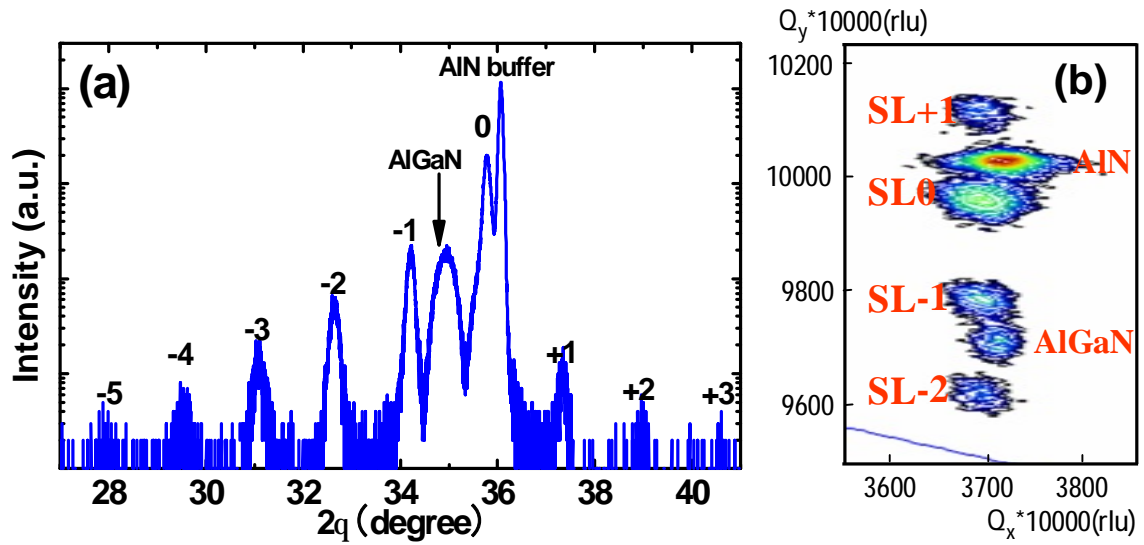
Fig. 3.6 (a) XRD (0002) 2θ-ω scan and (b) (10-15) RSM scan of a GaN/AlN MQWs
on AlN buffer with an AlGaN interlayer, r.l.u. is reciprocal lattice unit

3.4 Effects of Growth Temperature on MQWs Grown by Pulse Injection Method

In this section, one of two key parameters, the growth temperature of GaN/AlN MQWs has been investigated at 710, 740, 770, 800, 830, 860, 890 and 920°C by using pulse method. The investigated structure is again shown in Fig. 3.3(a). First, 0.5-μm thick AlN buffers were grown at 1175°C, 50 mbar, V/III=260, followed by 0.1-μm thick AlGaN interlayers grown at 1150°C, 100 mbar, V/III=1700, for all samples. Then, the growth temperatures were ramped down to the desired values, at reactor pressure of 50 mbar, and 40-period of GaN/AlN MQWs were deposited with pulse injection method which described in Fig. 3.3(b). V/III ratios during the growth of GaN well and AlN barrier were 5000 and 3000, respectively. After growth, the samples were evaluated using XRD, AFM and measured intersubband transition by FTIR. Let us consider the XRD (0002) 2θ-ω scans of each MQWs samples in Fig. 3.7. Clearly, GaN/AlN MQWs with excellent quality can be deposited at low temperature, especially at 800-860°C range, evidenced by the existence of high order satellite peaks (-5th to +3rd order) and their shape. This indicates that the abruptness of GaN/AlN interface is better at lower growth temperature.

41

However, once the growth temperature is too low, the uniformity of MQWs as well as the crystal quality of epitaxial layers dramatically drops due to short surface migration of adatoms. In addition, an ineffective chemical reaction is also though as a cause since NH_3, group V source, cannot well deform at low temperature. The MQWs grown at 710˚C, for example, exhibits poor quality as shown in Fig. 3.7. The (10-15) RSM scans of each sample are shown in Fig. 3.8. It is noted that good satellite peaks (denoted by numbers) can be observed in the samples grown at 800-860˚C agreeing with (0002) 2θ-ω scans. The samples grown at 710-770˚C had unclear -2nd and +1st order satellite peaks resulted from low MQWs quality as described before. By using the calculation procedures as described in section 3.3, the information of MQWs structures can be evaluated. The average GaN well and AlN barrier thicknesses for all samples could be determined to be 1.13±0.06 and 4.72±0.25 nm, respectively. The averages Al-content in AlGaN interlayer and in MQWs were 0.3 and 0.8, respectively. The transmittance spectra of p-polarized light in each sample are comparatively shown in Fig. 3.9. We can observe that intersubband transition wavelengths are blue-shifted with decreasing the growth temperature.
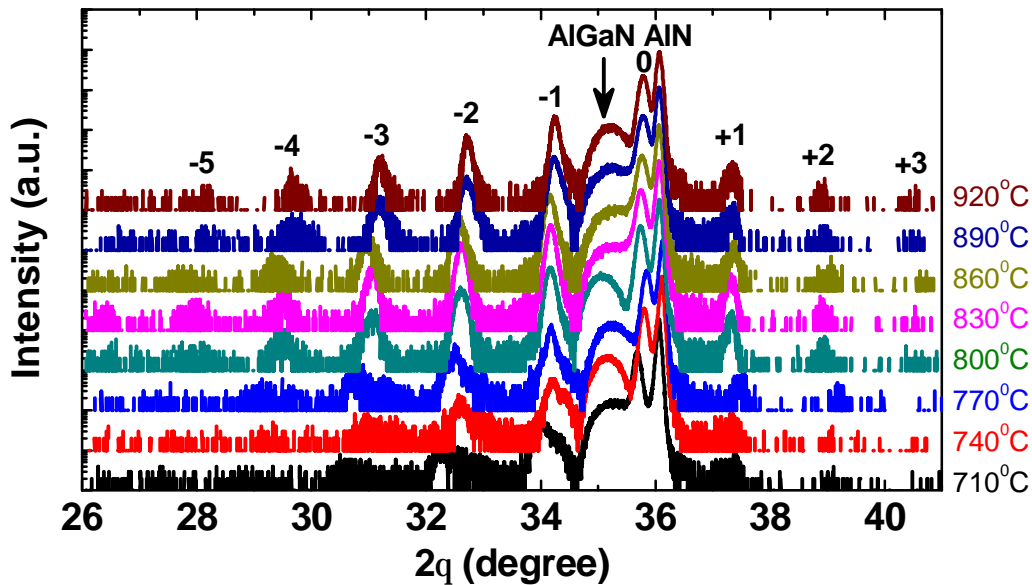
Fig. 3.7 XRD (0002) 2θ-ω scans of GaN/AlN MQWs grown at different temperatures on AlN buffers with $Al_{0.3}Ga_{0.7}N$ interlayer
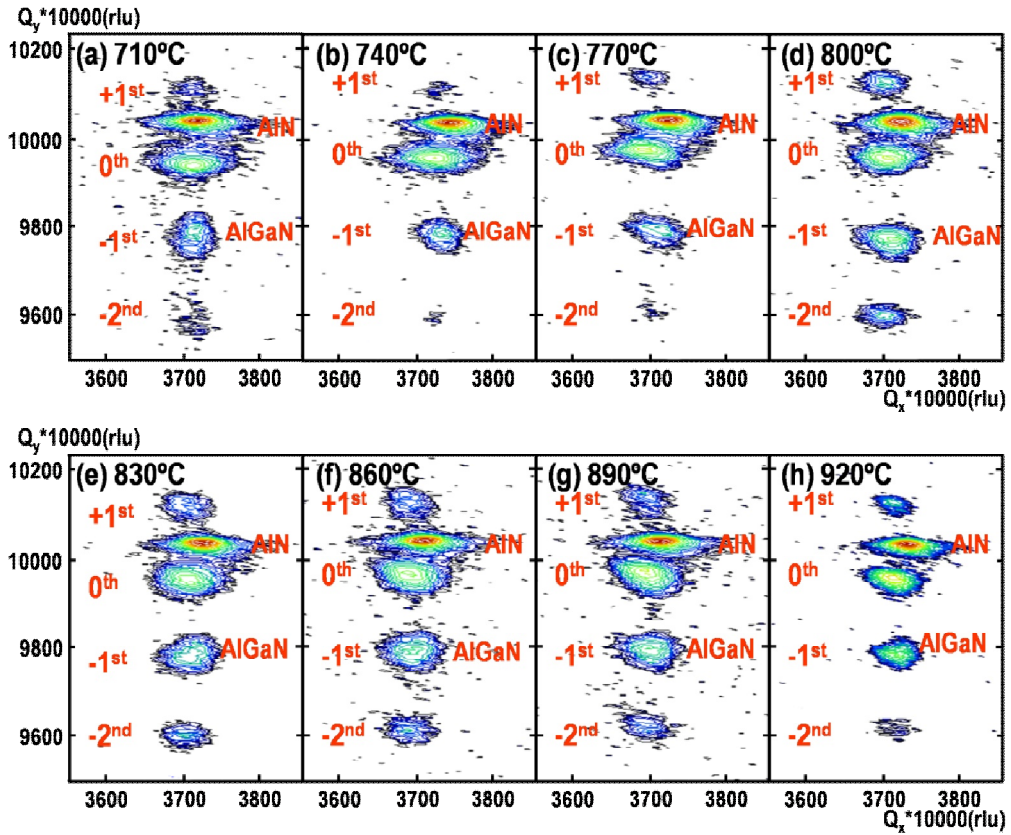
Fig. 3.8 (10-15) RSM scans of GaN/AlN MQWs grown at different
temperatures on AlN buffers with $Al_{0.3}Ga_{0.7}N$ interlayer

In order to explain the origin of blue-shift, the strain in GaN well and AlN barrier were calculated using Eq. 3-5. The intersubband transition wavelength, full-width at half-maximum (FWHM) of transition peaks and the strain in MQWs are plotted in Fig. 3.10(a) as 3.10(b) as functions of growth temperature.

First, considering the dependency of strain on the growth temperature in Fig. 3.10(b), since the substrates were AlN which has smaller lattice constants compared to that of GaN, the GaN layers in MQWs would be grown under compressive strain condition. At low temperature, the diffusion length of atoms and activity in epitaxial layers are limited by their low kinetic energy. Therefore, with the limitation of relaxation mechanism, the GaN epilayers grown at low temperature will more strain than that grown at high temperature. Strain in AlN can be inversely described, i.e. the AlN layers will more relax at lower temperature growth.
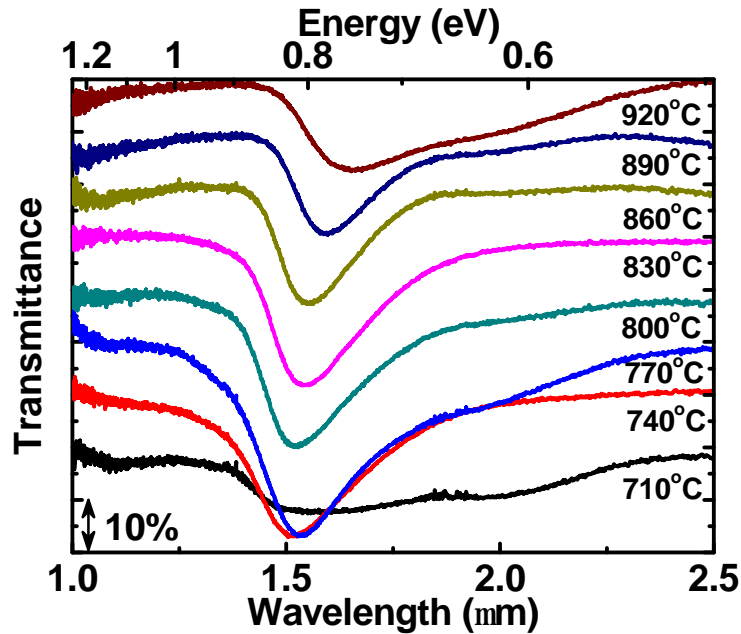
Fig. 3.9 Transmittance spectra of GaN/AlN MQWs grown at different

temperatures on AlN buffers with $Al_{0.3}Ga_{0.7}N$ interlayer

Focusing on the origin of the blue-shift of intersubband transition wavelength, S. Nicolay et al. [49] reported that strain in AlN barrier induces non-abrupt GaN/AlN interfaces in MQWs systems. Recalling from Fig 3.10(b), we can see that AlN layers trend to be more relaxed at low temperature. Therefore, it can be logically inferred that, not only due to the improvement of interdiffusion issue at low growth temperature, but interface between GaN/AlN is also improved by the relaxation in AlN layers. As a result, the thickness of non-abrupt region becomes thinner and shifts the intersubband transition to a shorter wavelength. This is clearly supported by the simulation of intersubband transition wavelength in GaN/AlN MQWs using a self-consistent Schrödinger-Poisson equation [91-93] implemented with effects of piezoelectric field [8, 94-96], strain in GaN/AlN MQWs [97-98], non-parabolicity [99-100] and non-abrupt interface (see Appendix B). As can see that, by fixing the non-abrupt interface thickness at 2.75 monolayer (ML) and using the thicknesses of GaN wells and AlN barriers evaluated from XRD measurements, the calculation results in Fig. 3.11 do not fit or even have a tendency with the experiment data. It is implied that only the thickness and the strain of GaN/AlN MQWs could not explain the tendency or determine the intersubband transition wavelength. In fact, when the

44

thickness of GaN wells becomes small, the effect of the non-abrupt region or graded interface becomes larger. It can be simply state that, the strain and relaxation in GaN/AlN MQWs affect on the abruptness of GaN and AlN interface and the thickness of resultant non-abrupt interface determines the intersubband transition wavelength. The dependency of intersubband transition wavelength on the thickness of graded interface in GaN/AlN (1.15 nm/4.50 nm) MQWs is plotted in Fig. 3.12.
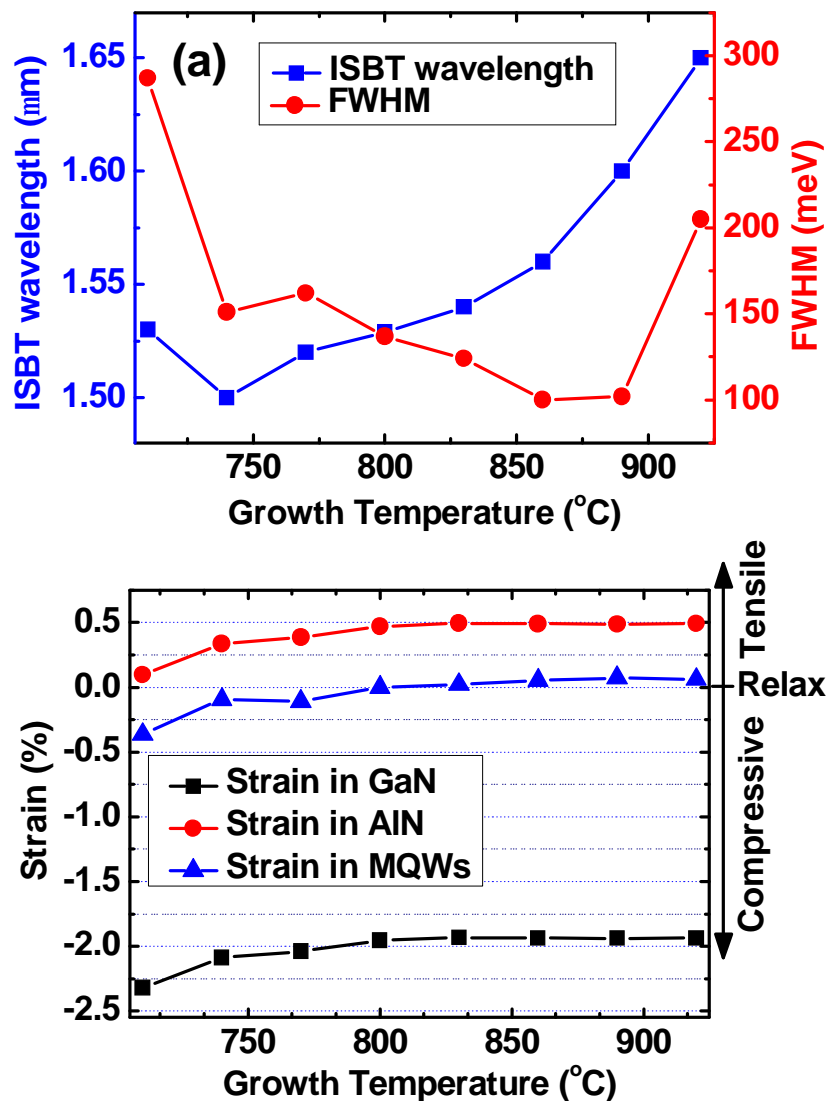
Fig. 3.10 Dependencies of (a) intersubband transition wavelength, FWHM of intersubband transition peak, and (b) strain in GaN wells, AlN barriers and MQWs on the growth temperature on MQWs

The FWHM of an absorption peak which attributes to the uniformity and surfactant of GaN/AlN MQWs had the least value at the growth temperature around 860 ℃ (Fig. 3.10(a)). This can also be explained by the improvement of GaN/AlN interface owing to low temperature and strain in AlN layers. However, at the growth temperature lower than 800 ℃, the crystal quality and the uniformity of MQWs became worse because of poor surface migrations that have more effects than the abruptness of MQWs which is improved at low temperature.

This experiment has proved the necessary of low temperature growth GaN/AlN MQWs for achieving short intersubband transition. The optimized temperature in this work was around 800-860˚C where the quality of GaN/AlN MQWs was the utmost.
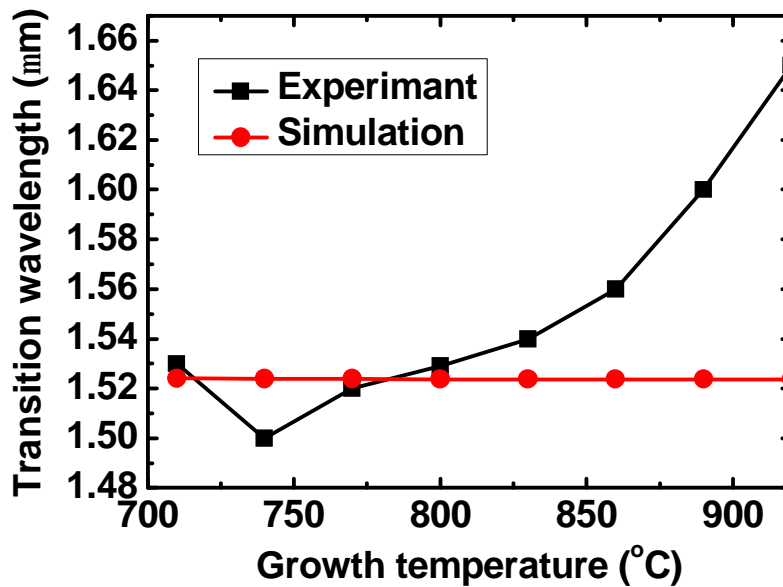
Fig. 3.11 Comparison between experiment and simulation data of the study of the temperature effects on intersubband transition wavelength. The calculation was performed fixing 2.75-ML thick of non-abrupt interface.
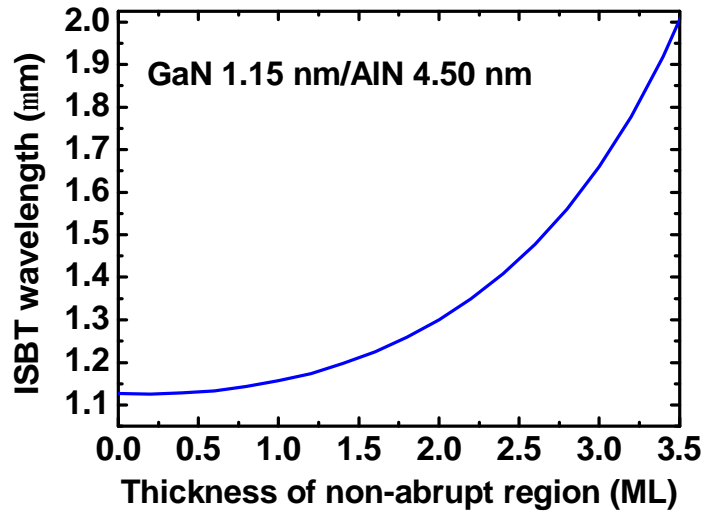
Fig. 3.12 The dependency of intersubband transition wavelength on the thickness of non-abrupt region

3.5 Effects of Al-content in AlGaN Interlayer on MQWs Grown by Pulse Injection Method

According to the previous experiment, the best temperature range for growing a high quality GaN/AlN MQWs by pulse injection method in the view point of abruptness of MQWs, crystal quality, intersubband transition wavelength and FWHM of intersubband transition peak has been proved to be around 800-860°C. Therefore, all of GaN/AlN MQWs in this section were grown at 830°C using different Al-content in AlGaN interlayer. The investigate structure is shown in Fig. 3.3(a) using the pulse injection growth method shown in Fig. 3.3(b). First, 0.5-μm thick AlN buffers were grown on 2-side c-plane sapphire at 1175°C, 50 mbar with V/III of 260. Next, 0.1-μm AlGaN interlayers were grown at 1150°C, 100 mbar. The Al-content in AlGaN layers (x_{Al}) were varied from 0 (GaN) to 1 (AlN) by adjusting the partial pressures of TMG and TMA gases. Note that, in the case of x_{Al} =1 (AlN), GaN/AlN MQWs was directly deposited on an AlN buffer layer, i.e. no interlayer. After that, 40-period GaN/AlN MQWs were grown at 830°C, 50 mbar using V/III of 5000 and 3000 during the GaN well and AlN barrier deposition, respectively. Similar to the previous section, XRD (0002) 2θ-ω and (10-15) RSM scans were

preformed to collect information from the MQWs and their lattice parameters were calculated using the methods in section 3.3. The intersubband transition characteristics were evaluated by FTIR at room temperature using multiple reflection method.

The comparison of XRD (0002) 2θ-ω scans of each sample is shown in Fig. 3.13. Most of GaN/AlN MQWs, except for the one which was grown on GaN interlayer (x_{Al}=0), showed the excellent quality so that satellite peaks from -5th to +3rd order could be clearly observed along with peaks of AlN buffer and AlGaN interlayer. The average Al-content in GaN/AlN MQWs was estimated by Eq. 3-4 to be approximately 0.8 for all samples. By Al-content and angular distance between satellite peaks of MQWs, the thicknesses of GaN wells and AlN barriers for all samples were estimated to be around 1.15±0.08 nm and 4.80±0.09 nm, respectively. Fig. 3.14 shows the RSM scans over AlN (10-15) plane of each sample. It agrees with the (0002) 2θ-ω scan in Fig. 3.13 that the quality of GaN/AlN MQWs grown on GaN interlayer was very poor evidenced by the relatively large satellite peaks' spots compared with that of the rest. While the samples deposited on AlGaN show good XRD pattern both (0002) 2θ-ω and (10-15) RSM scans, the sample grown without interlayer, x_{Al}=1, has excellent (0002) 2θ-ω scan but broad satellite peaks in (10-15) RSM scan. This indicated that the GaN/AlN MQWs grown without interlayer was gradually relaxation in the course of the growth of MQWs.
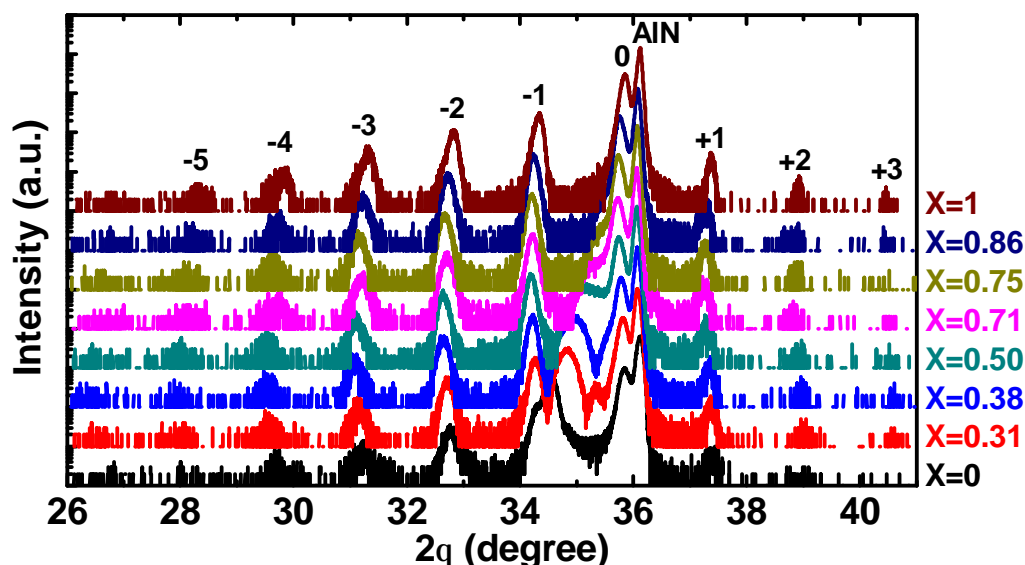
Fig. 3.13 XRD (0002) 2θ-ω scans of GaN/AlN MQWs grown at 830 ℃ on
AlN buffers with varied Al-content in AlGaN interlayer
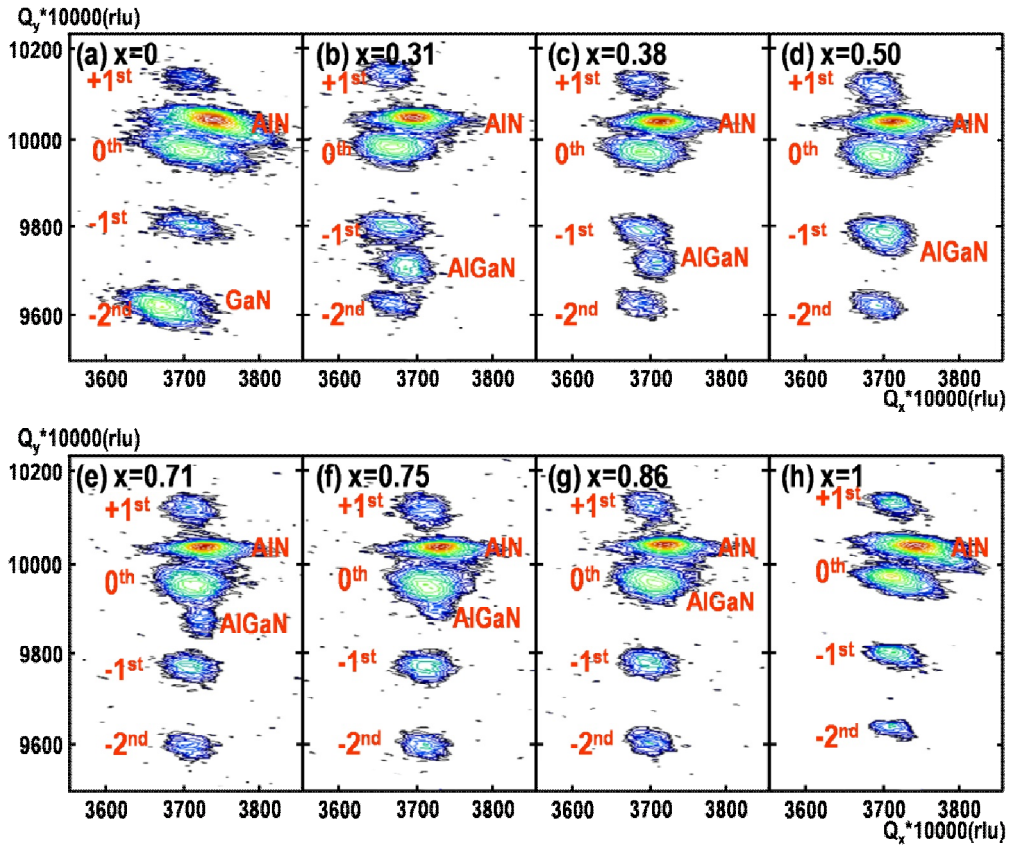
Fig. 3.14 (10-15) RSM scans of GaN/AlN MQWs grown at 830 ℃ on AlN
buffers with varied Al-content in AlGaN interlayer

The transmittance spectra of each sample are given in Fig. 3.15. We can observe that MQWs grown on GaN interlayer had no intersubband transition peak but only broad absorption because of its poor quality. The intersubband transitions were more clearly seen with the increasing of Al-content in AlGaN interlayer. The sample directly grown on AlN buffer also has no intersubband transition peaks although the XRD (0002) 2θ-ω scan was the most excellent. Because of the improvement of MQWs structure and the existence of intersubband transition, AlGaN interlayer has been proved to be necessary to achieve strong 1.5-μm range intersubband transition in GaN/AlN MQWs.
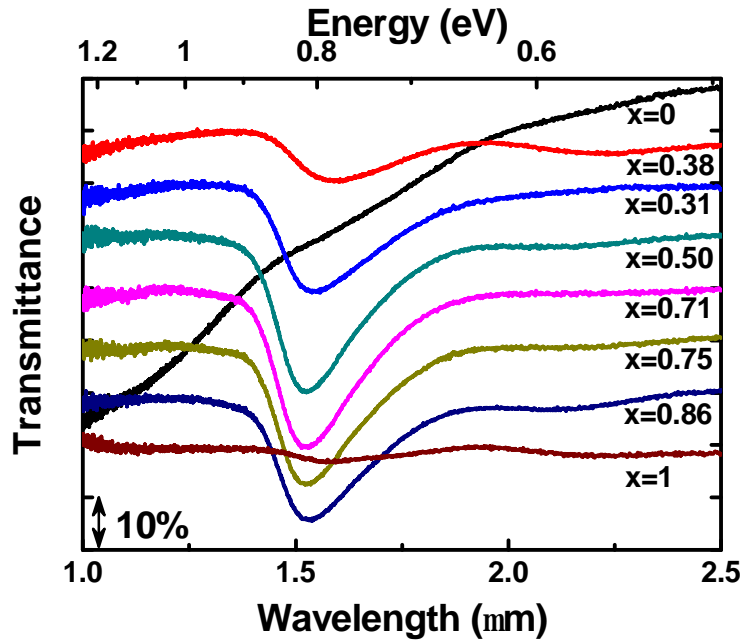
Fig. 3.15 Transmittance spectra of GaN/AlN MQWs grown at 830 ℃ on AlN
buffers with varied Al-content in AlGaN interlayer

In order to clarify the effects of Al-content in AlGaN interlayer, the dependencies of intersubband transition wavelength, FWHM of intersubband transition peak and strain in GaN well and AlN barrier are plotted as functions of Al-content as shown in Fig. 3.16(a) and 3.16(b). Obviously, all of them have similar parabolic dependency with the Al-content in AlGaN. First, let us focus on the left-hand side of Fig. 3.16(a) where $0 < x_{Al} < 0.7$. Since the lattice parameters of an AlGaN interlayer were smaller with an increased value of x_{Al}, the MQWs (x_{Al}=0.8) which were grown on Al-rich AlGaN would be grown with more compressive strain than that on Ga-rich AlGaN interlayer. The estimated compressive strain in GaN well increased while AlN barrier more relaxed when x_{Al} was raised from 0 to 0.7 as shown in Fig. 3.16(b). As described in the previous experiment that strain in AlN can induce surface instability and cause non-abrupt GaN/AlN interface. Thus, with the increase of x_{Al} from 0 to 0.7, the abruptness of MQWs could be improved and the intersubband transition wavelength was blue-shifted because the thickness of non-abrupt region was diminished. This better GaN/AlN interface was also favorable for the FWHM of intersubband transition peaks in which the FWHM was smaller when x_{Al} was

increased from 0 to 0.7. The shortest intersubband transition wavelength and the smallest FWHM value were achieved in the MQWs grown on AlGaN with Al-content around 0.7 where the GaN well was the most compressive strained and AlN barrier was the most relaxed.
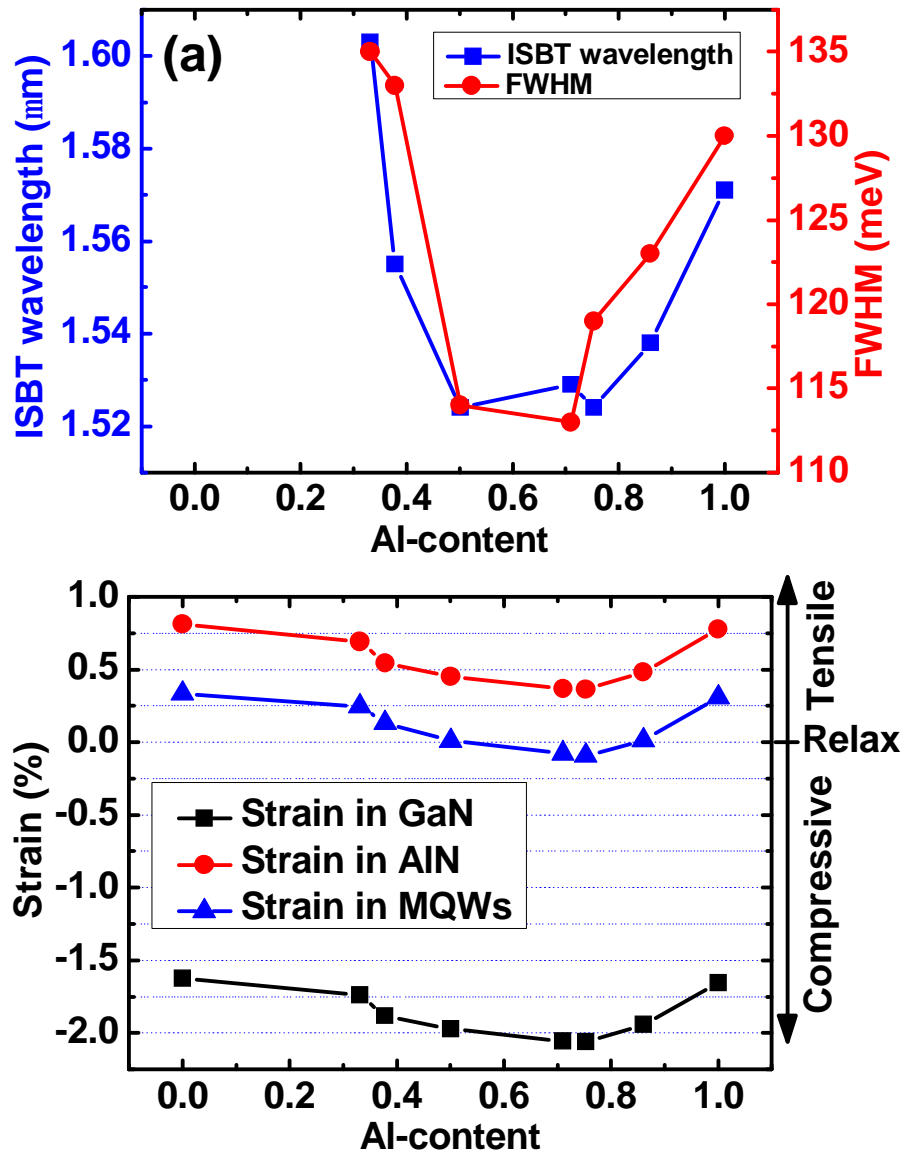
Fig. 3.16 Dependencies of (a) intersubband transition wavelength, FWHM of intersubband transition peak, and (b) strain in GaN wells, AlN barriers and MQWs on the Al-content in AlGaN interlayer

Although larger compressive strain in GaN wells is preferred, the strain management is not straightforward. Focusing on the range x_{Al} >0.8, the strain in GaN well layers rebounded to relaxed state instead of increasing toward more strained state, indicating that excess strain in GaN wells led to gradual relaxation in the course of the growth of MQWs. The MQWs sample grown on AlN buffer without interlayer was non-uniform, having gradual in-plane relaxation, resulting in broad and weak intersubband transition at a longer wavelength. This fact was supported by broad satellite peaks in Q_x direction (parallel to the surface) in Fig. 3.14(h).

In this experiment, the excellent intersubband transition properties had been achieved in the MQWs which have more relaxation in the AlN barrier rather than the MQWs with strained AlN. The Al content in the interlayer to realize this situation is not simply determined by the average Al content in the MQWs. The most relaxed AlN barrier was achieved with the AlGaN interlayer which had x_{Al} of approximately 0.7, which is a little bit smaller than the average x_{Al} of the MQWs.

3.6 Effects of Reactor Pressure during the Growth of GaN/AlN MQWs by Pulse Injection Method

At this point, the growth temperature of GaN/AlN MQWs and Al-content in AlGaN interlayer have already been investigated and optimized for a strong intersubband transition with a sharp FWHM at 1.5-μm range. In this section, the reactor pressure during the growth of MQWs has been studied in order to investigate its effects on the intersubband transition characteristics. The MQWs structure and the pulse injection sequence are, once again, shown in Fig. 3.3(a) and 3.3(b). First, 0.5-μm-thick AlN buffer layers were grown using conventional MOVPE at 1175 ℃, 50 mbar. Then, the growth of 0.1-μm-thick AlGaN interlayers was carried out at 1150 ℃, 100 mbar. The Al-content of AlGaN interlayer was designed to be a slightly lower than that of MQWs. For the growth of GaN/AlN MQWs, according to the study in section 3.4, the reactor temperature was 830 ℃. The effects of reactor pressure were investigated at 50 and 100 mbar. The other growth parameters were controlled and same for each growth. After the MQWs deposition, the samples were evaluated by XRD (0002) 2θ-ω and (10-15) RSM scans and the results are shown in Fig. 3.17 and 3.18. By using the calculation methods in section 3.3, the GaN

well and AlN barrier width of the MQWs grown at 50 and 100 mbar were estimated about 1.14 nm/4.86 nm and 1.21 nm/3.04 nm, respectively. The increasing of reactor pressure enhanced the GaN growth rate but decreased AlN growth rate. From Fig. 3.17, although the high order of satellite peaks could not be observed in the sample grown at 100 mbar due to the average thickness of 1-period QW became thinner, the other satellite peaks were very sharp and strong indicating good GaN/AlN interface and uniformity. The satellite peak spots of these two samples shown in Fig. 3.18 had similar width in both Q_x and Q_y -directions explaining that the uniformity and the relaxation of both MQWs were similar. Fig. 3.19 reveals the transmittance spectra of p-polarized light in the MQWs. We can clearly see that, the absorption rate of the sample grown at 100 mbar was almost twice as stronger than that of the other. The reasonable explanation is, at 100 mbar, the partial pressure of SiH_4 was doubled with the same V/III ratio. It means that the amount of Si atoms incorporating to GaN layers was also 2 times larger when the reactor pressure was doubled. With greater electron population in ground subband, the absorption rate by intersubband transition was also increased. In the view point of optical device fabrication, this study is very promising since it is possible to downsize the dimension of device without sacrificing the intersubband transition properties.
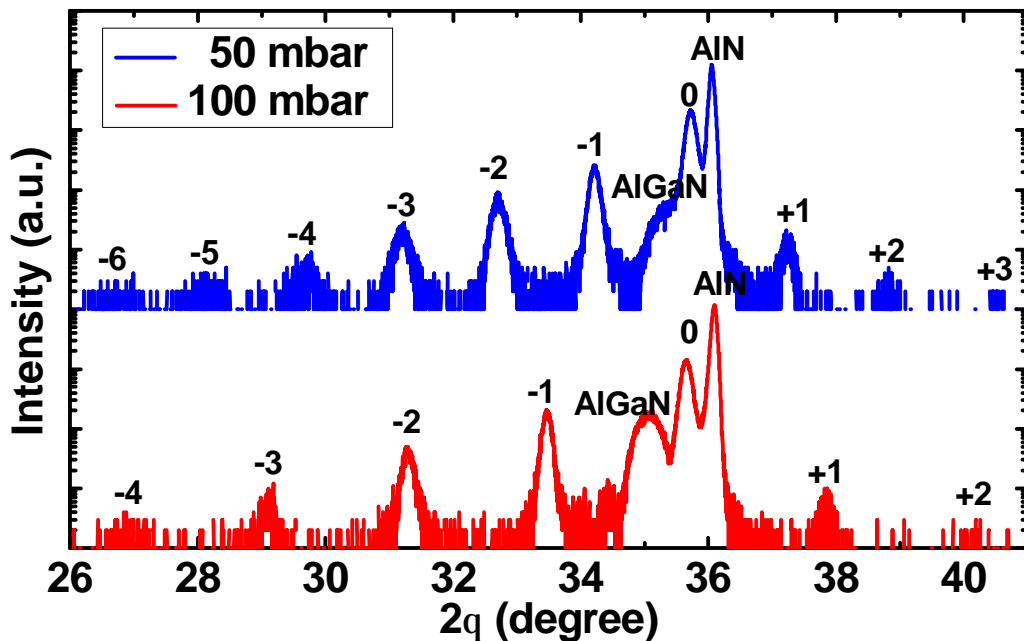
Fig. 3.17 XRD (0002) 2θ-ω scans of the GaN/AlN MQWs grown at 50 and 100 mbar
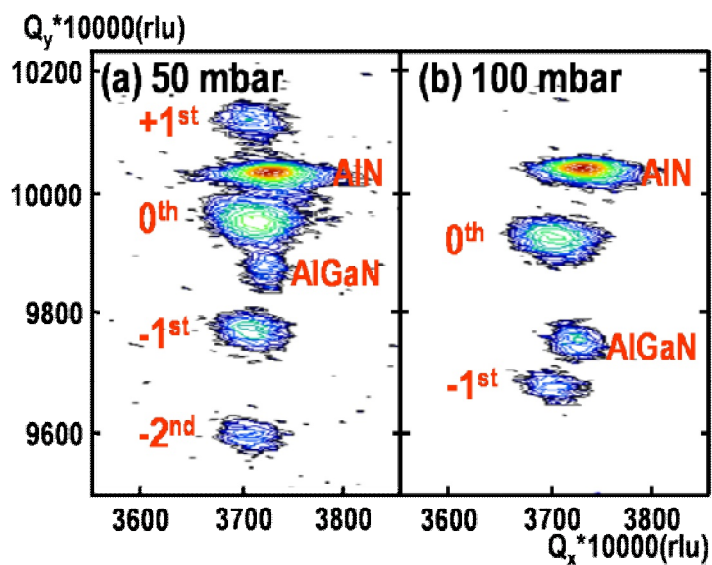
Fig. 3.18 (10-15) RSM scans of the MQWs grown at (a) 50 mbar and (b) 100 mbar
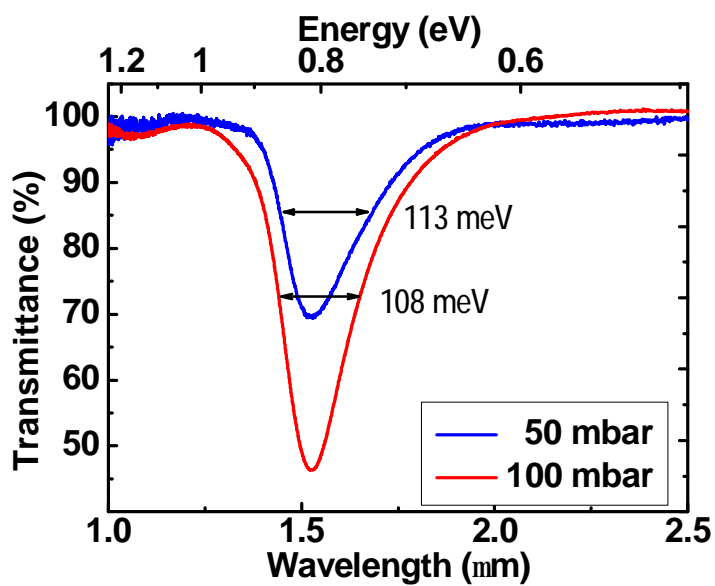
Fig. 3.19 Transmittance spectra of the GaN/AlN MQWs grown at 50 and 100 mbar

3.7 Conclusions

In this chapter, the pulse injection method has been proved to be a very effective method for the growth of GaN/AlN MQWs at low temperature. The intersubband transition at 1.5-µm-range has been achieved owing to the low temperature growth using pulse injection method and the strain management using AlGaN interlayer. The growth parameters of GaN/AlN MQWs have been investigated for the purpose of understanding their effects on the intersubband transition properties and optimizing the condition for a strong intersubband transition with small FWHM peak at 1.5-µm-range.

1. The abruptness of GaN/AlN MQWs is improved at low growth temperature but the uniformity of MQWs also becomes worse at extremely low temperature. The thickness of non-abrupt region determines the intersubband transition wavelength in which the thinner the non-abrupt region is, the shorter the intersubband transition wavelength becomes. The FWHM is controlled by the abruptness and the uniformity which is attributed to the growth temperature. The optimized growth temperature in this work is around 800-860 ℃.

2. The Al-content in AlGaN affects on the strain level in MQWs. The relaxation in AlN layer is preferred since the strain in AlN induces the surface instability and non-abrupt GaN/AlN interface. Al-content of AlGaN layer which is slightly lower that of MQWs is favorable for the shortest intersubband transition wavelength and the smallest FWHM value.

3. By doubling the reactor pressure, the absorption rate by intersubband transition becomes almost twice as stronger because of greater carrier concentration.

The behavior of intersubband transition wavelength in GaN/AlN MQWs has been explained by the simulation using a self-consistent Schrödinger-Poisson equation. It has been found that, in a GaN/AlN MQWs with thin GaN wells, the effects of non-abrupt interface (graded interface) becomes crucial as it determines the intersubband transition wavelength.

Chapter 4 Optimization of MQWs Structure for Fabrication of AlN Waveguide with GaN/AlN MQWs Core

T he achievement of 1.5-µm-range intersubband transition with a strong and small FWHM peaks in the last chapter has promoted the fabrication of optical devices using AlN waveguide (WG) with GaN/AlN MQWs active core. In this work, silicon nitride films (SiN, Si_3N_4) has been used as a waveguide cladding material. In section 4.1, the deposition of Si_3N_4 for the purpose of using as waveguide cladding material is discussed. The requirement of AlN upper cladding layer in order to compensate the effect of induced tensile strain from Si_3N_4 cladding is explained in section 4.2. After that, in section 4.3, the growth conditions of AlN upper cladding layer have been investigated and optimized for the best intersubband transition properties in the underneath GaN/AlN MQWs. In the last section, 4.4, the conclusion of this chapter is given.

4.1   Using of Si_3N_4 as a Material for Waveguide Cladding

As described in the previous chapters that the key parameters of short intersubband transition wavelength in MOVPE grown GaN/AlN MQWs are the low temperature growth and the AlGaN interlayers. Because of these proposes, the abruptness and the uniformity of GaN/AlN interface can be enhanced to the utmost and short intersubband transition wavelength can be realized. Considering the optical devices using AlN waveguide with GaN/AlN active core, it is necessary that GaN/AlN MQWs have to be embedded in semiconductors or dielectric materials, called cladding layers, in order to confine the light within the MQWs structures. The

choices of appropriated materials are limited by the refractive index of material and the fabrication process. It is strongly suggest that, to avoid the degradation of GaN/AlN MQWs by the thermal process, the fabrication of cladding layer should be performed at temperature lower than or at least equal to the growth temperature of MQWs. Therefore, there are few materials that can be used as cladding layers for AlN waveguide including low-temperature-grown AlN, low-temperature-grown GaN, silicondioxide (SiO_2), silicon nitride (Si_3N_4) and silicon oxidenitride (SiO_xN_y). Although the pulse injection method allows the growth of good-quality bulk AlN and GaN layer at low temperature, this process requires remarkably large amount of resources and the deposition rate is extremely slow [79-83]. Among these materials, Si_3N_4, are used in numerous applications such as gate dielectric in thin film transistors, as oxidation mask for selective oxidation of silicon, and as passivation and protection barrier layer [101-103]. Moreover, considering its refractive index of 1.85 and dielectric constant 10 [104], Si_3N_4 is one of the most appropriate material of waveguide fabrication. Several demonstrations of the use of Si_3N_4 films in nitride semiconductors waveguide have been reported [47,86]. Sputtered silicon nitride films are also used, for example, in magneto-optical storage disks where low process temperatures are essential to avoid damage of the polycarbonate substrate. Substoichiometric semi-insulating silicon nitride films could be used for similar applications as silicon rich oxide films [105]. Silicon nitride films are commonly made by CVD processes. These films contain relative high amounts of hydrogen which can lead to degradation of films in subsequent high temperature processing steps [106]. Therefore, sputtering of silicon nitride is an interesting technique for all applications where low process temperatures are desired [107], where the hydrogen content of the films should be low [107,108] or where the stoichiometry of the films should be controlled [109,110]. In particular, an RF magnetron sputtering is suited, because it allows for high deposition rates and is an industrial technique for large area applications. Considering the above advantages of sputtered Si_3N_4 layers:

- Refractive index of Si_3N_4 (~1.85@1.55μm) [111] which is match and a little bit lower than that of GaN (2.335@1.55μm) [112] and AlN (2.031@1.55μm) [112] allows the high efficiency optical coupling in AlN waveguide.

- Fabrication process can be performed at relatively low temperature or even at room temperature.

- Simple fabrication process, consume less resources.

- Low propagation loss at 1.5-μm range wavelength.

It is highly suggested to use sputtered Si_3N_4 for the fabrication of optical device based on AlN waveguide.

4.1.1 Si₃N₄ Fabricated by RF Magnetron Sputtering

All of Si_3N_4 films in this works were prepared in a ULVAC MNS 2000-RF sputter machine. The process chamber was equipped with an RF sputter magnetron with silicon targets. The base pressure in the chamber, which was pumped by a turbo-pump, was 1.5×10^{-4} mbar. Typical sputter conditions for the Si_3N_4 layers are: RF-power: 200 W; sputtering gas pressure: 0.70 Pa; argon flow: 15 sccm; nitrogen flow: 5 sccm; temperature: 250 ℃; deposition rate: 800 nm/h. The schematic of sputtering system is shown in Fig. 4.1. Optical properties of sputtered Si_3N_4 were evaluated by ellipsometry for the investigation of the refractive index and extinction coefficient by T. Shimizu [111]. The results were shown as functions of wavelength in Fig. 4.2.
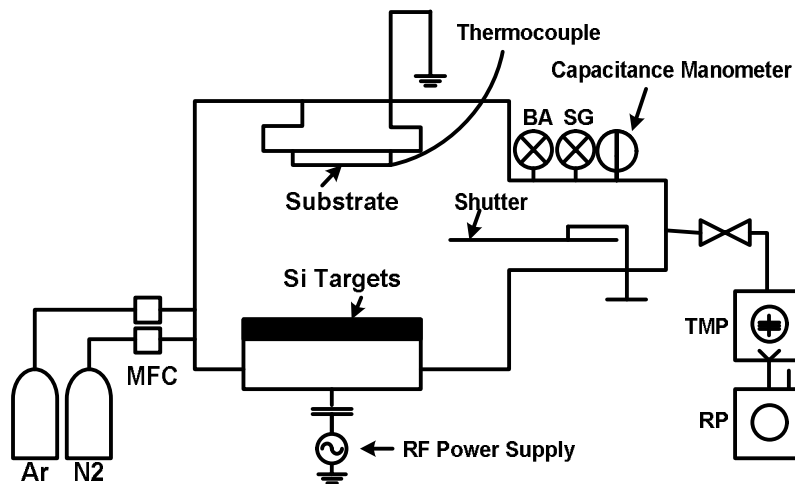
Fig. 4.1 Schematic of an RF magnetron sputtering apparatus: MFC, mass flow
controller; TMP, turbomodulator pump; RP, rotary pump
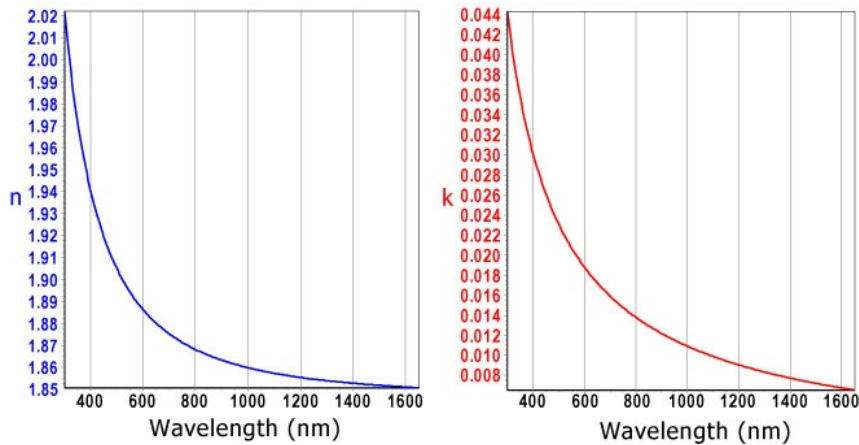
Fig. 4.2 Refractive index (n) and extinction coefficient (k) of Si_3N_4 film as functions of wavelength evaluated by ellipsometry [111]

4.2 Requirement of AlN Thin Layer for Waveguide Cladding

4.2.1 Properties of GaN/AlN MQWs with Sputtered Si_3N_4 Layer

From the previous section, Si_3N_4 was successfully deposited using sputtering process and its optical properties were investigated. Although Si_3N_4 has been widely used as passivation layer in GaN/AlGaN heterostructure field-effect transistors [148-150], the effects on intersubband transition characteristics in GaN/AlN MQWs have not been yet revealed. Hence, before fabricating AlN waveguides with Si_3N_4 clad layers, the effects of Si_3N_4 on the intersubband transition properties in GaN/AlN MQWs should be first studied. The sample structure investigated here was as same as in the chapter 3, Fig. 3.3(a). A high temperature grown 0.5-μm-thick AlN buffer layers was deposited by conventional MOVPE, followed by a 0.1-μm-thick AlGaN interlayer grown at 1150˚C. After that a 40-period GaN/AlN MQWs was deposited using pulse injection method shown in Fig. 3.3(b) by optimizing the intersubband transition at 1.5-μm-range. For being used as references, the sample was evaluated the MQWs structure by XRD (0002) 2θ-ω and (10-15) RSM scans. The intersubband transition property was measured by FTIR using multiple reflection method. The sample was, therefore, divided and deposited Si_3N_4 with thicknesses of 50, 100, 200 and 400 nm on the top of MQWs. The Si_3N_4-deposited samples were, again, measured the crystal structures by XRD and the intersubband

transition by FTIR. Fig. 4.3 and 4.4 show the XRD (0002) 2θ-ω scans and (10-15) RSM scans of the sample without and with Si_3N_4 layer, respectively. The MQWs properties and structure have been changed slightly after Si_3N_4 sputtering at 250°C as evidenced by Fig. 4.3 and 4.4. However, the transmittance spectra were greatly deformed as shown in Fig. 4.5. The absorption intensity via intersubband transition was much weaker in the samples with Si_3N_4 clad layer and found to be a function of Si_3N_4 thickness. There several reports on the effects of sputtered Si_3N_4 on the properties of the underneath structures including the damage of structure from sputtering [140-142] and the reduction of the surface state [143-145]. However, these reports could not clearly explain this investigation which the intersubband absorption intensity depended on the thickness of Si_3N_4 layer. Moreover, the intersubband transition properties of sputtered Si_3N_4 sample was recovered after removing Si_3N_4 by HF solution (concentration 25 mol/kg, temperature 60 °C) [146]. Considering the effects of Si_3N_4 clad layer in this work, it reasonably corresponds to the strain in GaN/AlN MQWs which has also been reported in Ref. 147. The Si_3N_4 clad layer induces more tensile strain to the GaN/AlN MQWs layers. Since the oscillation strength of intersubband transition determines the absorption intensity, the change of oscillation strength due to the shape of conduction band and strain in GaN/AlN MQWs will also greatly affect the absorption intensity [154]. Hence, it can be implied that Si_3N_4 deposited directly on the top of GaN/AlN MQWs restructures the strain in GaN/AlN MQWs and changes the oscillation strength resulting in decreasing of intersubband absorption intensity. This evidence is shown in Fig. 4.6 which the strain in GaN wells and the decrement of intersubband absorption intensity (respected to the sample without Si_3N_4 layer) are similarly depend on the thickness of Si_3N_4 clad layer. The relaxation of GaN wells weakens the oscillation strength and results in the decrement of intersubband absorption strength.
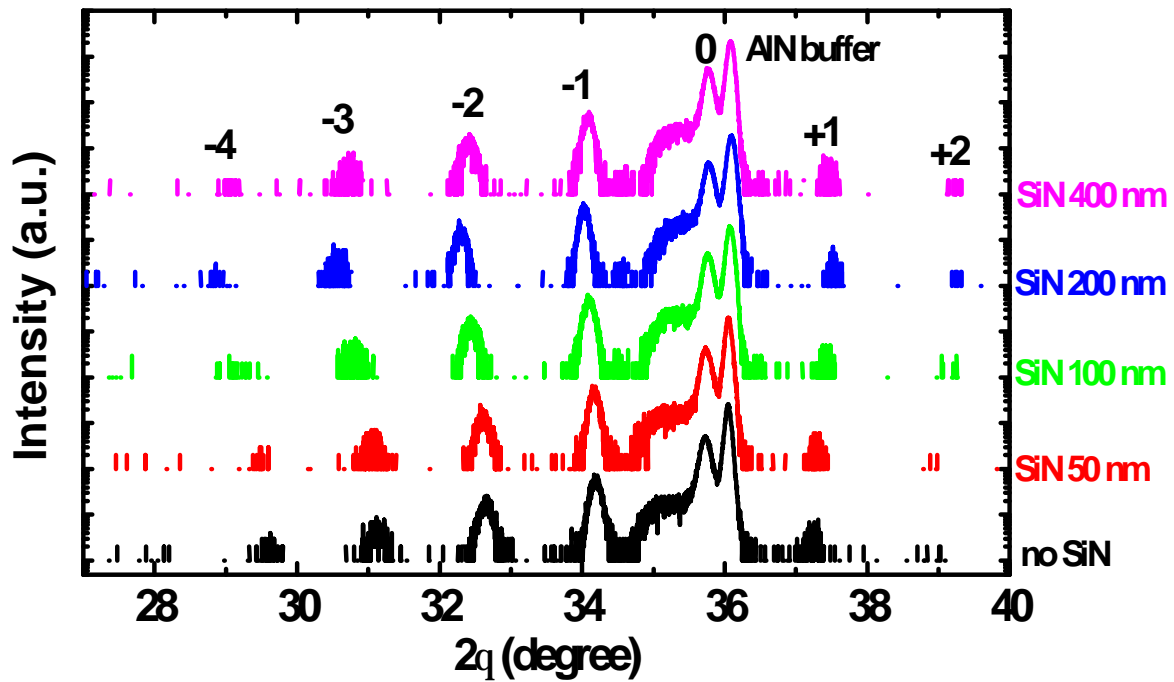
Fig. 4.3 XRD (0002) 2θ-ω scans of the samples without and with Si_3N_4 clad layer thicknesses of 50, 100, 200 and 400 nm deposited on the top on GaN/AlN MQWs

From the above reason, in order to prevent the effect of induced tensile strain from sputtered Si_3N_4 layer, a thin GaN, AlN or AlGaN layer deposited between Si_3N_4 and GaN/AlN MQWs is highly suggested as a strain compensating layer. This thin layer, so-called upper cladding layer, has been investigated including effects of material, thickness and growth conditions for purposes of the best intersubband transition properties and the fabrication of AlN waveguide with GaN/AlN MQWs core.
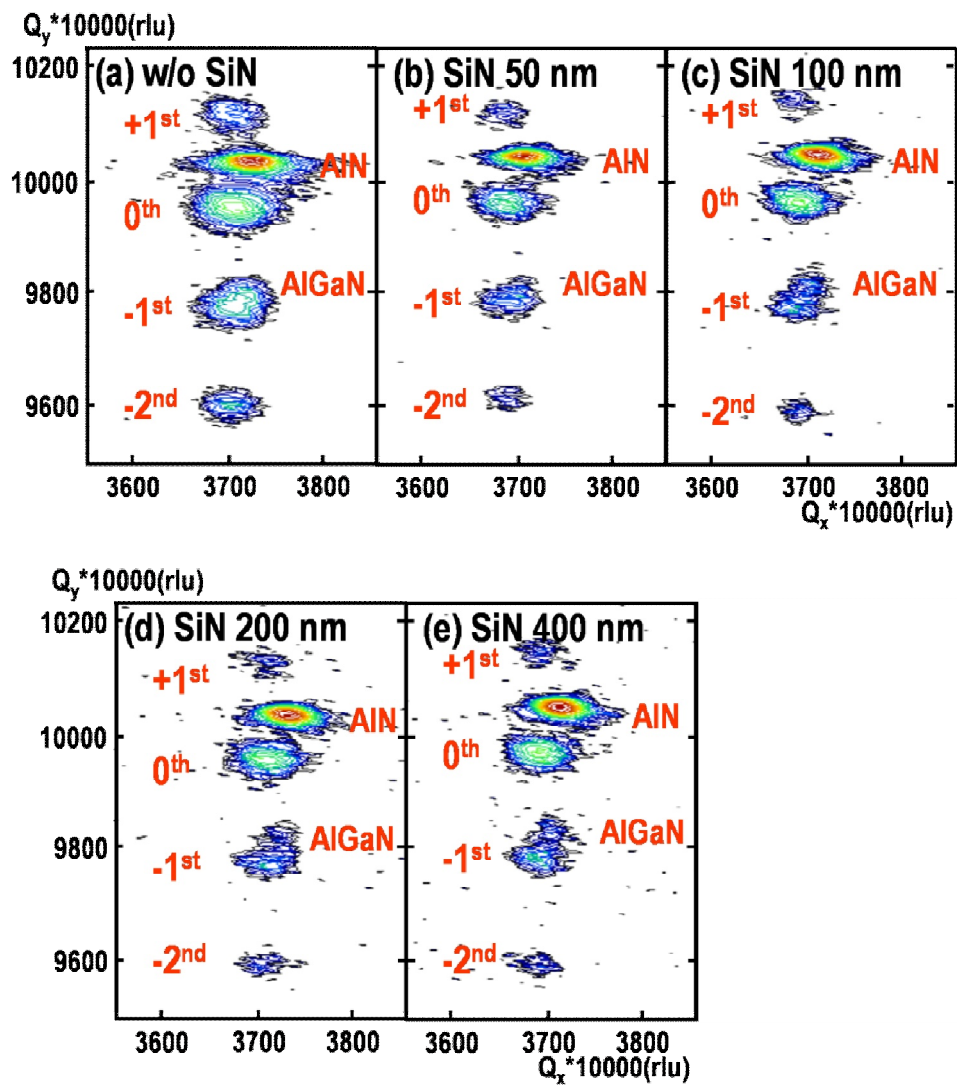
Fig. 4.4 XRD (10-15) RSM scans of the samples without and with Si_3N_4 clad layer thicknesses of 50, 100, 200 and 400 nm deposited on the top on GaN/AlN MQWs
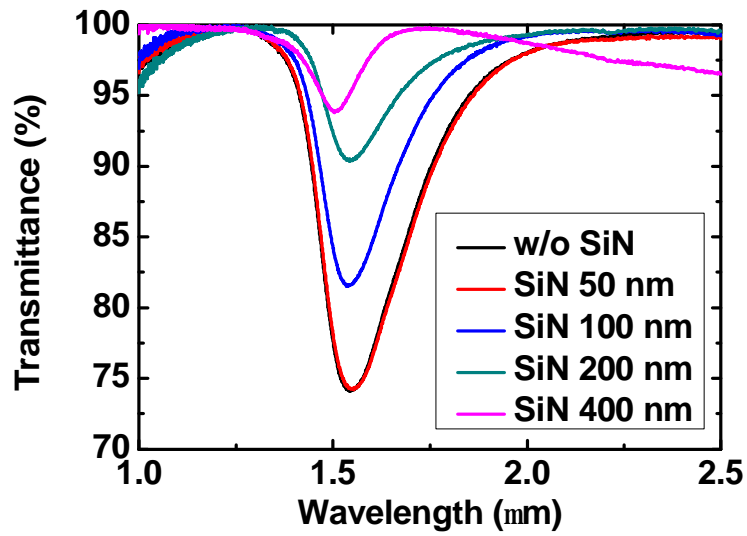
Fig. 4.5 Transmittance of p-polarized light in the samples without and with Si_3N_4 clad layer
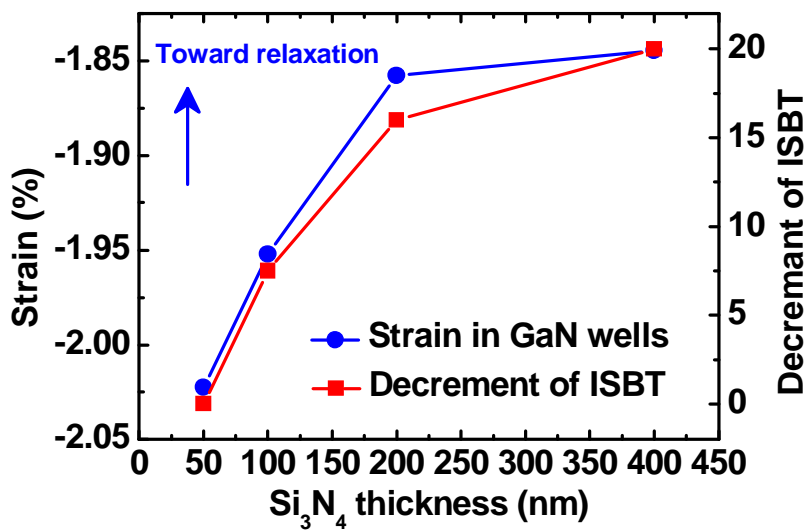
Fig. 4.6 Dependencies of strain in GaN wells and decrement of intersubband absorption intensity on the thickness of Si_3N_4 layer sputtered on GaN/AlN MQWs

4.2.2 Effects of AlN, AlGaN and GaN as Upper Cladding Layers

In this experiment, AlN, AlGaN and GaN have been investigated their effects on the GaN/AlN MQWs properties and intersubband transition characteristics when used as upper cladding layer to compensate induced tensile strain from Si_3N_4 layer. The experiment was carried out by growing 40-period GaN/AlN MQWs using pulse injection method on AlN buffers with AlGaN interlayers (see Fig. 3.3(a) and 3.3(b)). After that 0.1-μm-thick AlN or AlGaN (same Al-content with interlayer's) or GaN was deposited at 850 °C. The other parameters during the growth of upper cladding layer were similar to that of MQWs growth. After the growth by MOVPE, the samples were divided into two groups; one is control group and the other was deposited 0.5-μm-thick Si_3N_4 on the top of upper cladding layer.

Figure 4.7(a) and 4.7(b) provide the information of transmittance spectra in the samples without and with Si_3N_4, respectively. As evidenced in Fig. 4.7(a), each upper cladding layer had different effects on the properties of intersubband transition. It is understandably that, in the view point of absorption intensity, the sample with AlN upper cladding layer had the strongest intersubband transition. This is because its conduction band line-up was the most appropriated which the most of the ground subband in MQWs laid beneath the Fermi energy level [113]. In addition, a broaden intersubband transition peaks in the sample with AlN clad layer can relate to the crystal quality of upper cladding layer grown at relatively low temperature compared to that of conventional AlN growth with relatively high V/III ratio. Nevertheless, after Si_3N_4 deposition on the top of the MQWs, the intersubband transition properties were improved dramatically as indicated in Fig. 4.7(b). We can think that the issue of low crystal quality was suppressed during the sputtering of Si_3N_4 layer. Compared to this sample, the sample with AlGaN had better shape intersubband transition peak but weaker absorption intensity. This can be implied that the sample with AlGaN layer had better quality clad layer but the lattice constant of AlGaN was bigger than that of AlN. Since the purpose of nitride upper cladding layer is to compensate induced tensile strain generated by sputtered Si_3N_4, the AlN which has the smallest lattice constant among $Al_xGa_{1-x}N$ is the most suitable material. Note that, due to the disappearance of intersubband transition in the sample with GaN upper cladding layer as explained in [113], there is no meaning to deposit Si_3N_4 and investigate the resultant intersubband transition. Therefore, it was highly recommended to use AlN upper cladding layer for the purpose of a strong absorption peak.

In addition, the AlN layer was chosen to serve this purpose because of its simple deposition process. In this section, the AlN upper cladding layer was grown using the condition of AlN barriers of MQWs, low temperature and high V/III ratio. Hence, the crystal quality of AlN layer can be possibly improved by using higher growth temperature and lower V/II ratio which was the condition for AlN bulk layer grown by conventional MOVPE. These two growth parameters will be investigated in the next sections.
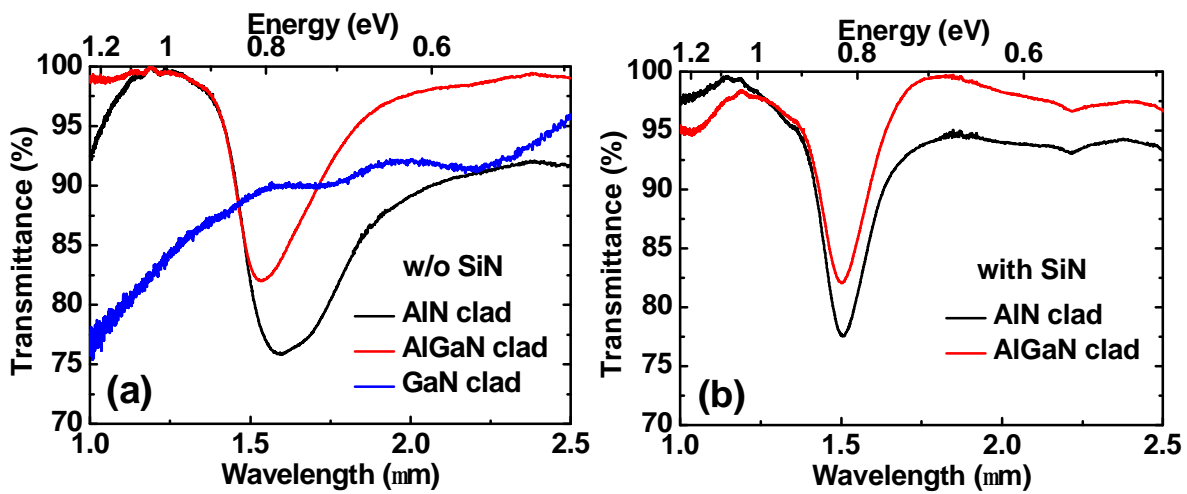
Fig. 4.7 Transmittance spectra in the MQWs with AlN, AlGaN and GaN upper cladding layer (a) without Si_3N_4 layers and (b) with Si_3N_4 layer

4.3 Optimization of AlN Upper Cladding Layer

4.3.1 Effect of Thickness of AlN Upper Cladding Layer

The influence of the thickness of AlN upper cladding layer has been studied in this section. On the top of 40-period GaN/AlN MQWs, AlN cladding layers were deposited at 850 ℃ using the growth condition of AlN barriers of MQWs (V/III = 3000). Three samples with AlN cladding layers 25 nm, 50 nm and 100 nm thick were fabricated in this study. After the growth by MOVPE, the samples were deposited with sputtered Si_3N_4, 0.5-μm-thick. Figure 4.7(a) and 4.7(b) reveal the FTIR measurement of p-polarized light transmittance in the samples without and with Si_3N_4 layers, respectively. These two graphs were intentionally plotted in the same

scale for easy comparison. We can observe that, before Si_3N_4 deposition, the sample with the thinnest AlN cladding possessed the strongest and the smallest FWHM of intersubband transition peak. It attributes to the poor crystal quality of AlN upper cladding layer grown by using the growth condition of AlN barriers of MQWs. Recalling from the experiment in chapter 2, we have assumed that AlN barriers in MQWs had relatively poor quality compared to that of GaN wells indicated by the AFM images in Fig. 2.15. This state is also applied for AlN cladding layers in this experiment since the growth conditions were similar. However, as shown in Fig. 4.8(b), it is clear that the sample with 100-nm-thick AlN upper cladding layer was the most robust to the effects of Si_3N_4 layer in the view point of absorption intensity via intersubband transition. The strength of intersubband transition peaks were greatly degraded in the samples with thin AlN cladding layers. From this result, AlN upper cladding layer for the purpose of compensating the strain effects of sputtered Si_3N_4 layer should be at least 100-nm-thick. Nevertheless, the thick AlN upper cladding layer could eventually lead to the degradation of the shape of intersubband transition peak. Moreover, the issue of poor crystal quality should be improved by optimizing the growth conditions which will be investigated in the next sections.
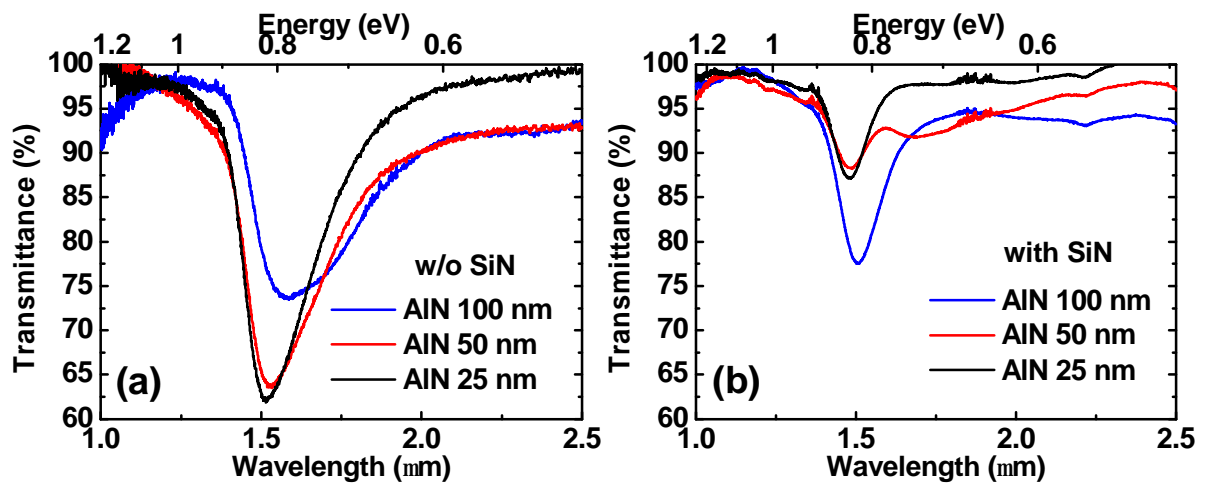
Fig. 4.8 Transmittance spectra in the MQWs with 100-nm-, 50-nm- and 25-nm-thick AlN upper cladding layer (a) without Si_3N_4 layers and (b) with Si_3N_4 layer

4.3.2 Effects of V/III Ratio during the Growth of AlN Upper Cladding Layers

At this point, we have known that a 0.1-µm-thick AlN upper cladding layer is the requirement for preventing the degradation of intersubband transition properties in GaN/AlN MQWs from Si_3N_4 layer. The problem here is to optimize the growth condition of AlN layer since its poor quality affects on the FWHM and shape of an intersubband transition peak. In this section, the effects of V/III ratio during the growth of AlN upper cladding layer have been studied. So far, the growth condition of AlN barriers in GaN/AlN MQWs has been used for the deposition of AlN upper cladding layer which V/III ratio is 3000. The reason of using high V/III ratio during the growth of AlN barriers is to balance the gas flow because the growth of GaN wells by pulse injection method requires sufficient amount of NH_3 (group V) for effective carbon reduction. Since there are several reports about the quality improvement of AlN bulk layer by lowering V/III ratio [114-117], this method has been adopted in order to solve the issue of low crystal quality of AlN upper cladding layer. Two samples with different 0.1-µm-thick AlN clad layers were fabricated using V/III ratios of 3000 and 500 at growth temperature of 850 ℃. After the growth, the samples were polished and measured intersubband transition properties by FTIR. The results are shown in Fig. 4.9. Without doubt, the intersubband transition properties were much better in the sample with AlN clad layer grown at low V/III ratio. This result was a good agreement with the above reference in which, at low V/III ratio, parasitic gas-phase pre-reactions between group-III and group-V precursors have been suppressed [117].
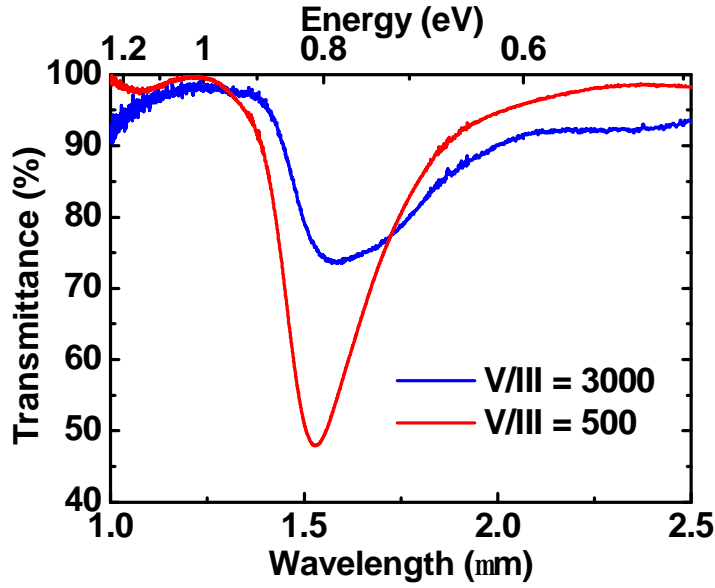
Fig. 4.9 Transmittance spectra of 40-period GaN/AlN MQWs with 0.1-μm-thick AlN clad layers grown at 850 ℃ using V/III of 3000 and 500

4.3.3 Effects of Growth Temperature of AlN Upper Cladding Layers

Continue from the accomplishment in the last section, the effects of the growth temperature of AlN clad layer on the intersubband transition properties has been studied. It is widely known that the elevated temperature enhances the lateral movement of deposited species resulting in a quasi 2D growth of AlN bulk layers and eventually reducing the pits [118,119]. However, there is a possibility that the low temperature grown GaN/AlN MQWs will be suffered from the relatively high temperature during of the deposition of AlN clad layer. Hence, the growth temperature of AlN upper cladding layer should be optimized in this section.

40-period GaN/AlN MQWs were deposited on the top of 0.1-μm-thick AlGaN interlayers grown on high-temperature 0.4-μm-thick AlN buffer layers. On the top of the MQWs, 0.1-μm-thick AlN upper cladding layers were deposited at 850 ℃, 950 ℃ and 1050 ℃ using V/III ratio of 500. A sample without AlN upper cladding layer was used as a reference. Transmittance spectra of p-polarized light of each sample are shown in Fig. 4.10. We can see that the sample with AlN clad layer grown at 1050 ℃ did not possess any intersubband transition peak. It can be interpreted that the quality and the abruptness of underneath GaN/AlN MQWs extremely

dropped during the growth of AlN layer at high temperature. In addition, the intersubband transition peak in the sample with 950-ºC-AlN layer began to broaden and evidenced the restructure of GaN/AlN MQWs. Among the samples with AlN upper cladding layers, the GaN/AlN MQWs with 850-ºC-AlN layer exhibited the best intersubband transition properties comparable to that of GaN/AlN MQWs without upper cladding. This indicates that the growth temperature of 850 ºC was high enough to deposit good quality AlN layer without degrading the underneath GaN/AlN MQWs. Therefore, the growth conditions of AlN upper cladding layer have been optimized for the purpose of waveguide fabrication in the next chapter.
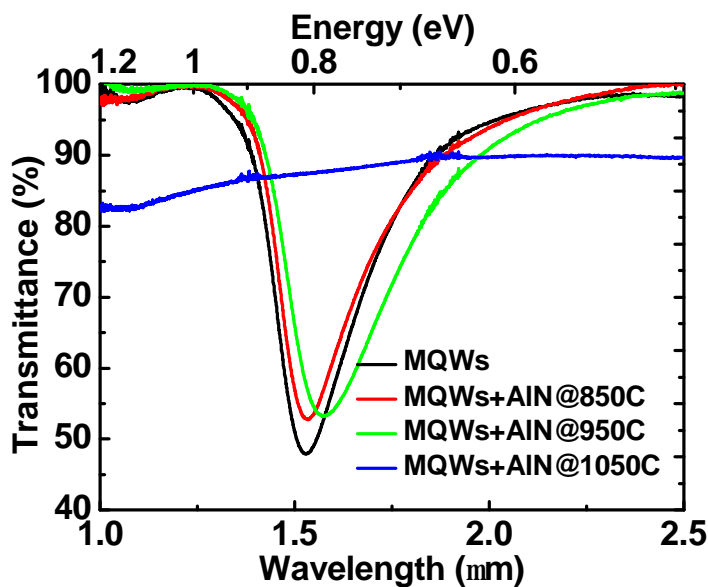
Fig. 4.10 Transmittance spectra of MQWs without and with AlN upper
cladding layer grown at different temperature

4.4 Conclusions

In this chapter, AlN upper cladding layer grown on the top of GaN/AlN has been proved to be mandatory for preventing the degradation of intersubband transition properties in underneath MQWs from sputtered Si_3N_4 layer. The origin of degradation is believed to be the change of strain level in GaN/AlN MQWs by induced tensile strain form Si_3N_4 layer which weakens the oscillation strength of intersubband transition and results in poor intersubband

absorption intensity. The AlN upper cladding layer and the effects of growth parameters have been investigated for the purpose of the best intersubband transition.

1. Considering its energy band gap, AlN or Al-rich AlGaN has been highly recommended to be used as upper cladding layer for the purpose of strong intersubband transition intensity.

2. From the study, a 0.1-µm-thick AlN is the minimum thickness required for preventing the underneath GaN/AlN MQWs from sputtered Si_3N_4 layer. However, with a thicker AlN cladding layer, the shape and the FWHM of an intersubband transition peak can possibly be suffered from poor crystal quality of AlN cladding layer.

3. Low V/III ratio during the growth of AlN upper cladding results in the excellent crystal quality. The sample with an AlN upper cladding layer grown using low V/III ratio showed superb intersubband transition properties both intensity and FWHM of absorption peak.

4. The high growth temperature of AlN cladding layer leads to the degradation of intersubband transition characteristic especially the absorption intensity even though the crystal quality of AlN layer can be improved. The growth temperature of 850 ℃ has been proved to be an optimum point for achieving good AlN layer in the view point of resultant intersubband transition properties in the beneath MQWs and crystal quality.

Chapter 5 Fabrication of AlN-Based Waveguide with GaN/AlN MQWs Absorption Core

A
ll effort from the previous chapters has been devoted in this chapter to fabricate optical devices utilizing intersubband transition in MOVPE grown GaN/AlN MQWs. This work has focused on all-optical switch based on AlN waveguide structure. The AlN-based waveguide has been designed in section 5.1 for the purpose of good optical confinement and single mode propagation. After that, ridge and high-mesa AlN waveguide with GaN/AlN MQWs core has been fabricated in section 5.2. In section 5.3, the intersubband (ISB) absorptions in AlN-based waveguides have been measured and compared with other studies. The intersubband absorption saturation has been evaluated in section 5.4. The conclusion of this chapter is given in section 5.5.

5.1   Design of AlN-Based Waveguide with GaN/AlN MQWs Core

In the last chapter, chapter 4, AlN upper cladding layer which is mandatory for compensating the effect of induced tensile strain originated by Si_3N_4 layer has been investigated. The optimized structure exhibited a very excellent intersubband transition peak in the viewpoint of absorption strength and FWHM of the intersubband transition peak. This thesis has focused on all-optical switch based on intersubband transition in GaN/AlN MQWs embedded in AlN-based waveguide. Hence, AlN-based waveguide has to be investigated, designed and fabricated. In fact, the design of optical waveguide is a very important issue, especially for optical devices utilizing the saturation of intersubband absorption including all-optical switches and modulators. This is

because the energy required for pumping the intersubband absorption in the waveguide to a certain saturation level relates to the size of active region (MQWs core) and the optical confinement in the waveguide. At the present time, the lowest pumping energy required for 10-dB saturation level is 38 pJ in a GaN ridge waveguide which has been reported in Ref. 25 owing to a good waveguide designing. This evidences the important and necessary of the designing of optical waveguide for the purpose of minimizing the switching energy.

Generally, in this work, two main parameters have been carefully considered during the designing of AlN-based waveguide including:

1. The optical confinement in GaN/AlN MQWs core which should be as high as possible in order to effectively utilize intersubband transition and saturate intersubband absorption with low pumping energy.

2. Mode of propagation which should be single mode in order to operate optical switches at high speed with stability and reliability using low switching pulse energy.

From the chapter 3, the growth and the optimization of GaN/AlN MQWs have been done on AlN buffer layers. In addition to the advantages of AlN described in chapter 3, AlN material also exhibits an outstanding property over GaN material which will be explained later in the designing of waveguide structure.

5.1.1   Optical Confinement and Mode Propagation in AlN-Based Waveguide

The designing of AlN-based optical waveguide in this work has been performed by the simulation of different structures using the beam propagation method (BPM). The refractive indexes of nitride material used in the simulation are 2.335[112], 2.031 [112], and 1.85 [111] at 1.55-μm wavelength for GaN, AlN and Si_3N_4, respectively. The refractive indexes of AlGaN interlayer and GaN/AlN MQWs (both have Al-content ~0.8) can be interpolated from that of AlN and GaN. Therefore, the structures with MQWs embedded between cladding layers have been studied by the one-dimensional waveguide simulation of propagation mode in z-axis (growth direction), followed by the two-dimensional waveguide simulation.

The simulation started with the structure shown in Fig. 5.1 which 0.5-μm-thick Si_3N_4 was sputtered on the top of 0.1-μm-thick AlN cladding layer optimized in the last chapter. The underneath layers were 40-period of GaN/AlN MQWs with the total thickness of 0.24 μm on

AlGaN interlayer and AlN buffer, 0.1-μm-thick and 0.5-μm-thick, respectively. Since this structure has been well investigated during the optimization process, it was considered as a good starting point with 0.5-μm-thick Si_3N_4 to make the MQWs at the center of the structure.
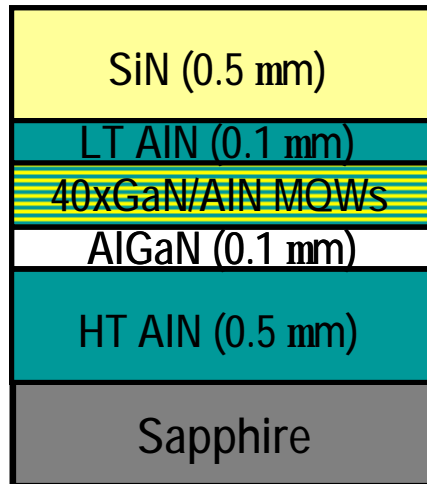
Fig. 5.1 Waveguide structure with GaN/AlN MQWs core buried with nitride material

The TE and TM mode intensity profiles on the waveguide structure in Fig. 5.1 are shown in Fig. 5.2 and 5.3, respectively. These TE and TM mode intensity profiles reveal that the optical confinement was maximized around the interface between AlGaN interlayer and MQWs core. Obviously, in both TE and TM mode intensity profiles, there exist two propagation modes including the fundamental mode and 1st higher order mode. This can be explained that the AlN buffer, AlGaN interlayer, AlN upper cladding layer and Si_3N_4 layer were thick and the optical confinement was large enough to confine multimode propagation. Although the coupling efficiency of higher mode from fiber to waveguide is generally lower than that of the fundamental mode, the higher mode propagation is considered as a loss. Particularly, the multimode propagations in the growth direction are undesirable since the most of higher mode intensities do not couple into the active region (MQWs core). This can be a major obstacle for the measurement and characterization of intersubband transition in waveguide as well as the pumping energy required for the saturation of intersubband absorption will be larger. From the above reasons, the single mode propagation in the waveguide is strongly preferred. There are several conservative methods for achieving this purpose including the use of materials that have

lower refractive indexes and the downsizing of the waveguide structure. Considering that AlN has the lowest refractive index among the AlGaN system, it suggests that the downsizing of the waveguide structure should be the best method for obtaining a single mode waveguide. Again, AlN buffer layer shows an outstanding merit over GaN layer in which MOVPE grown GaN buffer layer initially deposits in 3-D island mode and changes to quasi-2-D growth mode as its thickness exceeds 0.4 μm [120]. Generally, high quality GaN layer can be achieved when its thickness is around 0.8 μm. In the contrast, AlN layer deposits in 2-D growth mode from the initial state. Hence, it is possible to fabricate high quality AlN buffer layer as thin as 0.3-0.4 μm which is favorable for downsizing the waveguide structure. Moreover, GaN cladding layers in a waveguide structure easily lead to high optical confinement and multimode propagation due to large refractive index of 2.335. Consequently, AlN material is more preferred for optical devices based on waveguide structure owing to the above reasons including the relatively low dislocation density in AlN layer compared to that of GaN layer.
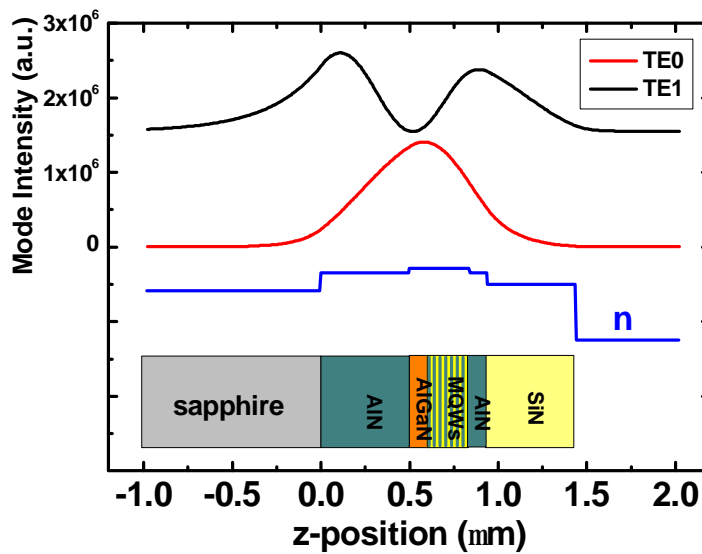
Fig. 5.2 TE mode intensity profiles and refractive index of waveguide structure shown in Fig. 5.1.
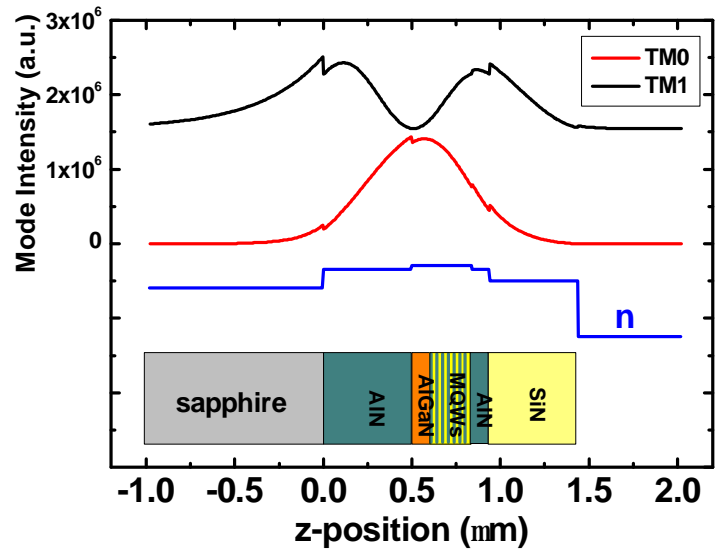
Fig. 5.3 TM mode intensity profiles and refractive index of waveguide structure in Fig. 5.1.

In order to design a single mode waveguide, the thickness of AlN buffer layer was, therefore, decreased to 0.4 μm, the limitation that ensures high-quality bulk AlN layers prepared by MOVPE. Using the optimization of intersubband absorption intensity by doubling the reactor pressure in chapter 3.6, the number of GaN/AlN MQWs can be reduced from 40 periods to 10 periods while the intersubband transition intensity is high enough for the measurement of intersubband characteristics in the waveguide. The total thickness of MQWs was 45 nm as a result. The Si_3N_4 layer was also decreased to 0.4 μm to align the MQWs at the center of the waveguide. The new designed structure is displayed in Fig. 5.4.
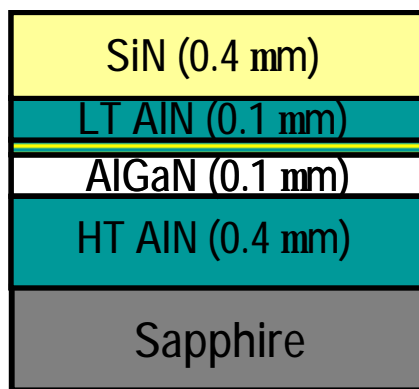
Fig. 5.4 The new designed waveguide structure by downsizing the thicknesses
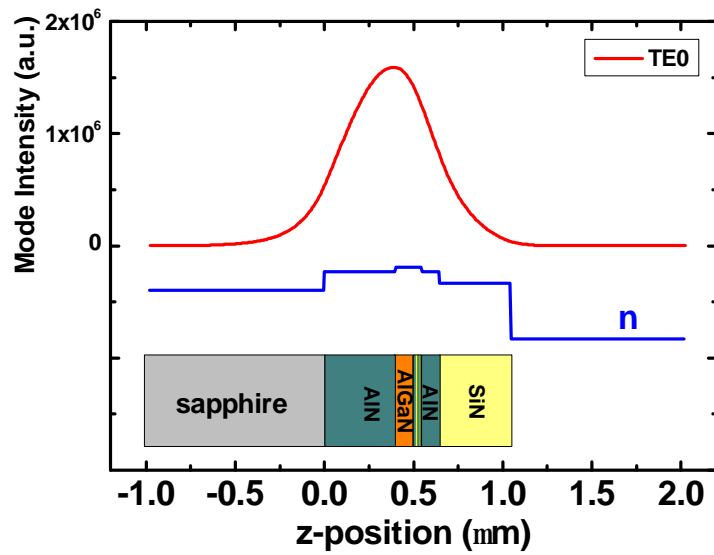
Fig. 5.5 TE fundamental mode intensity profile and refractive index of the new designed waveguide structure
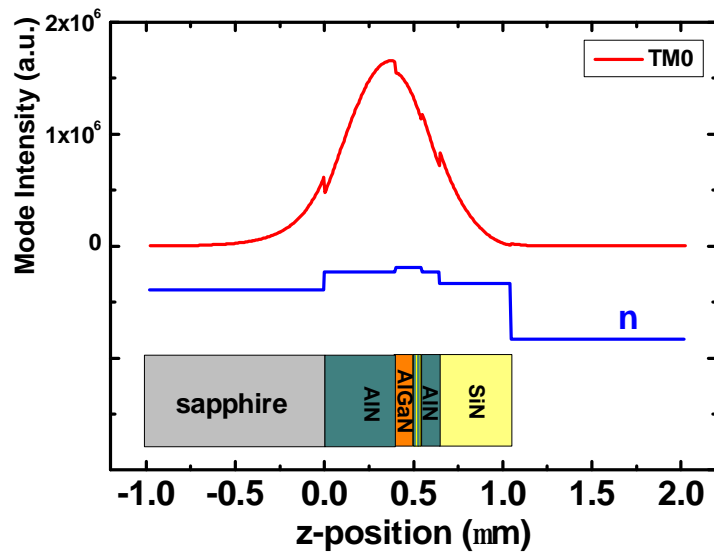
Fig. 5.6 TM fundamental mode intensity profile and refractive index of the new designed waveguide structure

Clearly, with the new designed structure, the AlN-based waveguide exhibits only single mode propagation. The mode intensity profiles both TE and TM mode in Fig. 5.5 and 5.6

indicate that the maximum optical confinement shifted to the bottom of AlGaN interlayer due to thinner MQWs core. The thicker MQWs core is favorable for the optical confinement but, in the contrast, can lead to multimode propagation in vertical direction. In addition, we can observe the larger optical leakage from the sapphire/AlN interface due to the thinner structure especially in TM mode light. However, compared with the multimode propagation in the old structure, the new designed waveguide has showed a potential for fabricating an optical switch requiring significantly low pumping energy.

5.1.2   Ridge and High-mesa Waveguide

The structure of AlN-based waveguide has already designed and optimized for single mode propagation. Before conducting the waveguide fabrication, the shapes of waveguide have been studied for good device characteristics. In this section, two famous types of waveguide geometries, ridge and high-mesa waveguides, are introduced.

Ridge waveguide, illustrated in Fig. 5.7(a), is the structure which is shallow etched, not reaching the active layer (MQWs core). The ridge waveguide is widely used for semiconductor optical waveguide owing to its properties, for example:

- Propagation loss in ridge waveguide is relatively low compared to that in high-mesa waveguide since the active core laterally expands in which the light can travel and be confined within the active core. Therefore, the propagation loss and interference from the roughness of sidewall of the above waveguide strip are relatively low.

- Because of the large cross section area of ridge waveguide, the coupling of light from fiber to waveguide is easy and yields a good coupling efficiency.

- The ridge waveguide is also famous for single mode waveguide because the optical confinement in lateral direction is not strong compared to that of high-mesa waveguide.

- However, because the active core is buried under the upper cladding layers, it is not an easy task to align the light from the fiber at the center of the active core. In fact, the energy of light coupled to the MQWs core can be greatly suffered from the difficult alignment.

- The large active region, especially in the lateral direction, can result in the requirement of high pulse energy to saturate the intersubband absorption.

79

Classified by the etching depth, high-mesa is the waveguide which is deeply etched pass through the active core as schematically shown in Fig. 5.7(b). The characteristics of high-mesa waveguide are different to that of ridge waveguide in which:

- The roughness of sidewall of the waveguide greatly determines the propagation loss in the high-mesa structure. The fabrication process requires advance technique in order to obtain deep-etched smooth sidewall.

- Considering the cross section area of high-mesa waveguide, the coupling efficiency of light from fiber to waveguide is not as good as ridge structure.

- The optical confinement in high-mesa waveguide is high both horizontal and vertical directions making an excellent light confinement within the waveguide. It can be expected that the large portion of light is delivered into the active core.

- However, such a high optical confinement, the multimode propagation can easily occur in this structure.

- Compared to ridge structure, the relatively small active region in high-mesa waveguide is favorable for lowering the pumping energy required to saturate the intersubband absorption.
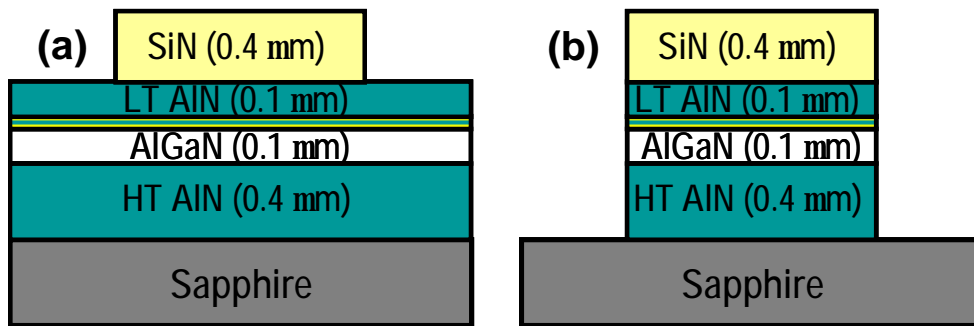
Fig. 5.7 2-μm-wide AlN-based optical waveguide with optimized thicknesses

(a) ridge waveguide and (b) high-mesa waveguide

Figure 5.8 displays the two-dimensional mode intensity profiles in the 2-μm-wide ridge waveguide which is shown in Fig. 5.7(a). Obviously, there exist single mode of TE propagation, TE 00, and two modes of TM propagation, TM 00 and TM 01. Note that the higher propagation mode does not appear in the vertical direction owing to the designing in the last section. We can

see that the intensities of each mode are maximum around the lower part of AlGaN interlayer, agreeing with the result in the last section. In addition, the portions of confined light into the MQWs core are also relatively high indicating a good designing.
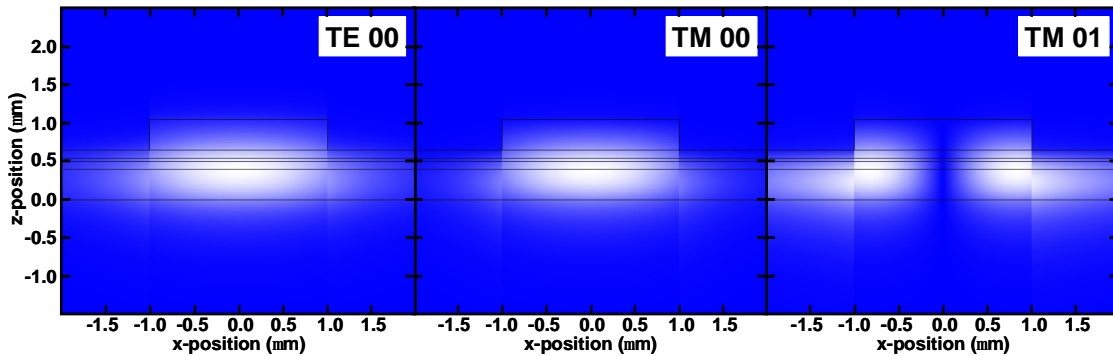
Fig. 5.8 2-D TE and TM mode propagation intensity profiles in 2-µm-wide ridge AlN-based waveguide

The TE and TM mode propagation intensity profiles of the high-mesa structure are shown in Fig. 5.9. We can see that the high-mesa waveguide designed in this work allows higher propagation mode compared with ridge structure. There exist 3 modes including fundamental mode, 1st and 2nd higher modes for both TE mode and TM mode. It should be noted that the issue of higher propagation mode in the vertical axis has been suppressed by the designing of waveguide structure in the last section. Hence, the higher propagation modes exist only in the horizontal direction which the loss from these propagation modes is much smaller than that of higher modes in vertical direction (if exists). Considering the intensity profiles in the high-mesa waveguide, the optical confinement of light into the MQWs core is remarkably better than the ridge waveguide case.

We can see that each waveguide structure has its own advantages. Ridge waveguide is easier to fabricate, easier to couple light from fiber, and yields low propagation loss, but the confinement of light into the center of active core is more difficult. For the high-mesa structure, on the other hand, the optical confinement is better but the fabrication is more advance and the propagation loss depends on the roughness of sidewall of the waveguide. For experimental comparison between two structures, in the following sections, ridge waveguide and high-mesa

waveguide have been fabricated and the intersubband transition characteristics in both structures have been evaluated.
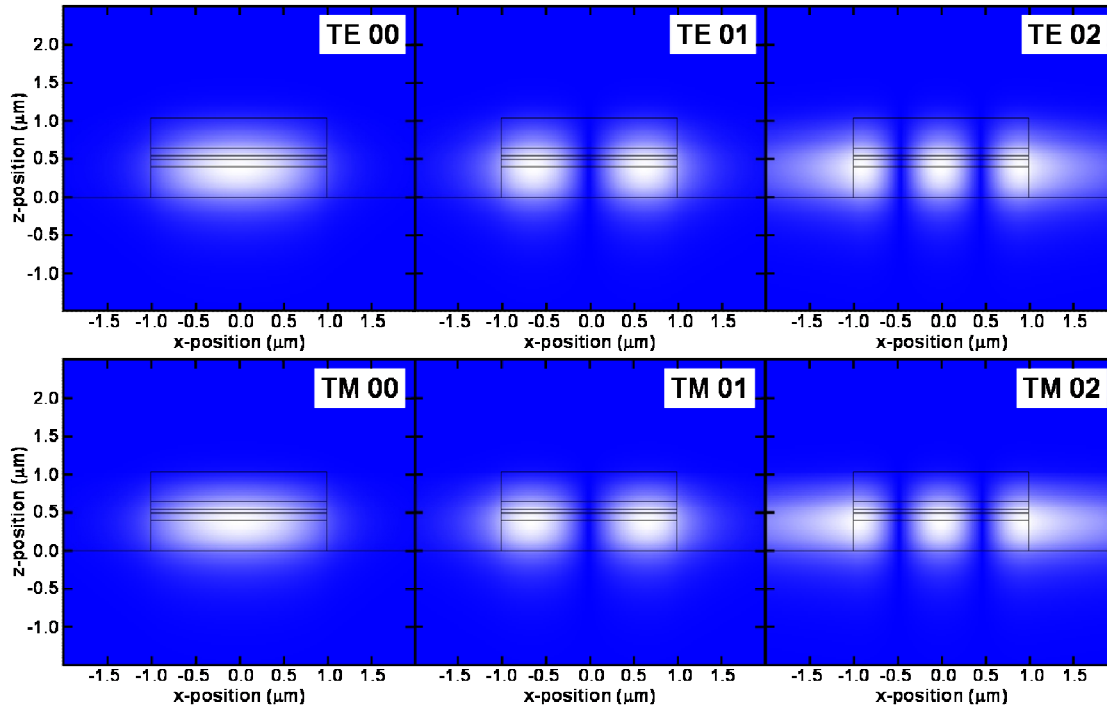
Fig. 5.9 2-D TE and TM mode propagation intensity profiles in 2-µm-wide
high-mesa AlN-based waveguide

5.2 Fabrication of AlN-Based Waveguide

In this section, the fabrication procedures of AlN-based waveguide are given in detail. First, the inductively coupled plasma reactive ion etching system (ICP-RIE) is briefly introduced as the most important instrument for the fabrication of nitride-based optical waveguide. The fabrication processes of high-mesa waveguide are quite similar to that of ridge structure and can directly derived from the fabrication of ridge structure. The only difference between two structures is etching depth. In the ridge structure, only Si_3N_4 layer is etched as illustrated in Fig. 5.7(a) while the etching in high-mesa structure is deep to sapphire substrate as shown in Fig. 5.7(b). Therefore, the fabrication procedures of two waveguide structures will be simultaneously

explicated. Note that the fabrication processes have been adopted from the optimized conditions which were thoroughly explained in Ref. 45-46, 111 and 120.

5.2.1 Inductively Coupled Plasma Reactive Ion Etching

Dry etching (reactive ion etching) is a key technology for the microfabrication. In contrast to wet etching, it is capable to yield structures with high pattern transfer fidelity and high aspect ratios. The etching is achieved by generating plasma from a suitable gas above the sample. The plasma is excited by applying RF (radio frequency) power. The capacitor formed by the chamber walls and the stage couples the energy capacitively to the reactive gas. In addition, the more sophisticated inductively coupled plasma reactive ion etching system (ICP-RIE) can also couple the energy inductively into the plasma by a coil around the chamber (Fig. 5.10). This two independent power sources, RF-power and ICP-power, allow controlling the plasma density and the ion energy independently, giving more degrees of freedom for process optimization.
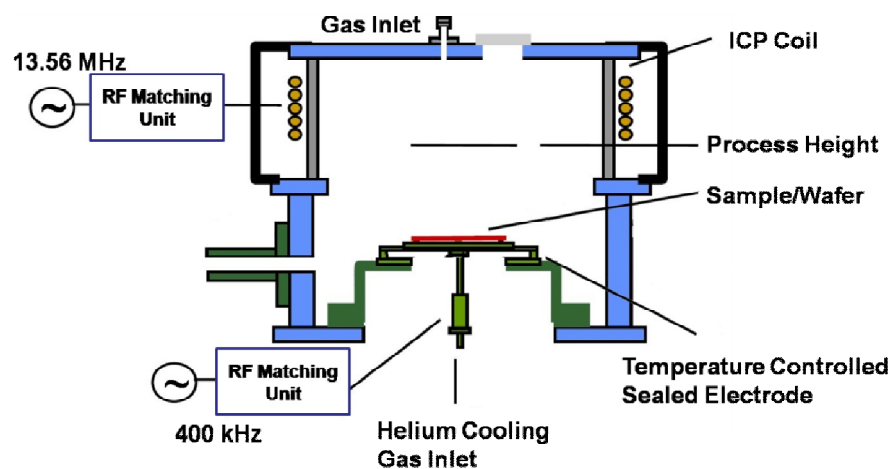
Fig. 5.10 Schematics of an ICP-RIE reactor

The different masses of the charge carriers (negative electrons and positive ions) cause a depletion of electrons close to the sidewalls of the plasma chamber, resulting in an electric field (DC-bias) between the plasma and the chamber wall. Through this field, electrically charged

positive ions are accelerated towards the sample, which they hit at almost normal incidence, causing vertical etching. These ions can either etch the underlying material chemically by forming volatile etch products, physically eject other atoms (sputtering or physical etching) or support chemical etching between the etched material and the neutral gas (ion-enhanced chemical etching).

In this work, the ICP dry etching was performed by ANELVA-201D ICP-RIE system. Rated powers and frequencies of ICP coil and RF source are 1000 W/13.56 MHz and 300 W/400 kHz, respectively. The machine is equipped with argon (Ar), oxygen (O_2), hydrogen (H_2), chlorine (Cl_2), methane (CH_4), trifluoromethane (CHF_3) and helium (He, for cooling) gases which allow the etching of various material systems.

5.2.2 Fabrication Processes of AlN-Based Waveguide

Figure 5.11 gives us the overview of AlN-based waveguide fabrication processes which their details are described as followed:
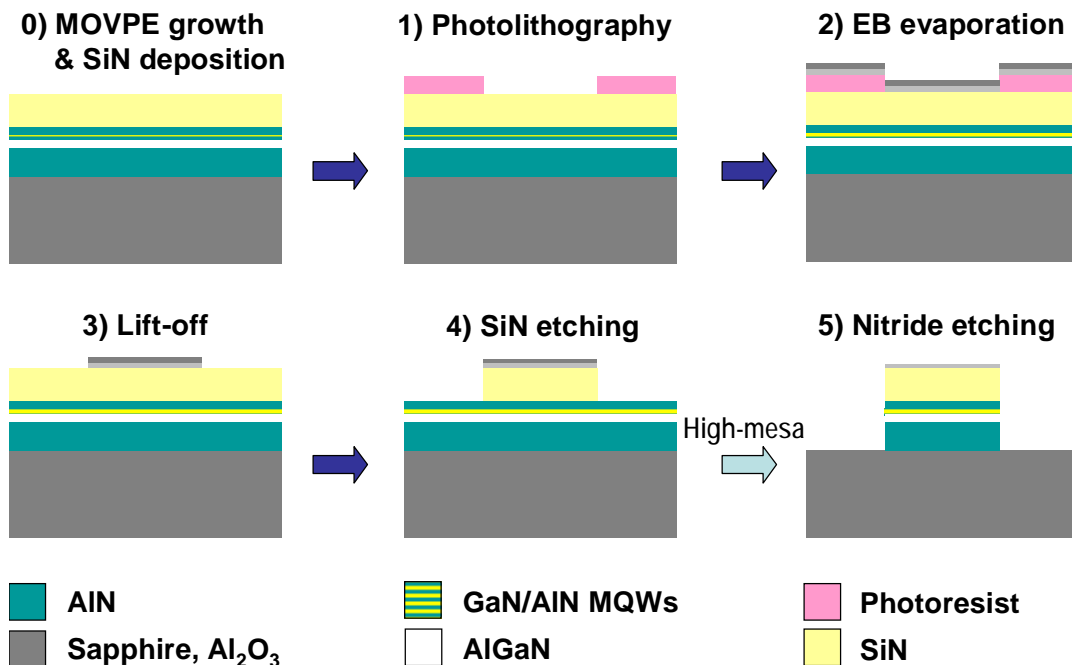
Fig. 5.11 Schematic diagram of waveguide fabrication processes

1) Photolithography

A sample which is deposited nitride semiconductor layers and sputtered Si_3N_4 layer is firstly cleaned with acetone and isopropanol. The cleaned sample is afterward dried with N2 and baked at 120 ℃ for 10 minutes to remove the remaining isopropanol. After that, the photolithography technique is performed to pattern a photoresist mask on the top of Si_3N_4. In this procedure, AZ 5214 which is favorable for lift-off technique is used as negative resist. The processes are listed as followed:

1. Spin Coating
   - 1st step: 500 rpm, 5 sec
   - 2nd step: 3000 rpm, 30 sec
2. Prebaking: 90 ℃, 60 sec
3. 1st exposure: 4 sec, hard contact with mask
4. Reversal baking: 120 ℃, 120 sec
5. 2nd exposure: 8 sec, soft contact without mask
6. Developing: Tetra-methyl-Ammonium-Hydroxide (TMAH, NMD3) 3min

Note that the exposure times are adjustable regarding to the intensity of Hg-lamp.

2) Electron-beam evaporation

The AZ 5214 photoresist itself cannot be used as a mask for ICP dry etching due to its softness. Hence, some harder materials have to be deposited as an etching mask. In this work, 300-nm-thick silicon dioxide (SiO_2) and 200-nm-thick aluminium oxide (Al_2O_3) have been used for this purpose. The deposition process is done by electron-beam (EB) evaporator using SiO_2 and Al_2O_3 targets.

3) Lift-off

The sample, which is already deposited SiO_2/ Al_2O_3 mask, is then lift-off the AZ 5214 photoresist using hot acetone, 80 ℃, for 5 minutes. This is followed by cleaning with acetone and IPA, each for 1 minute, in ultrasonic bath. After lift-off process, the mask pattern is clearly seen and ready for ICP dry etching.

4) ICP dry etching of Si$_3$N$_4$ layer

To form a ridge waveguide structure, the sample is shallow etched Si$_3$N$_4$ layer using ICP-RIE. The etching is perform in the ambient of gas mixture, Ar:CHF$_3$:O$_2$=7:2:4 sccm, at the pressure of 1 Pa. The ICP powers and RF power are maintained at, respectively, 200 and 75 watt during the process. The etching rate is approximately 1.5 nm/s. The ridge waveguide is finished in this step, while the high-mesa structure will be done in the next process.

5) ICP dry etching and wet treatment of nitride layers

In this step, the high-mesa waveguide is formed by deep etching all nitride layers using ICP-RIE. The process is utilizing two-step etching technique [46,111] which the conditions are summarized in the table 5.1. With 1 cycle of two-step etching, nitride layers can be removed by 600-700 nm thick.

Table 5.1 Summarization of conditions during two-step etching for nitride layers

Step No.	Time(min)	ICP Power	RF Power	Gas Press.	Ar:Cl$_2$ (sccm)	Temperature
1	3.5	600 W	175 W	7 Pa	2:8	RT
2	2.5	450 W	175 W	7 Pa	2:8	RT

After that, the wet treatment is carried out to remove spikes of remaining nitride layers. This procedure is done by TMAH at 70 ºC, 4 minutes.

At this point, two AlN-based waveguide structures have been successfully fabricated using the above procedures which the experimental results are shown in the next sections.

5.2.3 Ridge AlN-Based Optical Waveguide

By using the waveguide structure as discussed in section 5.2, Fig. 5.7(a), and the fabrication procedures, step 1 to step 4, from the last section, the practical ridge AlN-based waveguide has been fabricated. The scanning electron microscope (SEM) image of fabricated device is shown in Fig. 5.12. We can clearly observe each layer separated by different colors.

Nevertheless, we cannot distinguish the GaN/AlN MQWs from the AlGaN interlayer because their Al-contents were similar. The sidewall of the waveguide was smoothly etched so that it could be expected for the low propagation loss in this sample. Obviously, SiO_2 and Al_2O_3 mask layers still remained after the ICP etching of the Si_3N_4 layer. Since the refractive index of SiO_2 and Al_2O_3 are 1.46 and 1.75, by using the thicknesses of each layers as measured by the SEM image, the propagation mode in this structure was still single mode, both TE and TM, confirmed by the simulation method described in section 5.1.
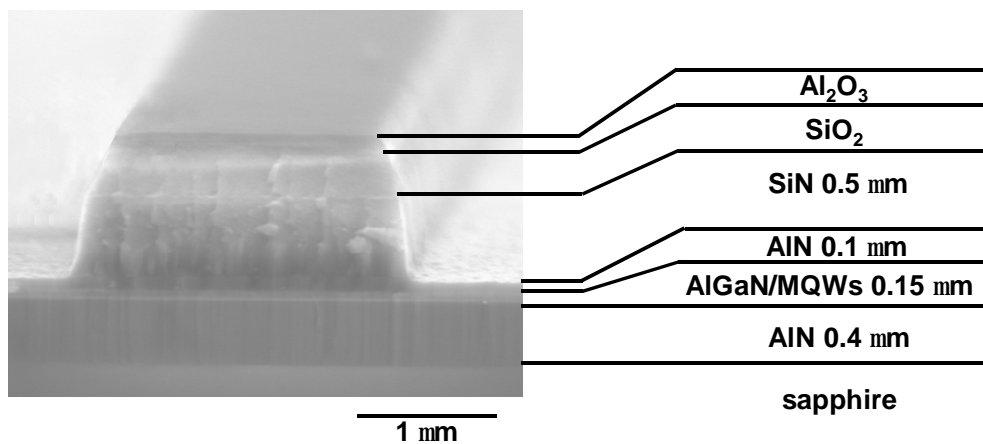
Fig. 5.12 SEM image of 2-μm wide ridge AlN-based waveguide

5.2.4 High-mesa AlN-Based Optical Waveguide

The high-mesa waveguide structure in this work was based on the ridge type but performed the deep etching of nitride layers as mentioned above. Figure 5.13 reveals the practical result by SEM image of a high mesa waveguide using the fabrication process from step 1 to step 5. Each layer was clearly observed separately from the others by different colors except the GaN/AlN MQWs and AlGaN layer. The Al_2O_3 layer was completely vanished while the SiO_2 layer was several removed by the nitride etching using Cl_2 gas. The roughness of sidewall of the high-mesa waveguide, which crucially affects the propagation loss, was a little bit rough. However, by looking at the entire structure, the intersubband transition characteristics should be expectedly observed from this sample. The two AlN-based waveguide structures, ridge type and

high-mesa type, have been successfully fabricated using the procedures described in the previous section. This indicates that the fabrication processes have been well performed but leaves room for further optimization. The measurement of intersubband transition characteristics in both samples is carried out in the next section.
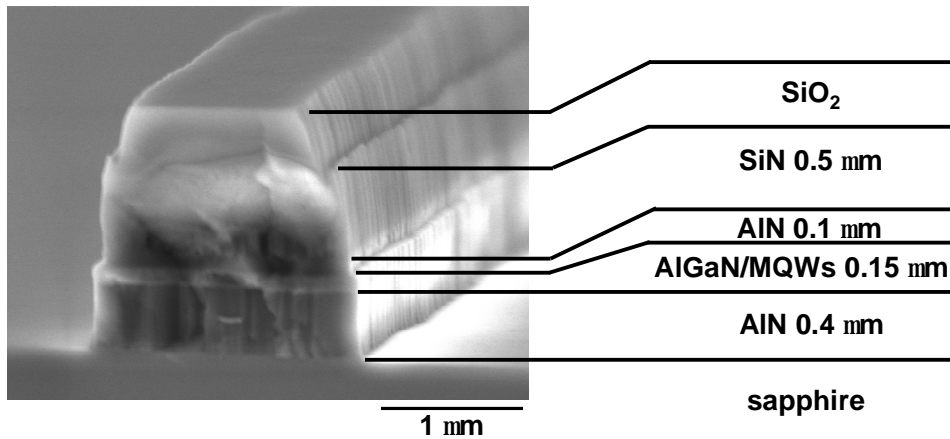
Fig. 5.13 SEM image of 2-µm wide high-mesa AlN-based waveguide

5.3 Intersubband Absorption in AlN-Based Waveguide with GaN/AlN MQWs Core

Before the measurement of intersubband transition characteristics in AlN-based waveguide, the functionality of waveguide should be confirmed by the light propagation test. A 1.55-µm light from a tunable laser is directly coupled to the waveguide. A lens is used for focusing the output from optical waveguide to an infrared camera. The functionality of the waveguide is considered from the near-field image of the propagating light. Captured by the infrared camera, Fig. 5.14(a) and 5.14(b) show the near-field images of propagating light through the ridge waveguide and the high-mesa waveguide which were fabricated in the last section, respectively. For the ridge type, the beams from the neighbor waveguides can also be seen as satellite spots. As shown in both figures, the round beams of propagating lights were clearly observed, indicating the functionality of fabricated waveguides. This means that the optical waveguides can be evaluated and characterized the intersubband transition properties in GaN/AlN MQWs.

88
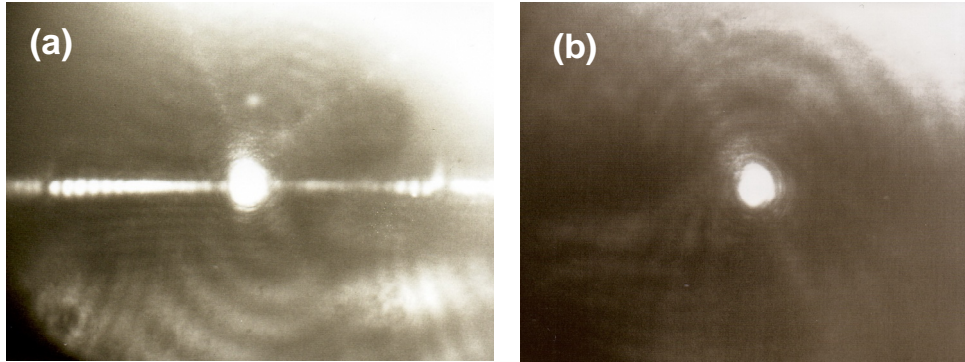
Fig. 5.14 Near-field images of propagating light through (a) ridge AlN-based waveguide
(b) high-mesa AlN-based waveguide which were fabricated in section 5.2

5.3.1 Measurement Setup Using Direct Coupling Method

In this section, the measurement and characterization of propagating light through optical waveguide is performed. The quantities and parameters especially concerned are propagation spectrum, propagation loss and polarization dependency. The measurement system called direct coupling method was setup as illustrated in Fig. 5.15 [46,111,120]. A supercontinuum light source was used as an ultra-wideband light generator. Supercontinuum generation is a process where laser light is converted to light with a very broad spectral bandwidth (i.e., low temporal coherence), whereas the spatial coherence usually remains high. The spectral broadening is usually accomplished by propagating optical pulses through a strongly nonlinear device, such as an optical fiber [121-126]. The supercontinuum light source in this work has a high power and wide range from 1100 nm to 1750 nm. Hence, it is suitable for the measurement of 1.5-µm-range intersubband transition which is the most interesting wavelength in this study. The supercontinuum light is directly coupled from a fiber to the waveguide and the propagating light from the opposite facet is focused to a small beam by 100X lens. The focused light is then directly coupled to a large-diameter multimode propagation fiber using a collimating lens, preparing for measurements by power meter or optical spectrum analyzer (OSA). To get rid of unnecessary information and noise, a pin hole is placed between the 100X lens and the collimating lens and filters only the light propagating through the waveguide. Because the supercontinuum light is typically non-polarization, the polarization of propagating light from the

89

waveguide can be selected by placing a polarizer behind the 100X lens. In the last, with the measurement setup, transmission spectra of both TE mode and TM mode light can be separately evaluated and characterized by OSA. Finally, intersubband transition properties can be analyzed using the fact that only TM mode light can be absorbed via intersubband transition which is so called the selection rule in quantum well.
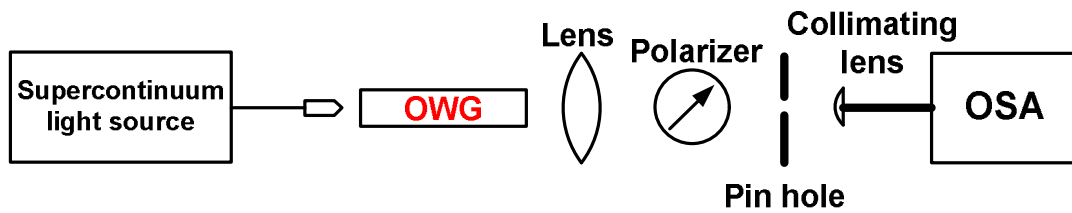
Fig. 5.15 Schematic diagram of measurement setup for intersubband transition characterization using direct coupling method

5.3.2 Characterization of Intersubband Transition in GaN/AlN MQWs Embedded in AlN-Based Optical Waveguide

The measurement results of intersubband transition characteristics in AlN-based waveguide both the ridge type and the high-mesa type are discussed and analyzed in this section. Before that, the optical loss occurs during the measurement is discussed and explained. Typically, we can classify the optical loss into two types. The first occurs within the optical waveguide which is called the propagation loss. The origins of propagation loss are defects in the waveguide, shape of the waveguide, roughness of the sidewall, optical leakage and multimode propagation. These are the parameters that can be controlled by carefully designing and fabricating of the waveguide. The second is the loss outside the optical waveguide. The optical coupling mismatch, reflection of light at cleaved area of the waveguide and scattering of light at cleaved area of the waveguide are classified as this loss. Figure 5.16 schematically shows the optical loss in the measurement classified into two groups, loss inside and outside of the optical waveguide. Before the measurement of optical waveguide, transmittance spectra of TE and TM mode light have been evaluated by fiber-to-fiber measurement to estimate the insertion loss of measurement system as illustrated in Fig. 5.17.
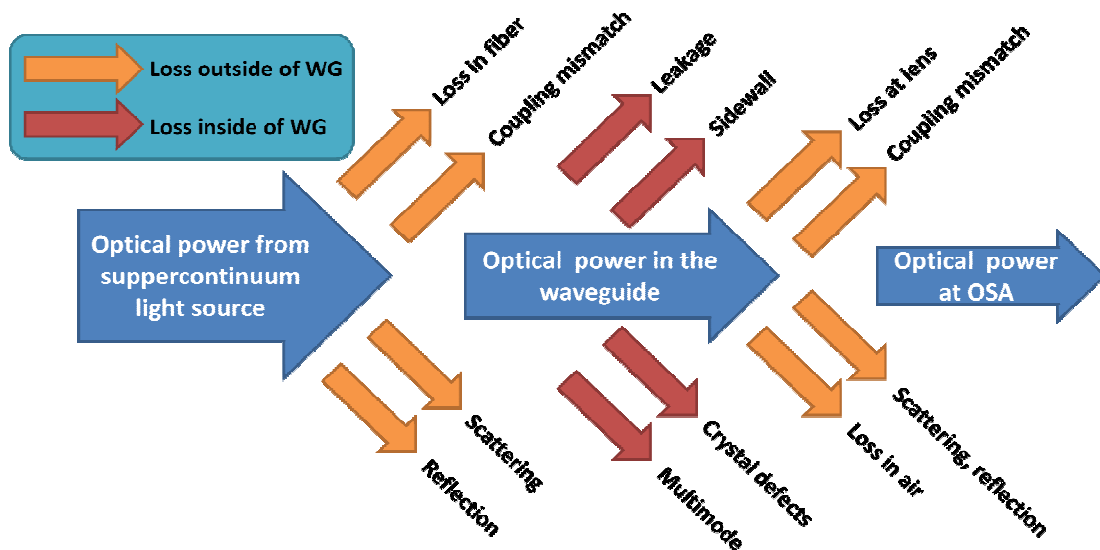
Fig. 5.16 Losses in the measurement of intersubband transition in AlN-waveguide
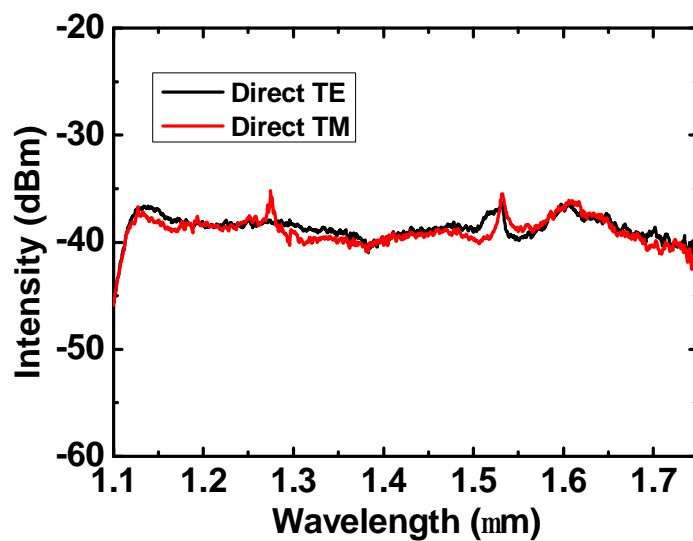
Fig. 5.17 Transmission spectra of TE mode light and TM mode light evaluated

by fiber-to-fiber measurement

1) Ridge optical waveguide

The transmission spectra of TE mode light and TM mode light in 400-µm-long ridge AlN-based waveguide with GaN/AlN MQWs core are plotted in Fig. 5.18(a). As mentioned before, the ridge waveguide is favorable for low propagation loss structure. Hence, by comparing with fiber-to-fiber propagation spectra in Fig. 5.17, the summation of propagation loss and coupling loss at input facet of the waveguide, which is a non-saturated loss, was noticeably low in TE mode light, i.e. around 5-6 dBm for the 400-µm-long waveguide. Obviously, we can clearly see that the transmittance of TM mode light had a valley which was an absorption peak covered the wavelength from 1.45 µm to 1.75 µm with a center around 1.57 µm and a full-width at half-maximum of 160 meV. Besides the propagation loss and coupling loss, this relatively large absorption was due to the intersubband transition in GaN/AlN MQWs. The polarization dependent transmission spectrum including absorption via intersubband transition approximated by the ratio of TM and TE (subtraction in the log scale) is also plotted in Fig. 5.18(b). Without any doubt, the strong intersubband absorption has firstly been realized in MOVPE grown AlN-based waveguide with GaN/AlN MQWs core. The absorption rate was around 21 dB in the 400-µm-long waveguide, estimated 52 dB/mm. The interference and resonance in ridge waveguide have minor effects on the transmission spectra so that we can observe smooth transmittances in both TE mode light and TM mode light.
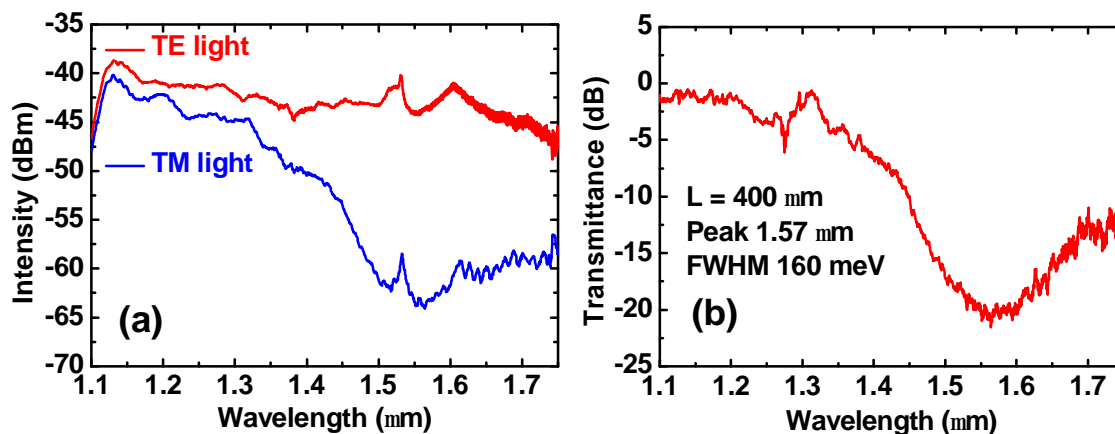
Fig. 5.18 (a) Transmission spectra of TE mode and TM mode lights and (b) TM/TE ratio in the 400-µm-long ridge AlN-based waveguide with GaN/AlN MQWs core

2) High-mesa optical waveguide

Similar with the ridge waveguide structure, the intersubband transition properties in GaN/AlN MQWs in high-mesa waveguide was evaluated by measuring the transmittance of TE mode light and TM mode light. The measurement results of 400-µm-long high-mesa waveguide are plotted in Fig. 5.19(a). It is clear that the propagation loss in this sample was noticeably lager than that in the ridge structure, estimated around 5-10 dB at all wavelength. The TE loss in this high-mesa structure was estimated around 10-15 dB over 400-µm-long waveguide. The larger loss than the ridge structure attributed to the low coupling efficiency at input facet and the roughness of sidewall of the waveguide which was not completely smooth (Fig. 5.13). Hence, the travelling light can easily be scattered at the rough sidewall resulting in a large propagation loss. The spike-like transmission spectra or oscillation were originated from the resonance and interference in the waveguide structure. This is evidenced by the fact that the oscillation changes with the alignment of fiber. Nevertheless, we can also clearly observe the absorption via intersubband transition in GaN/AlN MQWs by the ratio of TM and TE transmission spectra as evidenced in Fig. 5.19(b). The absorption region covered the wavelength from 1.45 µm to 1.75 µm with a peak around 1.60 µm and a full-width at half-maximum of 150 meV. The absorption rate was about 21 dB in 400-µm-long waveguide equaling to 52 dB/mm. The absorption via intersubband transition in this sample was similar to that of ridge waveguide regardless the large propagation loss in both TE- and TM-polarized light.
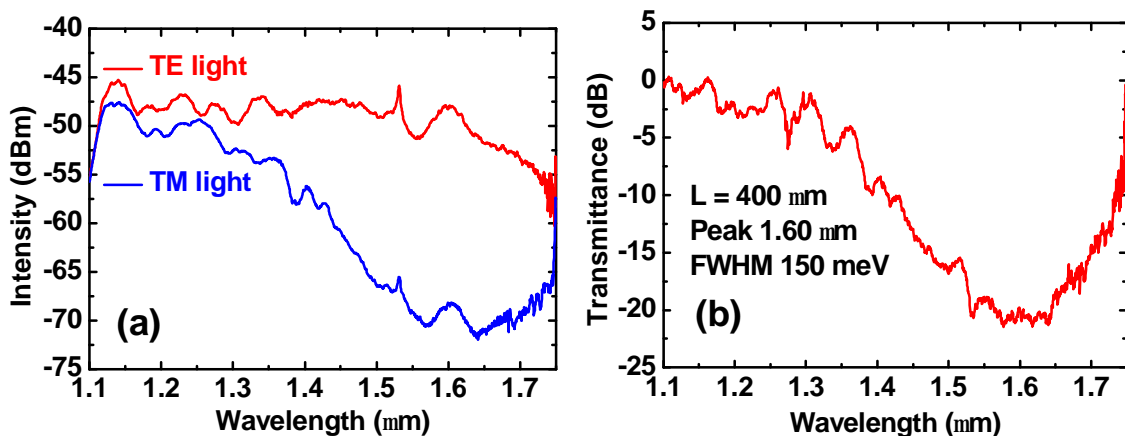
Fig. 5.19 (a) Transmission spectra of TE mode and TM mode lights and (b) TM/TE ratio in the 400-µm-long high-mesa AlN-based waveguide with GaN/AlN MQWs core

5.3.3 Comparison of Intersubband Absorption with Other Researches

The intersubband transition properties in AlN-based waveguide with GaN/AlN MQWs in this work are analytically compared with the data from the researches in Ref. 45, 120, labeled as sample "*A*", and in Ref. 46, 111, labeled as sample "*B*", which are the precedence of this thesis. Therefore, the fabrication processes from the growth to the device are partially similar while the measurement setup is same. The comparison of waveguide structures and related parameters are listed in the table 5.2. The major difference between this work and the others is that the GaN/AlN MQWs and cladding layers in this study were grown by MOVPE at low temperature instead of MBE. The doping concentrations in MBE grown samples, *A* and *B*, are approximately 5 times higher than the value which can be achieved in this work. Hence, the numbers of MQWs period are also different by the factor of 5. A great outstanding of this work is that the crystal growth processes can be performed by MOVPE at once compared with the regrowth by MBE in the other works. It should be noted here that, up to the present, the intersubband absorption in AlN-based waveguide with GaN/AlN MQWs grown by MOVPE is first observed in this work. The fabrication processes in this work were partially optimized owing to the investigations of sample *A* and *B*, i.e. the fabrications of waveguide with utilizing the low temperature MOVPE were different with the fully optimized processes of sample *B*. It should also be remarked that the coupling efficiency of the waveguides in this work was relatively low compared with the other since the lack of fine polishing process. Hence, the coupling loss in this work was not optimized and higher than that of the rest.

Figure 5.20 and 5.21 show the data of transmission spectra and TM/TE ratio of the sample *A* and *B*, respectively. Focusing on the results in Fig. 5.20(a), we can see that the propagation losses of TE mode and TM mode were greater than this work although the coupling efficiency was better. The absorption via intersubband transition was observed (Fig. 5.20(b)) which covered the wavelength from 1.15 µm to 1.65 µm with a center at 1.40 µm. This absorption result was not clear since the transmittance of TM mode light was very low which can easily be interfered from noise. Nevertheless, the absorption peaks was considerably broad compared to the results of both ridge waveguide and high-mesa waveguide in this work. The absorption rate was 25 dB in 400-µm-long waveguide, approximated 60 dB/mm, which was high considered the fact of high propagation loss.

Table 5.2 Lists of waveguide structure and related parameters of the AlN-base waveguide in this work and sample *A* and *B*

Parameter		This work	*A* [45,120]	*B* [46,111]
Year		2009	2006	2007
Sample	Buffer	MOVPE 0.4-µm AlN	MOVPE 0.4-µm AlN	MOVPE 0.4-µm AlN
	Interlayer	0.1-µm AlGaN	-	-
	MQWs	MOVPE 10xGaN/AlN	MBE 2xGaN/AlN	MBE 2xGaN/AlN
	Doping	2×10^{19} cm^{-3}	1×10^{20} cm^{-3}	1×10^{20} cm^{-3}
	Cladding	MOVPE 0.1-µm AlN/ 0.4-µm Si$_3$N$_4$	MBE 0.4-µm AlN	MBE 0.4-µm AlN
Waveguide	Structure	Ridge/ High-mesa	High-mesa	High-mesa
	Optimized	Partially	Partially	Fully
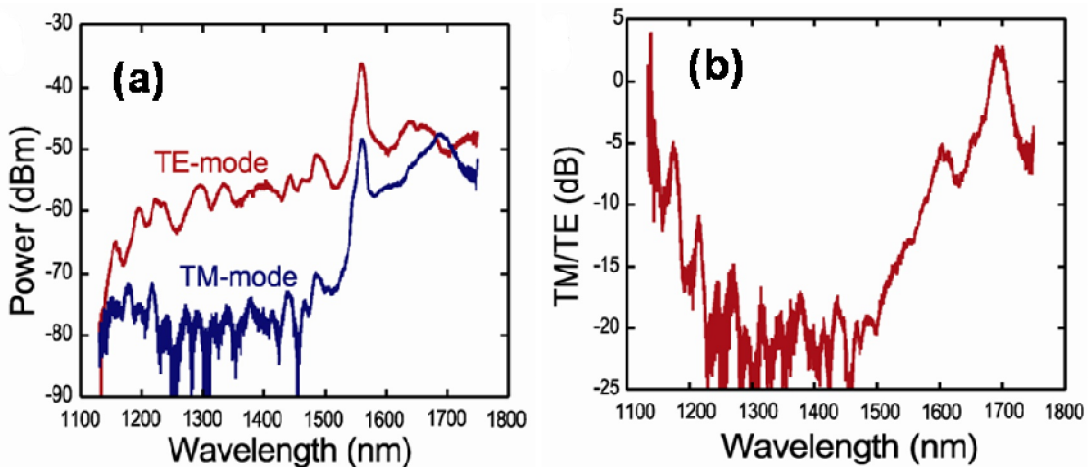
Fig. 5.20 (a) Transmission spectra of TE mode and TM mode lights and (b) TM/TE ratio in the 400-µm-long high-mesa AlN-based waveguide with MBE grown GaN/AlN MQWs core (sample *A* [45,120])

The result in Fig. 5.21 is the successor of the previous study in which the fabrication processes of the waveguide were fully optimized to achieve the lowest propagation loss. In addition, before the measurement, the backside of the sample was polished to improve the cleaved surface and coupling efficiency. Without doubt, the transmission spectra revealed the excellent propagation with low loss even in the high-mesa structure, completely outrunning the high-mesa waveguide in this work. However, the ridge waveguide in this work also exhibited comparably good transmittance spectra although the fabrication procedures were not fully optimized. The intersubband absorption peak was clearly observed from 1.30 µm to 1.65 µm with a peak center at 1.50 µm. The absorption strength was 25 dB over 800-µm-long waveguide equaling to 30 dB/mm. Comparing with 52 dB/mm in the ridge waveguide and the high-mesa waveguide in this work, it indicates that the optical waveguide in this study were well fabricated without the fully optimization.
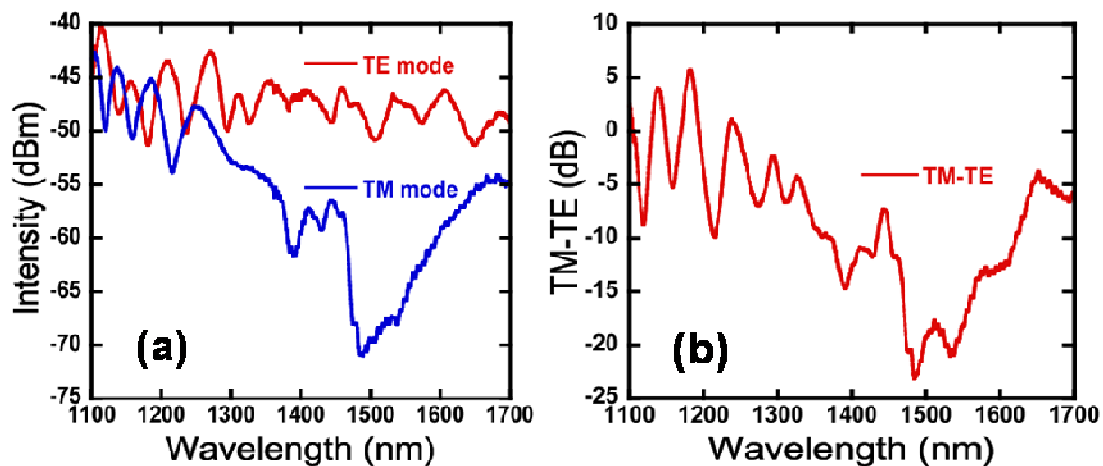
Fig. 5.21 (a) Transmission spectra of TE mode and TM mode lights and (b) TM/TE ratio in the 800-µm-long high-mesa AlN-based waveguide with MBE grown GaN/AlN MQWs core (sample B [46,111])

It has been clearly shown that the intersubband absorption in MOVPE grown AlN-based waveguide can competitive with the MBE grown sample which so long dominated the 1.5-µm-range intersubband transition in GaN/AlN MQWs as followed:

- The crystal quality of GaN/AlN MQWs and AlN upper cladding grown at low temperature are excellent. There is no evidence for addition losses from defects or dislocation in these layers.

- The carrier concentration in GaN wells grown at low temperature by pulse injection method is sufficient for intersubband absorption in AlN-based waveguide.

- The AlN upper cladding layer has been well optimized in which strong intersubband absorption can be achieved.

- The Si_3N_4 layer exhibits good performance as a cladding layer for nitride-based waveguide which can be deposited using sputtering method at low temperature.

This achievement is very promising for the optical device utilizing intersubband transition in nitride waveguide. Therefore, the non-linear properties and saturation of intersubband transition in the waveguide which determine the functionality of optical devices are investigated in the next section.

5.4 Intersubband Absorption Saturation in AlN-Based Waveguide with GaN/AlN MQWs Core

The saturation of intersubband absorption in GaN/AlN MQWs is one of the most importance characteristics for the optical devices utilizing saturation absorption including all-optical switch. The saturation can occur by exciting carriers from first subband energy level to higher subband energy levels, generally second subband. In this section, the attempt of evaluating the saturation absorption is carried out using high energy pulse laser.

5.4.1 Measurement Setup

It should be mentioned first that the measurement setup here is not the best configuration for observing the intersubband absorption saturation in GaN/AlN MQWs. This is because the intersubband relaxation in GaN/AlN MQWs is extremely fast [11-12,127-128]. Therefore, for evaluating the pumping energy required to saturate intersubband absorption, it is necessary to use

an ultrashort optical pulse which has a temporal width less than the intersubband relaxation time. In general, a femtosecond pulse generator with a pulse width around 150 fs is suitable for this purpose [12,23-25,44-47]. With the limitation of laboratory equipment here, the measurement of saturation absorption is carried out using self-saturation measurement instead of generally used pump-probe measurement. So that, the measurement cannot directly evaluate the required pumping energy in time-domain but determine the power of output light propagating in AlN-based waveguide with GaN/AlN MQWs core. The measurement system was setup according to the schematic diagram in Fig. 5.22. A 63-MHz 1.56-µm laser with a pulse width of 0.4 ps (FWHM) was generated from a laser diode (LD) and used as an exciting source. In order to maintain the pulse width, the measurement setup was designed and eliminated unnecessary component as much as possible. The intensity of optical pulse can be adjusted by using optical attenuator (OA). The TE mode and TM mode of the optical pulse was adjusted by a polarization controller (PC). The propagating light through the optical waveguide was collected by 100X lens. After filtering unnecessary light using a pin hole, the focused light was coupled to a multimode fiber using a collimating lens and analyzed by a powermeter. Before the measurement, the average power of input light with varying the optical attenuator was evaluated. The energy of pumping optical pulse was calculated by the product of the average power and the repetition rate of optical pulse.
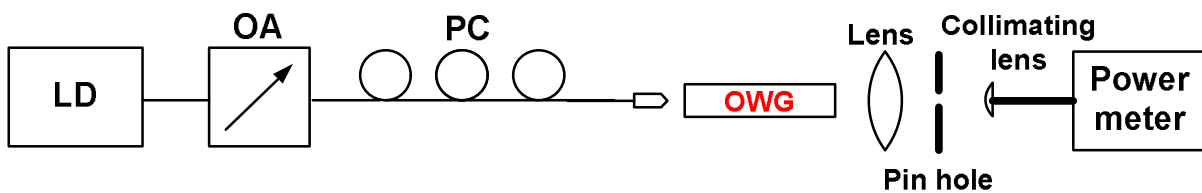
Fig. 5.22 Schematic diagram of self-saturation absorption measurement

5.4.2 Intersubband Absorption Saturation in Ridge AlN-Based Waveguide with GaN/AlN MQWs Core

The total loss in both TE- and TM-polarized light can be determined by the ratio of output power of TE-polarized light or TM polarized light and power of input light. The total loss

consists of coupling loss at both facets of a waveguide, the propagation loss, loss from defects in waveguide (only TM polarized light) and loss via intersubband absorption (only TM mode light). The coupling loss at the output facet of a waveguide can be estimated by measuring the power of optical pulse using fiber-to-fiber configuration, i.e. Fig. 5.22 but without waveguide. This coupling loss was estimated around 9 dB both TE and TM mode light. The coupling loss at input facet can be approximately determined by the calculation of coupling efficiency. The intersubband absorption saturation in the AlN-based waveguides both ridge and high-mesa structures are shown as following:

1) Ridge waveguide

The dependencies of total loss in both TE and TM mode light on the input pulse energy have been plotted in Fig, 5.23. Non-saturated TE-polarized loss was around 15 dB at each input energy value. By the mean of beam propagation method, around 36% of input power can be delivered in this structure which equals to 4.4 dB loss (ideal case). Since the coupling loss at output facet was 9 dB, around 1.6 dB was the summation of propagation loss in waveguide and scattering loss at facets. The propagation loss at most 1.6 dB over 400-µm-long waveguide was remarkably low. This waveguide utilized a merit of low dislocation MOVPE-grown layers. As can clearly observe, the absorption saturation occurred in TM-polarized light. 5-dB saturation can be achieved with an input energy of 115 pJ. This required input energy was relatively high compared with the record from Ref. 25 and Ref. 47 which 10-dB and 5-dB absorption saturation were reported using pumping energy of 38 pJ and 25 pJ, respectively. One of the explanations is that the temporal width of exciting pulse in this work was 0.4 ps, longer than the typical intersubband relaxation time, while the pulse widths used in Ref. 25 and 47 were 160 and 130 fs, respectively. N. Suzuki et al have calculated the influence of the pulse width on the saturation characteristics of the intersubband absorption [151] and found that the energy required for saturation decreases with decreasing the pulse width as evidenced in Fig. 5.24. Therefore, we can expect the better result using a short pulse width comparable with the record form Ref. 25 and 47. Nevertheless, this is the first result of the intersubband absorption saturation in MOVPE grown AlN-based waveguide with GaN/AlN MQWs core.
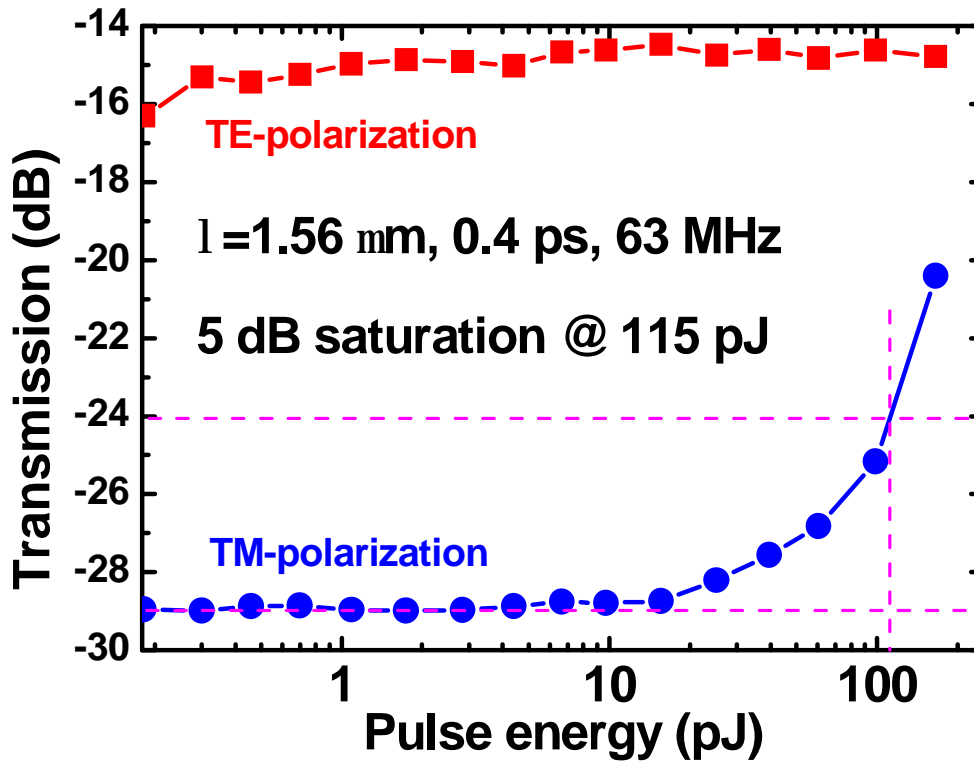
Fig. 5.23 Transmittances of TE and TM mode light in the ridge AlN-based waveguide with GaN/AlN MQWs core as functions of input pulse energy
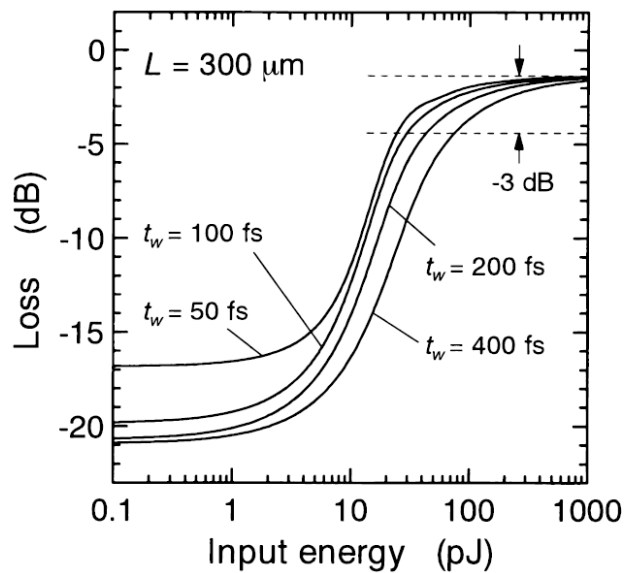
Fig. 5.24 Saturation Characteristics of the intersubband absorption for short pulse [151]

2) High-mesa waveguide

The transmission spectra of both TE- and TM-polarized light in the AlN-based high-mesa waveguide were evaluated using the same manner with the ridge structure and plotted as functions of input pulse energy in Fig. 5.25. In this high-mesa waveguide, the non-saturated total loss in TE mode light was around 24 dB. By the simulation, the power guided in this high-mesa structure was around 30%, or 5.2-dB loss equivalent. Since the coupling loss at output facet was 9 dB, the summation of propagation loss in the waveguide and scattering loss at facets was 9.8 dB, 8.2 dB higher than that in the ridge structure. The major cause of this high propagation loss in TE mode mainly attributed to the sidewall roughness of the waveguide. This propagation loss also affected the TM polarized light as a non-saturable loss. Because of this loss, the absorption saturation in TM-polarized light was difficult and needed large amount of input pulse energy. Only 3-dB absorption saturation can be achieved with a pulse energy of 145 pJ. It should be noted here that the extinction ratio at low pulse energy was not different in both structures.
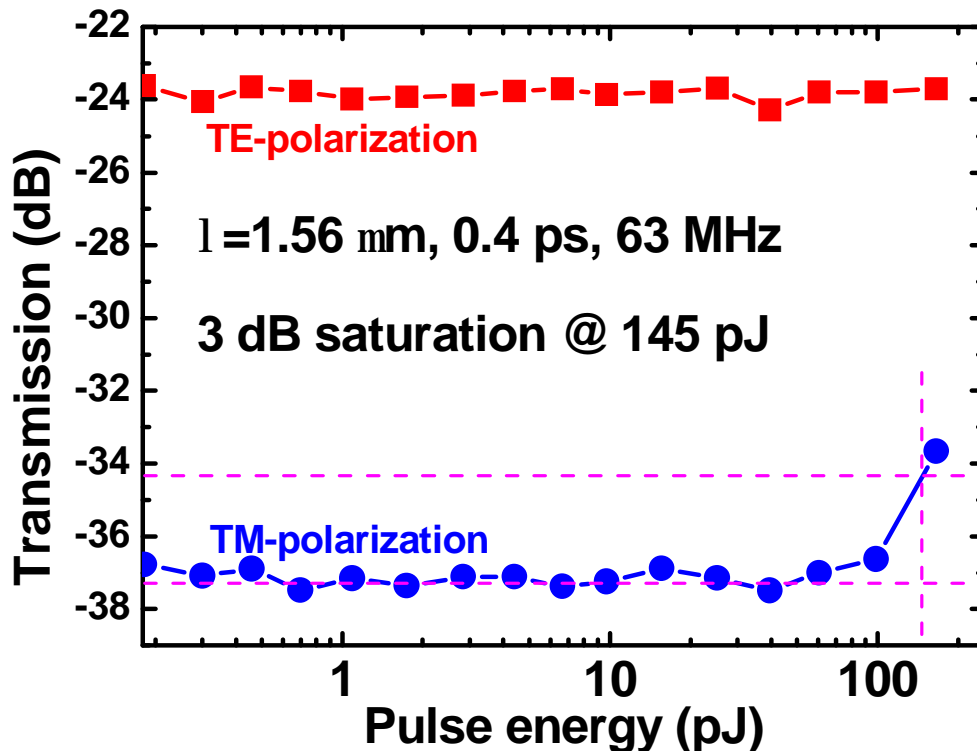
Fig. 5.25 Transmittances of TE and TM mode light in the high-mesa AlN-based waveguide with GaN/AlN MQWs core as functions of input pulse energy

The results of intersubband absorption saturation in the ridge and high-mesa waveguide indicate that the waveguides in this study can function and are promising for the fabrication of all-optical switch operated at communication wavelength. The issue of high required pumping energy can be further improved. First, the propagation loss can be suppressed by the improvement of crystal growth and waveguide fabrication. The background loss, originated from abnormal shape of waveguide including the roughness of sidewall, can be overcome by the designing of waveguide structure and improving fabrication process. The defects and dislocation in crystalline structure, causing extra propagation loss particularly in TM mode light, can be suppressed by improving the growth technique. Second, it is suggested that the required operating energy can be lowered by downsizing the cross-sectional area of the waveguide. Hence, although suffered from high propagation loss, the high-mesa structure is still promising for low-energy optical switches. The issue coupling loss in high-mesa structure can be overcome by introducing spot-size converters which is given thoroughly in the next chapter.

5.5   Conclusions

In this chapter, AlN-based waveguide with GaN/AlN MQWs core were designed and fabricated. The intersubband transition characteristics in fabricated waveguides were evaluated. The saturable intersubband absorption was observed in AlN-based waveguides both ridge and high-mesa structures.

1. The designing of AlN-based optical waveguide with GaN/AlN MQWs core has been done in order to realize low loss but high optical confinement waveguide. Two waveguide structures, ridge type and high-mesa type have been designed for the purpose of single mode propagation waveguides.

2. The ridge and high-mesa AlN-based waveguides have been successfully fabricated using ICP dry etching. However, the fabrication procedures can be fully optimized for the improvement of waveguide shape including sidewall roughness for the purpose of low propagation loss waveguide and low pumping pulse energy.

3. The world first intersubband absorption in as-fabricated AlN-based waveguides with GaN/AlN MQWs core grown by MOVPE has been observed and characterized. Both

ridge and high-mesa waveguides exhibited excellent intersubband absorption peaks with an absorption rate of 52 dB/mm for each samples.

4. The intersubband absorption characteristics in AlN-based waveguides with GaN/AlN MQWs fabricated by MOVPE have been compared with the MBE grown samples. The results of MOVPE grown samples are in the same league with the MBE grown sample.

5. By self-saturation measurement using 1.56-μm pulse laser with a temporal width of 0.4 ps and repetition rate of 63 MHz, 5-dB absorption saturation has been observed in a 400-μm-long ridge waveguide using pumping energy of 115 pJ. The propagation loss in this ridge waveguide was remarkably low. However, suffering from high propagation loss due to sidewall roughness, only 3-dB absorption saturation has been achieved in a 400-μm-long high-mesa waveguide using pumping energy of 145 pJ. The lower pumping energy can be expected using a shorter exciting optical pulse.

6. These results confirm the functionality of fabricated AlN-based waveguide with GaN/AlN MQWs core. The performance can be further enhanced by optimizing the fabrication process and using a better measurement setup.

In the next chapter, the AlN-based waveguide with integrated spot-size converters promising for enhancement of the coupling efficiency and lowering the saturation energy has been investigated.

Chapter 6 Fabrication of AlN-based Optical Waveguide with Integrated Spot-Size Converter

T he ridge AlN-based optical waveguide fabricated in the last chapter exhibited 5-dB absorption saturation with an input pulse energy of 115 pJ which was still high. This can be explained by the large lateral dimension of the GaN/AlN MQWs core. Hence, the down scaled cross-sectional area of waveguide is one method in order to lower the required pulse energy for intersubband absorption saturation. In contrast with the ridge waveguide, the high-mesa structure possesses a better optical confinement with relatively small cross-sectional area of the MQWs core. From this reasons, the high-mesa waveguide can be considered as a solution for the issue of high pumping energy. The interesting structure, however, exhibited poor propagation spectra both in TE and TM modes because of excess loss from waveguide shape including sidewall roughness. This issue can be suppressed by careful fabrication. Moreover, the coupling efficiency of optical pulse from single-mode fiber to the waveguide is considerably lower than that of the ridge waveguide causing ineffective power transmission. In this chapter, the spot-size converter (SSC) integrated to AlN-based waveguide is introduced as an effective method for achieving high coupling efficiency in the downscaled cross-sectional waveguide. The brief introduction of spot-size converter is given followed by the designing of spot-size converter in section 6.1. After that, in section 6.2, the fabrication process which utilizes the ICP dry etching is explained in detail. The characterization of intersubband absorption and the absorption saturation in fabricated structure is evaluated in section 6.3. The last section is the conclusions of this chapter.

6.1 Spot-Size Converter

6.1.1 Introduction

In fiber-optical network, most of optical components consist of III-V semiconductor devices. As each of these devices is connected to at least one optical fiber, it is important to obtain a good coupling of light between optical device and fiber. In a semiconductor optical waveguide, the cross-sectional area is, generally, smaller than the spot-size of a light beam from optical fiber. This is because of the mode size of semiconductor waveguide is typically small due to refractive index of semiconductor. In addition to the cross-sectional area, the field mismatch, due to the geometrical contrast between fiber (cylindrical) and semiconductor (rectangular) is considered as an origin of coupling loss.

Focusing on the ridge AlN-based waveguide fabricated in this study, it is obvious that the intersubband absorption saturation required a great amount of pumping energy. As consider an origin of this issue, the lateral size of GaN/AlN MQWs is suggested to be down-scaled by fabricating the high-mesa waveguide structure. However, the issue of coupling loss from a fiber to high-mesa waveguide becomes more serious when the cross-sectional area of the waveguide is small. Although, there are several methods to improve the fiber-to-waveguide coupling efficiency including the use of microlens or taper fibers [129-130], these methods still suffer from the difficult of the alignment and the fabrication cost. The other effective approach to achieve an effective coupling is the integration of spot-size converter to the waveguide. Although, there are several types of spot-size converter, they share a similar idea which one facet size is large for good coupling with optical fiber and diverges light to the small facet to couple with waveguide. Figure 6.1, 6.2 and 6.3 schematically show various types of spot-size converters using lateral tapers, vertical tapers and combined lateral and vertical tapers, respectively [131]. However, those types of spot-size converters have been designed for silicon and arsenide-phosphide semiconductors which are not fully compatible with III-nitride semiconductors. One of reasons is that III-nitride, especially GaN/AlN MQWs and the other epilayers, are typically hexagonal structure which anisotropic wet etching is not available. Moreover, the hardness and robustness of nitride semiconductors to almost all of wet etchants make the fabrication of patterned nitride semiconductors more difficult. Because of these reasons, the spot-size converter

for AlN-based waveguide should be designed for compatibility with available nitride semiconductors related fabrication processes.
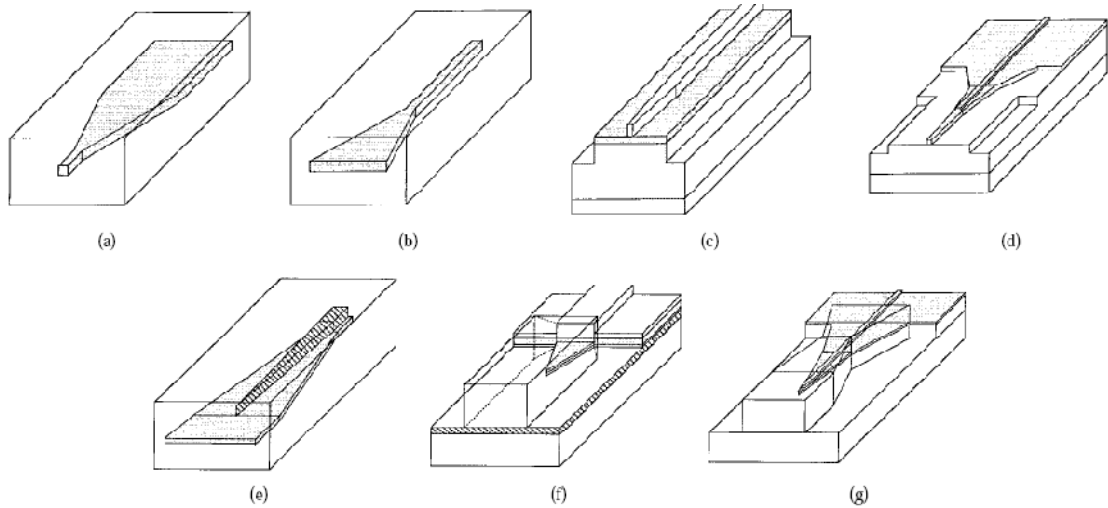
Fig. 6.1 Lateral taper designs: (a) Lateral down-tapered buried waveguide. (b) Lateral up-tapered buried waveguide. (c) Single lateral taper transition from a ridge waveguide to a fiber-matched waveguide. (d) Multisection taper transition from a ridge waveguide to a fiber-matched waveguide. (e) Dual lateral overlapping buried waveguide taper. (f) Dual lateral overlapping ridge waveguide taper. (g) Nested waveguide taper transition from a ridge waveguide to a fiber-matched waveguide. [131]
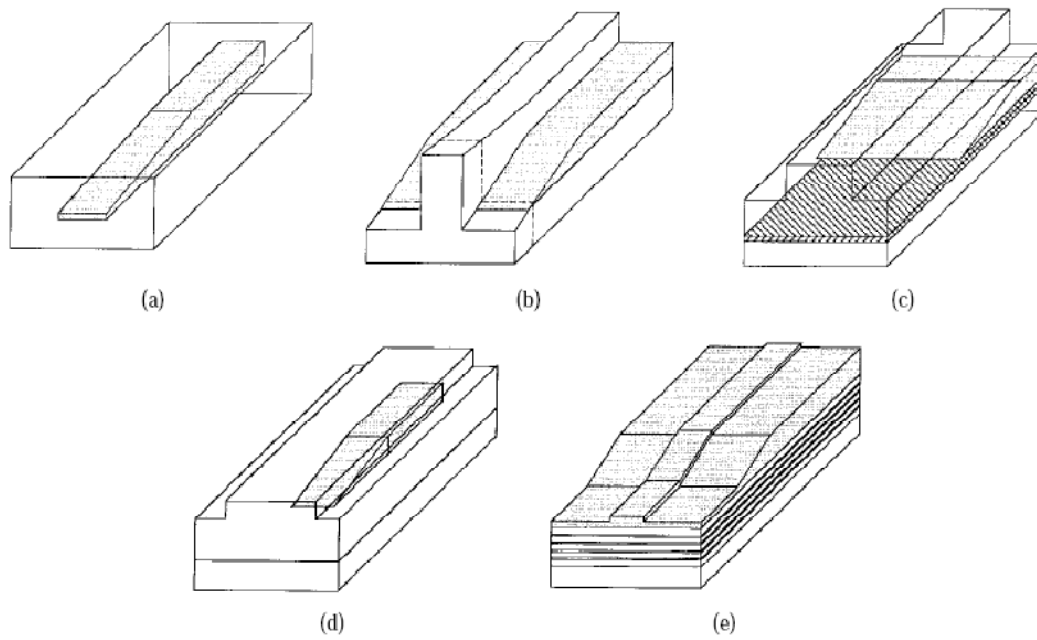
Fig. 6.2 Vertical taper designs: (a) Vertical down-tapered buried waveguide. (b) Vertical down-tapered ridge waveguide. (c) Vertical overlapping ridge waveguide taper. (d) Vertical overlapping waveguide taper transition from a buried waveguide to a fiber-matched waveguide. (e) Vertical overlapping waveguide taper transition from a ridge waveguide to a fiber-matched waveguide. [131]
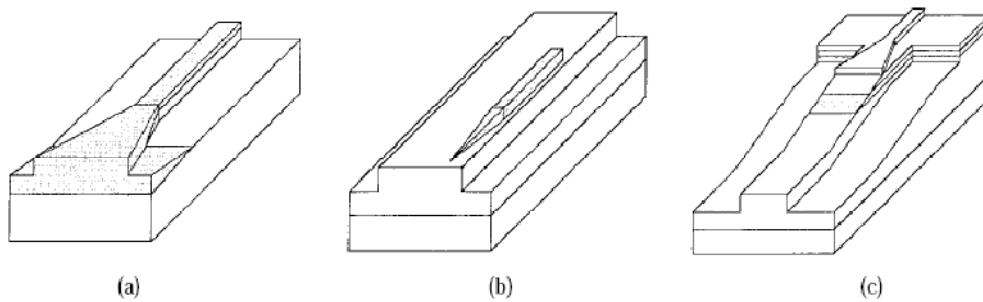
Fig. 6.3 Combined vertical and lateral taper designs. (a) Combined lateral and vertical ridge waveguide taper. (b) 2-D overlapping waveguide taper transition from a buried waveguide to a fiber-matched waveguide. (c) Overlapping waveguide taper transition with two sections from a ridge waveguide to a fiber-matched waveguide. [131]

108

6.1.2 Design of AlN-Based Waveguide With integrated Spot-Size Converter

The spot-size converter in this study has been designed based on available nitride fabrication technologies while the fabrication procedures should be simple. Figure 6.4 shows the design of the AlN-based waveguide with integrated spot-size converters. The structure consists of three parts: the guiding region, the taper region and the active region. The Si_3N_4 layer is employed as spot-size converter region. As illustrated in the figure, AlN/MQWs core is buried between Si_3N_4 upper cladding and AlN lower cladding. Hence, the active core is down-scaled and the spot-size converter couples and transmits light from and to optical fibers.

The dimensions of guiding part and spot-size converter were, therefore, designed for achieving a good coupling efficiency. Since, the thicknesses of AlN buffer layer, AlGaN interlayer, GaN/AlN MQWs and AlN upper cladding layer as well as the width of absorption core have already been designed in the last chapter, only spot-size converter was simulated by varied the height (H), width (W) and taper length (L) as illustrated in Fig. 6.4. Therefore, the MOVPE growth structure consists of AlN buffer/AlGaN interlayer/MQWs/AlN upper cladding layer with the thicknesses of 0.4-μm, 0.1-μm, 0.045-μm and 0.1-μm, respectively. First, by the mean of beam propagation method (BPM), the coupling efficiency at junction between taper and active core was calculated by (a) fixing H at 3 μm and varying L and W and (b) fixing W at 4 μm and varying L and H. The simulation results are shown in Fig. 6.5(a) and 6.5(b), respectively, Note that the diameter of beam spot from fiber was set as 3 μm. The value of coupling efficiency which is functions of dimensions of spot-size converter is shown in the color mapping with the color bar. It is indicated by both results that, when the length of taper is 15-20 μm and 32-37 μm, the value of coupling efficiency is relatively large and tolerance to the height and width of spot-size converter. Since, the diameter of a light beam from optical fiber is around 3-μm, the spot-size converter of 4-μm-wide (W) is reasonably enough for coupling most of input light. The problem is the height of spot-size converter. Although it was suggested from the simulation results that the height of Si_3N_4 layer of spot-size converter part should be more than 1.5-μm-height for the best coupling efficiency, such a thick Si_3N_4 layer resulted in the multimode propagation in the active region which decreased the power coupled to the MQWs core. This can be solved by using a stair-step etching at the taper part of the structure to make vertical spot-size converter. In fact, the fabrication procedures will become much more difficult and need a very

advance technique and skill. So that, in this thesis, the designing of spot-size converter focused on the lateral spot-size converter. The propagation mode of light in the active region was calculated to find the thickest Si_3N_4 layer which allows single mode propagation in the active region. Hence, the simulation suggested that the Si_3N_4 layer should be 0.8-μm-thick. The length of active core was varied as 100, 200 and 400 μm long. The total of entire structure was 1000 μm by adjusting the length of guiding region according to the length of active region. The top view and the side view of final structure is showed schematically in Fig. 6.6
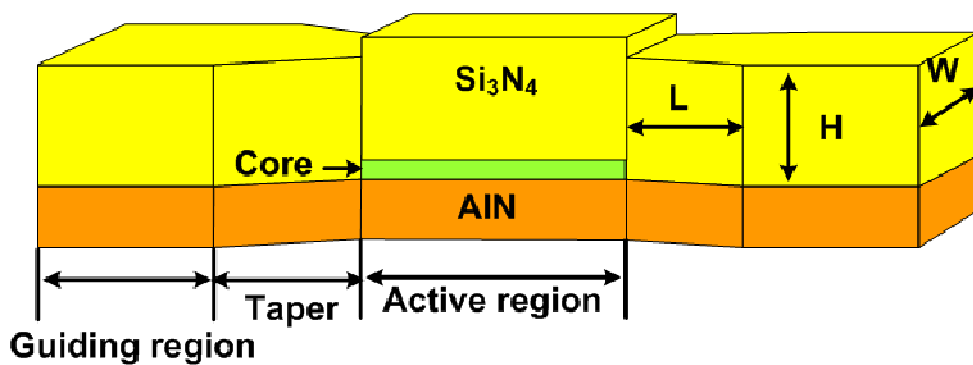
Fig. 6.4 The designed structure of AlN-based waveguide with integrated spot-size converter, the parameters H, W and L represents the height, width and length of the taper region, respectively.
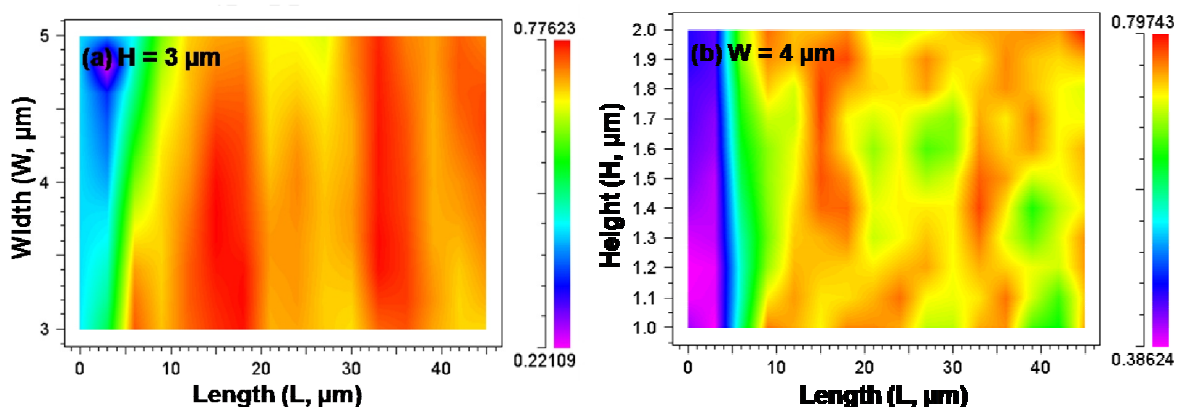
Fig. 6.5 Simulation results of coupling efficiency between 3-μm-diameter optical fiber and AlN-based waveguide with integrated spot-size converter: (a) Fixing H = 3 μm, varying W and L and (b) Fixing W = 4 μm, varying H and L. (Simulated by Haruhiko Yoshida, Corporate Research & Development Center, Toshiba Corporation)

110
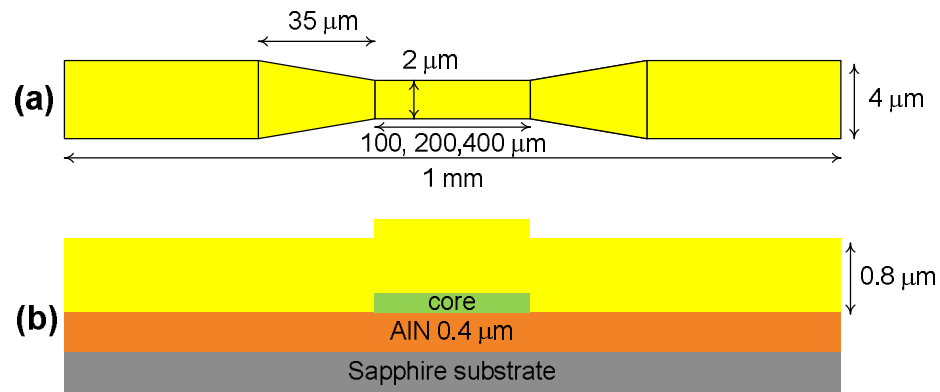
Fig. 6.6 The final designed structure of AlN-based waveguide with integrated spot-size converter: (a) top view and (b) side view

6.2 Fabrication of AlN-Based Waveguide With integrated Spot-Size Converters

6.2.1 Fabrication Procedures

The fabrication procedures of AlN-based waveguide with integrated spot-size converter are partially similar to that of AlN-based waveguide. Figure 6.7 is giving an extensive scope of all fabrication processes in order to make the explanation easier and clearer. The fabrication procedure employs six steps including two photolithography processes, Si_3N_4 sputtering, EB-evaporating and two ICP dry etchings. The details are described as followed:

1) Photolithography

The sample was deposited nitride semiconductor layers by MOVPE and cleaned with acetone 5 minutes, followed by isopropanol 5 minutes. Then, the cleaned sample was dried with N_2 gun and baked at 120 ℃, 10 minutes to eliminate remaining isopropanol. The photolithography was conducted using a positive resist, TSMR8900 which is hard enough for a mask to etching core layer. The conditions were listed below:

    1. Spin Coating

    a. 1st step: 500 rpm, 5 sec

    b. 2nd step: 6000 rpm, 40 sec

2. Prebaking: 110 ℃, 90 sec

3. Exposure: 4.5 sec, hard contact with mask

4. Developing: Tetra-methyl-Ammonium-Hydroxide (TMAH, NMD3) 1min

5. Post baking: 120 ℃, 60 sec

The expose time can be adjusted according to the intensity of Hg lamp. Note that, the hardness of TSMR photoresist depends on the baking temperature and time. The higher temperature and longer time results in harder resist but more difficult to be cleaned after etching.

2) Core removal by ICP dry etching

After patterning the mask, the core layer consisting of AlN upper cladding layer and GaN/AlN MQWs was therefore etched by ICP dry etching using mixture Ar:Cl$_2$ gases, 2:8 sccm. The two-step etching was employed using same conditions as listed in the table 6.1, except the time intervals which are 60 sec and 30 sec for the first step and the second step, respectively. The time of each steps required for core etching were estimated and determined by using a dummy sample. Because there is no etching stopper layer compatible with nitride semiconductors, the etching depth can only be controlled by etching times. Lots of spikes, which were unetched core layer, generally remained after ICP dry etching can be removed by dipping the sample into TMAH (70 ℃, 45 sec). After that, the remaining TSMR-8900 photoresist was completely cleaned by boiled acetone and boiled isopropanol and dried with N$_2$ gun.

3) Si$_3$N$_4$ sputtering

As-cleaned sample was deposited Si$_3$N$_4$ layer by an RF magnetron sputtering machine. The sputtering was done under Ar and N2 ambient at 250 ℃ with the designed thickness of 0.8 μm.

4) 2nd photolithography

After cleaning and baking the sample, the AZ-5214 negative photoresist was spin-coated for a mask used in lift-off technique. The condition of photolithography can be referred with the chapter 5, section 5.2.2.

5) EB-evaporating and lift-off

The sample with the mask was deposited 300-nm-thick SiO_2 and 200-nm-thick Al_2O_3 by electron-beam evaporator. Then, the lift-off process was carried out using hot acetone and isopropanol.

6) Waveguide etching

The AlN-based waveguide with integrated spot-size converter was fabricated by ICP dry etching. First, the Si_3N_4 etching was perform followed by nitride etching which the etching conditions can be referred with section 5.2, chapter 5. After that, the remaining spikes were removed by wet treatment using TMAH.
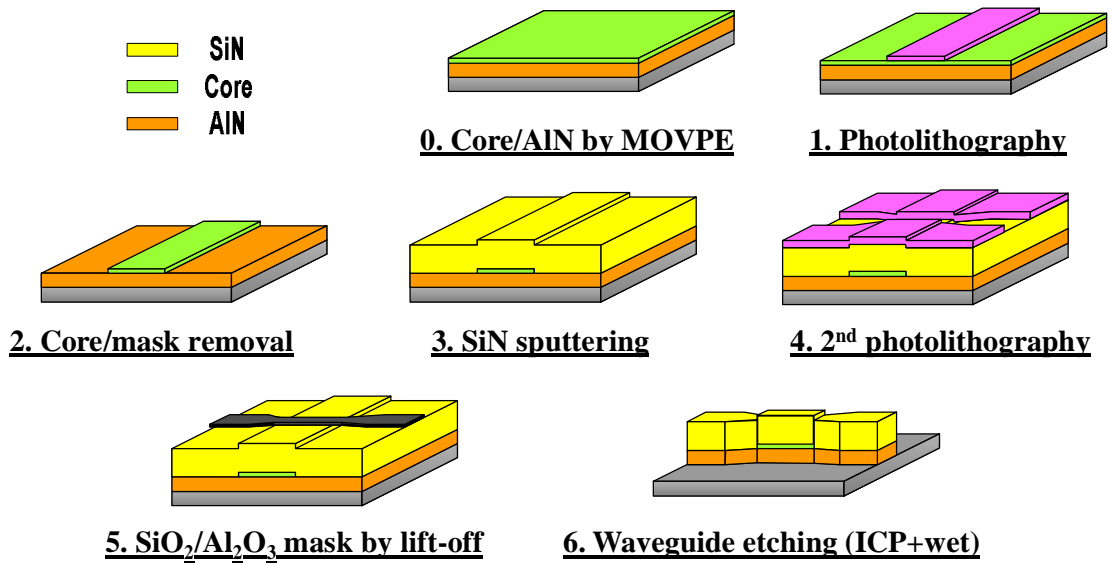
Fig. 6.7 Fabrication process of AlN-based waveguide with integrated spot-size converter

With the above fabrication procedures, AlN-based waveguide with integrated spot-size converter was fabricated. The fabrication results are revealed in the next section.

6.2.2 AlN-Based Waveguide with integrated Spot-Size Converters

The dimension and shape of fabricated structure were evaluated by SEM images. The pictures AlN-based waveguide with integrated spot-size converter are shown in Fig. 6.8(a) to 6.8(d) for the images of (a) top view, (b) cross-sectional active region, (c) cross-sectional guiding region, and (d) side view of junction between active region and guiding region, respectively. We can see that the AlN-based wave guide as well as spot-size converter were well fabricated. The top view shows an array of 3 waveguides which the active region, taper and guiding region were clearly observed. The shape of waveguide both in active region and guiding region was not perfectly rectangular due to the over-etch Si_3N_4 layers during the nitride etching. Observing in Fig. 6.8(b) to 6.8(d), the sidewall of the waveguide was quite smooth. In the Fig 6.8(d) the junction between active region and guiding region was clearly seen together with the absorption core embedded in the active region. In addition to the SEM scans, the quality of AlN-based waveguide with integrated spot-size converter was examined using a near-field image. The 1.55-µm light was directly coupled to the waveguide which was cleaved by cutting with a diamond-pen. The near-field image of output light from the waveguide was captured by an infrared camera. The round shape of beam indicates the functionality of fabricated AlN-based waveguide which the intersubband absorption should clearly be observed in this sample.
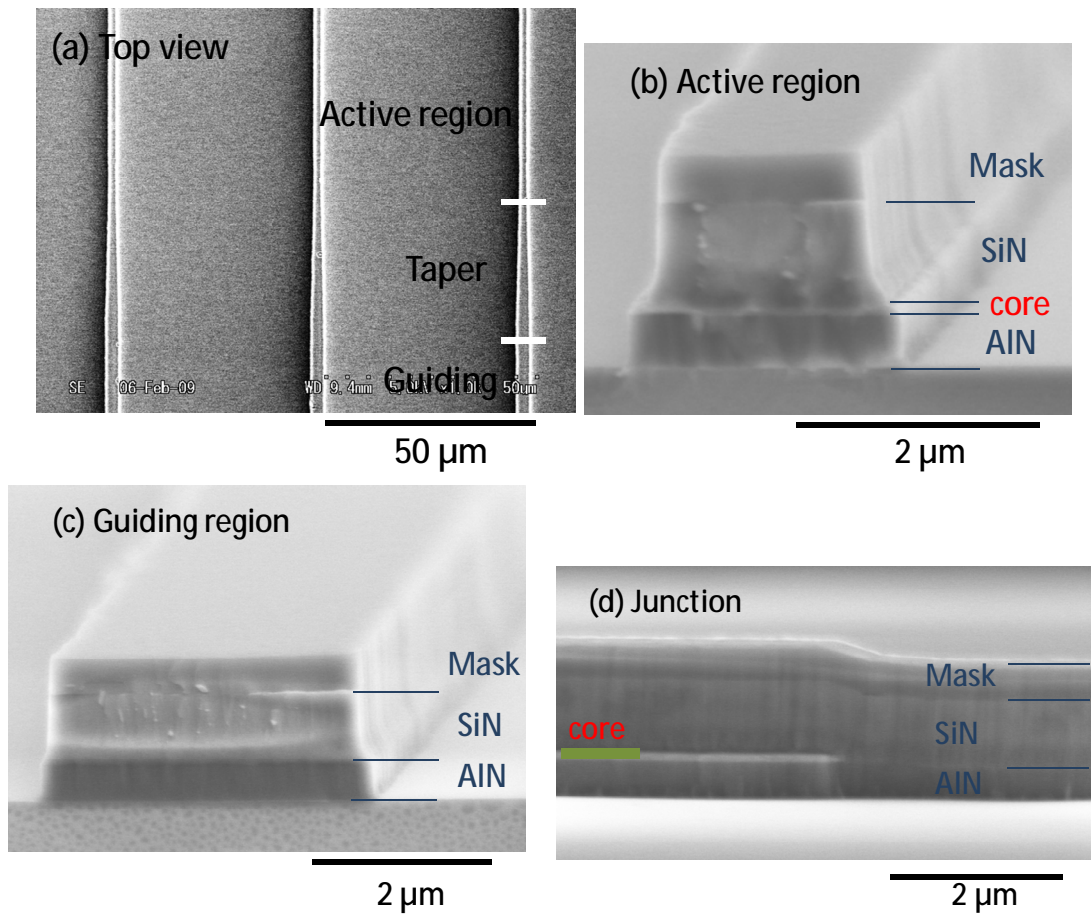
Fig. 6.8 SEM images of AlN-based waveguide with integrated spot-size converter:
(a) top view, (b) cross-sectional active region, (c) cross-sectional guiding region, and
(d) side view of junction between active region and guiding region
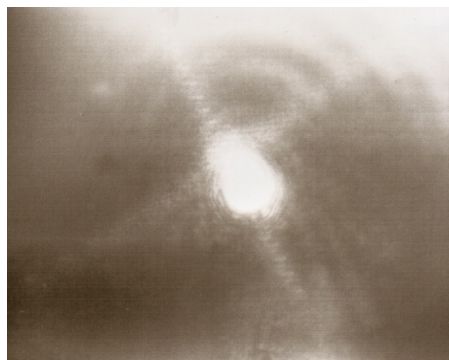
Fig. 6.9 Near-field images of propagating light in fabricated AlN-based
waveguide with integrated spot-size converter

115

6.3 Intersubband Characteristics in AlN-based Waveguide with Integrated Spot-Size Converter

6.3.1 Intersubband Absorption

After testing the functionality, the AlN-based waveguide with integrated spot-size converter was evaluated the intersubband transition properties by transmission spectra of propagating light both TE mode and TM mode. The measurement setup was similar with the setting in Fig. 6.15. The back-side-polished sample was cleaved by cutting with a diamond-pen. The transmission spectra of TE mode light and TM mode light in a waveguide with 400-μm-long active core were plotted in Fig. 6.10(a). For comparison, the spectra of propagating light in the ridge AlN-based waveguide and in high-mesa AlN-based waveguide were also shown in Fig. 6.10(b) and 6.10(c), respectively. The y-axis of each figures were intentionally balanced. As can obviously see, compared with the ridge waveguide, the AlN-based waveguide with integrated spot-size converter had similar loss in TE mode at 1.5-μm-range but a little poorer at short wavelength. This indicated that the deeply etched structure had smooth sidewall and good waveguide shape so that the total loss in TE-polarized light was comparable with that of ridge structure. Compared with the propagation loss in the high-mesa waveguide, the propagation loss in AlN-based waveguide with integrated spot-size converter was much improved although the two structures had similar active core shape. Considering the AlN-based waveguide with integrated spot-size converter, the propagation loss in TM mode light was noticeably large especially at short wavelength range. Since this TM-polarization loss was not found in the ridge and the high-mesa AlN-based waveguide, the fabrication procedures of spot-size converter induced some additional loss to TM-polarized light including (1) interface roughness between AlN buffer layer and Si_3N_4 layer during the ICP dry etching of MQWs core and (2) sidewall roughness of etched MQWs core. N. Iizuka et al. has reported excess TM polarization loss caused by edge dislocations parallel to the growth axis [24]. The edge dislocations introduce acceptor centers along the dislocation lines and electrons are captured by the acceptor centers [152,153]. Then, charges perpendicularly align and work like a wire-grid polarizer [44]. Hence, the damages along the growth direction occurred during MQWs removal process by ICP-RIE can induced excess TM-polarization loss in the same manner evidenced by propagation spectrum of TM mode light in Fig. 6.10(a). Figure 6.11(a) shows the SEM image of the sample after

MQWs removal process. It clearly displays the damages induced by ICR dry etching especially the damage perpendicular to the surface which can be act as a wire-grid polarizer as shown in Fig. 6.11(b). The oscillations in transmission spectra of light in AlN-based waveguide with integrated spot-size converter are due to the reflection and resonance in the waveguide especially at the spot-size converter regions.
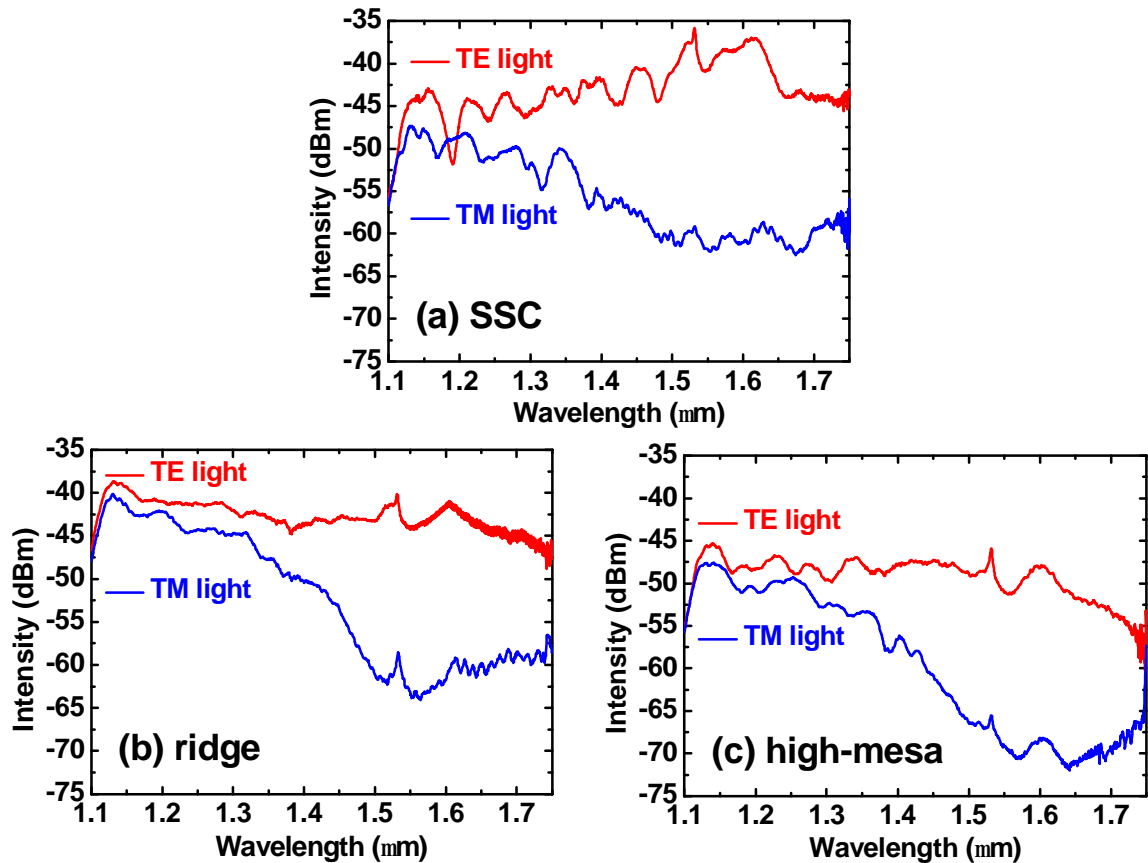
Fig. 6.10 Transmission spectra of TE mode light and TM mode light in (a) AlN-based waveguide with integrated spot-size converter, (b) ridge AlN-based waveguide and (c) high-mesa AlN-based waveguide
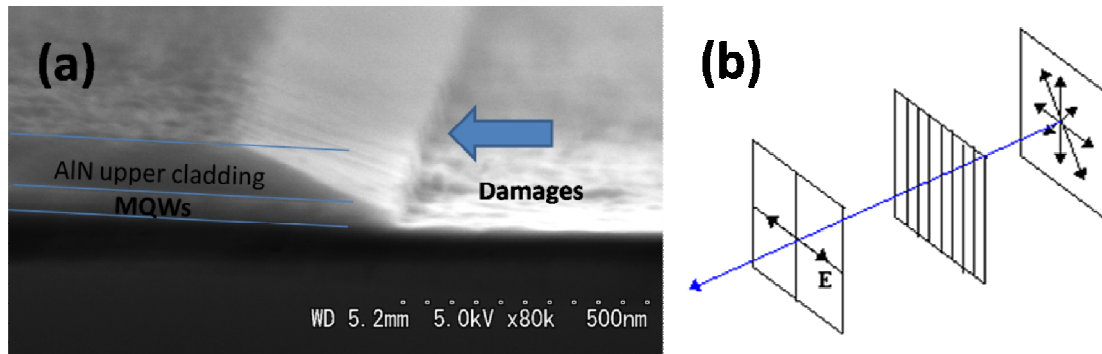
Fig. 6.11 (a) SEM image of the sample after MQWs removel showing the damages induced by ICP- dry etching (b) wire-grid polarizer passing only the component that perpendicular to the grid

The analyzing of polarization dependent transmission spectra including absorption via intersubband transition has been done using the ratio of TM mode light transmittance to TM mode light transmittance (subtraction in log scale). The results of the AlN-based waveguide with integrated spot-size converter, ridge waveguide and high-mesa waveguide are plotted as functions of wavelength in Fig. 6.12(a), 6.12(b) and 6.12(c), respectively. The absorption intensity in AlN-based waveguide with integrated spot-size converter was around 24 dB in 400-µm-long active core which was slightly higher than the ridge AlN-based waveguide and the high-mesa AlN-based waveguide. It can be explained by the additional non-saturated TM-polarization losses due to the fabrication of spot-size converter. It was also evidenced by large absorption at short wavelength range. The polarization dependent loss including absorption via intersubband transition was cover the wavelength from 1.35 to 1.75 µm with a peak at 1.59 µm and a full-width at half maximum of 160 meV. It should be noted that all of the AlN-based waveguides in this work were fabricated using a same epitaxial wafer.
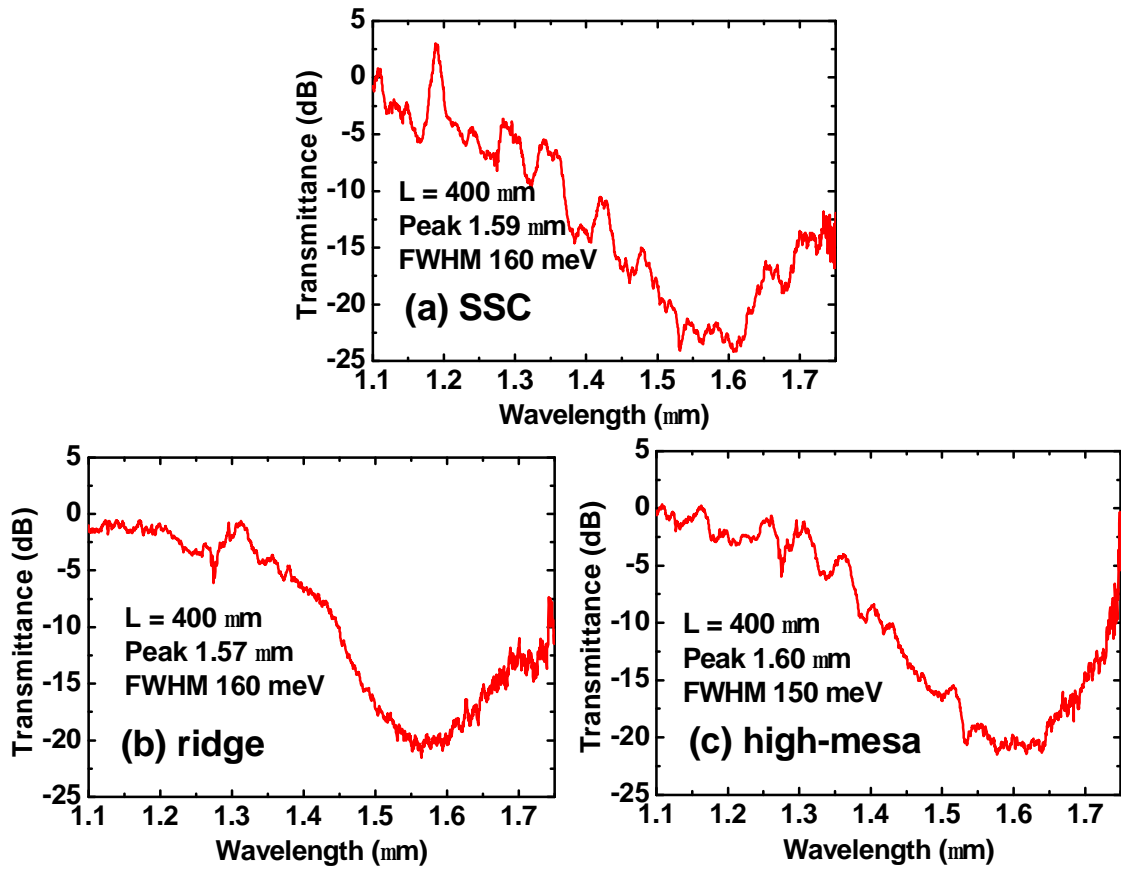
Fig. 6.12 Polarization dependent of transmission spectra including absorption via intersubband transition in (a) AlN-based waveguide with integrated spot-size converter, (b) ridge AlN-based waveguide and (c) high-mesa AlN-based waveguide

6.3.2 Intersubband Absorption Saturation

The original purpose of introducing the spot-size converter to AlN-based waveguide is to reduce the required pumping pulse energy for intersubband absorption saturation. In the previous chapter, the ridge AlN-based waveguide exhibited 5-dB absorption saturation with the pumping energy of 115 pJ. Therefore, the AlN-based waveguide with integrated spot-size converter should theoretically exhibit 5-dB absorption saturation at lower pumping power or deeper absorption saturation at 115 pJ pumping energy. The measurement was carried out in the same manner with the measurement of intersubband absorption saturation in chapter 5, section 5.4. The AlN-based waveguide with integrated spot-size converter evaluated in this study had a 400-

μm-long active core with the total length of 1 mm. The measurement result is shown in Fig. 6.13. The y-axis is the power transmittance of propagation light in dB unit, determined by the difference between the transmission power and input pumping power. The results of each waveguide structure were given in Fig. 6.14 for a comparison. The AlN-based waveguide with integrated spot-size converter had non-saturated TE-polarization loss around 15.3 dB regardless the input pulse energy. It was comparable with low-loss ridge waveguide indicating the improvement of high-mesa structure by introducing spot-size converters. By simulation, it was revealed that 50% of input optical power can be coupled to the waveguide and spot-size converter can transmit 38% of input optical power to the active core which is a slightly higher than the ridge waveguide (36%). Hence the coupling losses at input facet and output facet were 4.2 dB and 9 dB, respectively. The propagation loss and scattering loss were at most 2.1 dB, compared with 1.6 dB and 9.8 dB in ridge waveguide and high-mesa waveguide, respectively. This evidence confirmed a merit of integrating spot-size converters to a high-mesa structure. In Fig. 6.13, 5-dB absorption saturation in TM-polarization light can be achieved with an input pulse energy of 125 pJ, slightly higher than 115 pJ of ridge structure. One of explanations is the higher extinction ratio in AlN-based waveguide with integrated spot-size converter due to the additional non-saturated TM-polarization losses. At low absorption saturation, this higher extinction ratio needs more energy for saturating. However, by looking at the tendency of saturation curve and fitting with exponential curves, it seems that AlN-based waveguide with integrated spot-size converter can surpass the ridge AlN-based waveguide at high saturation level, i.e. the curve of AlN-based waveguide with integrated spot-size converter and ridge AlN-based waveguide had exponential growth constant of $\frac{1}{116} \times 10^{12}$ and $\frac{1}{145} \times 10^{12}$, respectively. Therefore, the spot-size converter structure is still promising for an optical switching with low operating energy. The issue of saturation energy can be further improved by optimizing the fabrication process of spot-size converter and introducing vertical converting effect for enhancing the coupling efficiency.

This achievement indicates that the MOVPE grown AlN-based waveguide with GaN/AlN MQWs core can be in the same league with MBE grown sample. Although we cannot directly compare the results from this work with the reports from N. Iizuka in Ref. 47 and Y. Li in Ref. 25 due to the limitation of short pulse laser, the absorption saturation in AlN-based waveguide with GaN/AlN MQWs fabricated by MOVPE has been demonstrated.
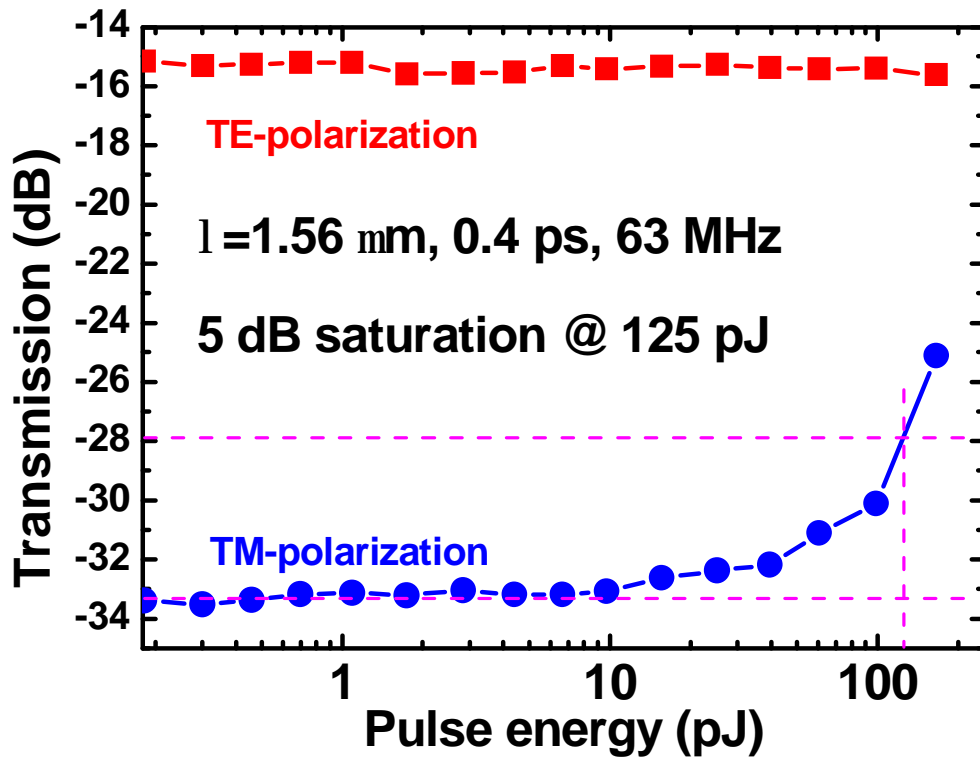
Fig. 6.13 Transmittances of TE and TM mode light in the AlN-based waveguide with integrated spot-size converter with GaN/AlN MQWs core as functions of input pulse energy
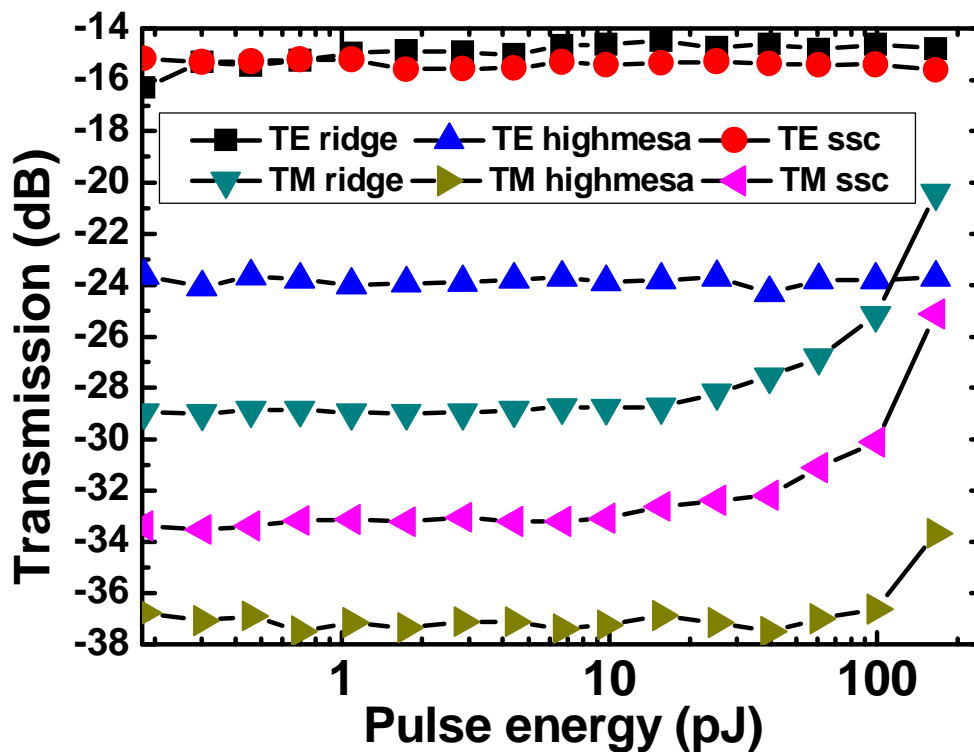
Fig. 6.14 Transmittances of TE and TM mode light in the ridge AlN-based waveguide, high-mesa AlN-based waveguide and AlN-based waveguide with integrated spot-size converter with GaN/AlN MQWs core as functions of input pulse energy

6.4 Conclusions

The spot-size converter has been introduced to the AlN-based high-mesa waveguide as a promising technology for improving the saturation energy issue. The sputtered Si_3N_4 has been used as the material for spot-size converter and cladding layer. The AlN-based waveguide with integrated spot-size converter has been designed for compatibility with nitride semiconductors. In order to simplify the fabrication procedures, the spot-size converter only affects on the lateral direction. However, the design has a potential to integrate vertical spot-size converting effect. The fabrication of AlN-based waveguide with integrated spot-size converter has based on the optimized fabrication processes of high-mesa AlN-based waveguide found in literature [46,111]. Although the fabrication processes were not fully optimized, the fabricated AlN-based

waveguide with integrated spot-size converter possessed a good shape and smooth sidewall which its functionality was tested by the near-field image of propagating light. Compared with two AlN-based waveguide from the last chapter, the intersubband absorption characteristics in AlN-based waveguide with integrated spot-size converter was quite similar to the ridge AlN-based waveguide and the high-mesa AlN-based waveguide from the last chapter. However, at short wavelength range TM-polarization loss in AlN-based waveguide with integrated spot-size converter was noticeably higher than the others. This was due to the additional non-saturated TM-polarization losses induced by the fabrication of spot-size converter and by the waveguide structure. Coupling loss at input facet of the AlN-based waveguide with integrated spot-size converter was around 4.2 dB improved from 4.4 dB and 5.2 dB in the ridge waveguide and the high-mesa waveguide, respectively. The TE propagation loss was 2.1 dB over 400-µm-long core, 1-mm-long devices, compared with 1.6-dB loss of 400-µm-long ridge structure and 9.8-dB loss of 400-µm-long high-mesa structure. For 5-dB absorption saturation, the AlN-based waveguide with integrated spot-size converter required 125-pJ of input pulse energy, slightly higher than 115-pJ in the ridge AlN-based waveguide but much better than 3-dB saturation at 145-pJ in the high-mesa AlN-based waveguide. Although there was no improvement at 5-dB absorption saturation compared with the ridge waveguide due to the additional non-saturated TM-polarization losses, the AlN-based waveguide with integrated spot-size converter was still promising at high absorption saturation. By the exponential fitting curves, the exponential growth constant of saturation curve of the AlN-based waveguide with integrated spot-size converter was of $\frac{1}{116} \times 10^{12}$ higher than $\frac{1}{145} \times 10^{12}$ of the ridge AlN-based waveguide. It should be noted here that the structure of spot-size converter can be further improved by introducing the vertical converting effect to the current spot-size converter which can increase the optical power coupled to the active core. The achievement in this thesis clearly indicates the potential of MOVPE grown AlN-based waveguide with GaN/AlN MQWs core as an optical switch.

Chapter 7 Conclusions

T his work has focused on the growth and fabrication of 1.5-µm-range all-optical switches utilizing intersubband transition in GaN/AlN MQWs. The unique points of this work from previous reports and publications are as followed:

1. All nitride semiconductors layers were deposited using metalorganic vapor phase epitaxy. This is an outstanding point of this work, since at the present time all of publications related to intersubband GaN/AlN MQWs optical switches were fully or partially fabricated by molecular beam epitaxy, especially GaN/AlN MQWs layer and upper cladding layer.

2. The sputtered Si_3N_4 spot-size converter has been designed for the most compatible with nitride fabrication technologies. Although the structure of AlN-based waveguide with integrated spot-size converter inspiration from the other publications, the structure in this work has been designed for lateral spot-size converting in order to simplify the fabrication procedures and increase fabrication yield.

The experiments in this thesis have been carried out step-by-step from the investigation of GaN/AlN MQWs, the optimization of GaN/AlN MQWs for the best intersubband transition properties, the design and fabrication of AlN-based waveguide and the measurement and investigation of intersubband transition characteristics in fabricated AlN-based waveguide.

In chapter 1, the basic knowledge of intersubband transition in GaN/AlN MQWs has been introduced followed by some examples of intersubband optical devices. The motivations and objectives of this thesis have also been given in this chapter.

The chapter 2 has related to the growth of GaN/AlN MQWs by conventional MOVPE. Several experiments have been performed to point out the possible factors that hinder the

accomplishment of short intersubband transition wavelength in MOVPE grown GaN/AlN MQWs. The growth temperature of GaN/AlN MQWs has been highly expected to be an answer as it plays a crucial role on the abruptness of GaN/AlN MQWs. This evidenced by many reports and publications which several methods have been put to improve the surface morphologies and abruptness of GaN/AlN MQWs, for examples, the use of indium as a surfactant, the growth at low temperature, and the pulsed MOVPE grown GaN/AlN MQWs. However, as evidenced in this work and by other references, the GaN/AlN MQWs grown at low temperature generally exhibit very weak intersubband absorptions which the carrier concentration in GaN wells has been assumed as a cause of this issue.

In chapter 3, the pulse injection growth method which has been investigated and used in our group has been adopted and employed for depositing GaN/AlN MQWs on AlN buffer layers. This method allows the growth of high quality *"n-doped"* GaN at low temperature. The GaN/AlN MQWs grown by pulse injection method exhibited superb quality in terms of crystal quality, surface morphologies and the interface abruptness. Later in this chapter, a strong intersubband transition in GaN/AlN MQWs has been realized by inserting a strain-tailoring thin AlGaN interlayer between GaN/AlN MQWs and AlN buffer. The effects of growth parameters on the intersubband transition properties have been investigated. In order to explicate the behavior of intersubband transition wavelength in GaN/AlN MQWs, the simulation has been performed using finite-different method implemented with non-parabolicity and non-abrupt interface effects. A strong intersubband at 1.5-µm-range with a small full-width at half-maximum value has been achieved after investigating and optimizing the growth parameters. Hence, in this chapter, the GaN/AlN MQWs with a good intersubband transition characteristic has been prepared for the fabrication of AlN-based waveguide with GaN/AlN MQWs core.

The chapter 4 has introduced the utilizing of Si_3N_4 as a material for waveguide fabrication which is compatible with nitride semiconductors. However, the Si_3N_4 directly deposited on the top of GaN/AlN MQWs dramatically degrade intersubband transition properties. This phenomenon is possibly due to the additional tensile strain in GaN/AlN MQWs induced by sputtered Si_3N_4 layer which restructures the energy band diagram and affects the oscillation strength of intersubband transition. For this reason, a thin AlN layer, called upper cladding layer, has been inserted before the sputtering of Si_3N_4 in order to protect the underneath GaN/AlN

MQWs. The growth parameters of AlN upper cladding layer have been investigated to realize the best intersubband transition properties and effectively protect the beneath GaN/AlN MQWs.

In chapter 5, the AlN-based waveguide structures have been designed for a purpose of low loss single-mode propagation waveguide. The design has been done by down-sizing the layer thicknesses, from the bottom AlN layer to the top Si_3N_4 layer. The 2-µm-wide ridge AlN-based waveguide and 2-µm-wide high-mesa AlN-based waveguide have been designed and clarified the propagation mode by the mean of beam propagation method. The intersubband absorption in AlN-based waveguides has been examined and found that both waveguide structures existed clearly 1.5-µm-range intersubband absorption. The absorption spectrum and the absorption intensities of the ridge AlN-based waveguide and the high-mesa AlN-based waveguide were similarly around 52 dB/mm. However, the high-mesa waveguide had much higher propagation loss due to the sidewall roughness of the waveguide. The intersubband absorption saturations in the ridge AlN-based waveguide and in the high-mesa AlN-based waveguide pumped by 1.56-µm laser with a temporal width of 0.4 ps and repetition rate of 63 MHz were 5 dB and 3 dB at the input pulse energy of 115 pJ and 145 pJ, respectively. Although the result could not be directly compared with other related reports which utilizing intersubband transition in MBE grown GaN/AlN MQWs because of the limitation of short pulse laser, AlN-based waveguide fabricated by MOVPE showed a good prospectiveness for practical used all-optical switches. It should be remarked here that the required input energy can be decreased with decreasing of temporal width of exciting laser.

In chapter 6, the issue of high demanded pumping power for saturating intersubband absorption in the ridge AlN-based waveguide has been challenged. By analyzing the ridge waveguide structure fabricated in this work, the optical confinement in MQWs layer and the large active core in lateral direction have been though as causes of this problem. Hence, the downscaling of active core and the utilizing of high-mesa structure were recommended. For these purposes, the Si_3N_4 spot-size converter has been introduced to enhance the coupling efficiency of high-mesa waveguide. The structure has been designed for the simplest fabrication procedures and the most compatible with nitride fabrication technologies. However, the fabrication of spot-size converter and the waveguide structure caused some additional non-saturated TM-polarization loss. For 5-dB absorption saturation, the AlN-based waveguide with integrated spot-size converter required 125-pJ of input pulse energy, slightly higher than the

ridge AlN-based waveguide but much better than the high-mesa AlN-based waveguide. By the exponential fitting curves, the exponential growth constant of saturation curve of the AlN-based waveguide with integrated spot-size converter was of $\frac{1}{116} \times 10^{12}$ higher than $\frac{1}{145} \times 10^{12}$ of the ridge AlN-based waveguide. Therefore, the AlN-based waveguide with integrated spot-size converter was promising at high absorption saturation.

This thesis has clearly demonstrated the potential and capability of MOVPE grown AlN-based waveguide with GaN/AlN MQWs core as an optical switch. The strong intersubband transition in MOVPE grown GaN/AlN MQWs has been successfully realized. The 5-dB intersubband absorption saturation has been demonstrated in the ridge AlN-based waveguide and in the AlN-based waveguide with integrated spot-size converter. It has shown a potential for further improvement and the utilizing as a practical all-optical switch. This study has renewed the interest of GaN intersubband optical devices and is an importance milestone of the development in GaN intersubband devices.

Appendex A   Material Parameters

Table A.1 Material parameters of AlN and GaN

	wurtzite	AlN	GaN
Lattice constant	a_0 (Å)	3.111	3.189
	c_0 (Å)	4.978	5.185
Energy bandgap	E_g	6.25	4.88
Effective mass	m^*/m_0	0.33	0.20
Dielectric constant	e_s	8.5	9.5
Spontaneous polarization	P_{SP} (C/m^2)	-0.081	-0.029
Piezoelectric constant	e_{31} (C/m^2)	-0.60	-0.49
	e_{33} (C/m^2)	1.46	0.73
Stiffness	C_{13} (GPa)	106	120
	C_{33} (GPa)	398	395

Table A.2 Lists of scientific constants used in this work

Boltzmann's constant	k	1.380662×10^{-23} JK^{-1}
Electron charge	q	$1.602189246 \times 10^{-19}$ C
Electron rest mass	m_0	9.109534×10^{-31} kg
Permittivity of vacuum	e_0	$8.854187827 \times 10^{-12}$ Fm^{-1}
Pi	p	3.1415926535897932384
Plank's constant	h	$6.626176583 \times 10^{-34}$ Js
Reduced Plank's constant	$\mathbf{h}$	$1.054588757 \times 10^{-34}$ Js

Appendex B   Simulation Model

This section is giving a brief theory of a simulation mode for calculating the intersubband transition wavelength in GaN/AlN MQWs. The numerical model is based on a self-consistent Schrödinger-Poisson equation implemented with the effects of piezoelectric field, strain in GaN/AlN MQWs, band non-parabolicity and non-abrupt interface between GaN and AlN.

B.1 Polarization in Quantum Well

It is widely recognized that there exists a very large built-in field due to spontaneous and piezoelectric polarization in the (0001)-oriented wurtzite nitride-based structures [8,94-97]. This built-in electric field plays a crucial role in the electrical and optical properties of the group III nitride materials. Optical transition energy and oscillator strength are typical physical parameters that strongly depend on the built-in field. It is necessary to take the effect of spontaneous and piezoelectric polarization into account in the realistic calculations in order to obtain accurate results.

The piezoelectric tensor of wurtzite group-III nitrides InN, GaN, and AlN has three independent components. Two of these components, e_{31} and e_{33}, determine the piezoelectric polarization, P_{PE}, induced by strain along the c-axis. The relevant relationship is

$$P_{PE} = 2\frac{a-a_0}{a_0}\left(e_{31} - e_{33}\frac{C_{13}}{C_{33}}\right)$$ (B-1)

where C_{13} and C_{33} are the elastic stiffness constants.[6] The lattice structure can be defined by the length of the hexagonal edge a_0 or a, and the height of the prism c_0 or c for relaxed and strained crystals, respectively.

Bernardini et al. predicted that in addition to the piezoelectric polarization, a spontaneous polarization (polarization of an unstrained, equilibrium lattice) is present in wurtzite group-III nitride crystals [95,132]. The calculated values of spontaneous polarization are very large. The sign of the spontaneous polarization of AlN and GaN is found to be negative (Table A-1). The orientation of the spontaneous and piezoelectric polarization is defined assuming that the positive

direction goes from the metal (cation) to the nearest neighbor nitrogen atom (anion) along the c-axis. Since $\left(e_{31}-e_{33}\left(C_{13}/C_{33}\right)\right)<0$ for AlGaN over the whole range of compositions, from equation (B-1), it follows that the piezoelectric polarization is negative for tensile and positive for compressive strained crystals. As a consequence, the orientation of the piezoelectric and spontaneous polarization is parallel in the case of tensile strain, and anti-parallel in the case of compressive strained layers.

<div align="center">without built-in electric filed   "with" built-in electric field</div>
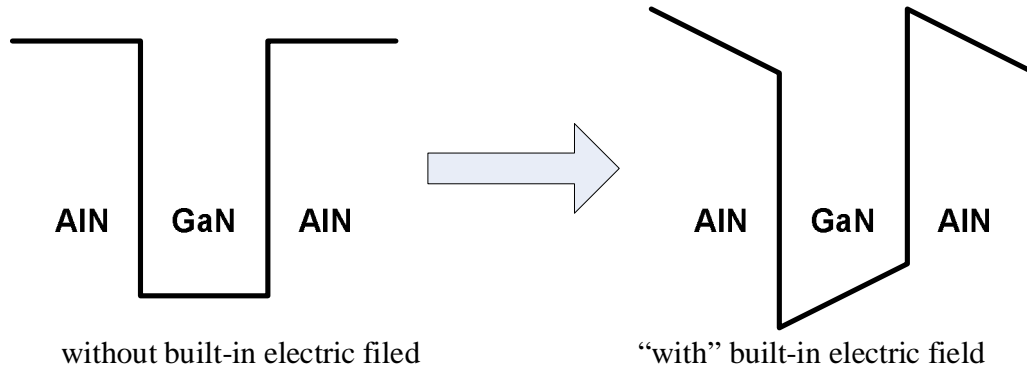
Fig. B.1 Effect of built-in electric field on a conduction band of a GaN/AlN quantum well

Consequently, the negative spontaneous polarization of GaN and the alloys as well as the piezoelectric polarization of the tensile strained layers are pointing from the nitrogen towards the nearest neighbor metal atom along the c-axis. The value of the total polarization inside one layer is the sum of the piezoelectric and spontaneous polarization, $P = P_{PE} + P_{SP}$ [98]. The presence of spontaneous and piezoelectric polarization induces immobile polarization charges at the interface between the two layers and the surface density of immobile polarization charges at the interface k can be expressed as:

$$s(z_k) = P(z_k^+) - P(z_k^-) \qquad\qquad \text{(B-2)}$$

where z_k only has values at the heterointerfaces, and $P(z_k^+)$ and $P(z_k^-)$ are the polarizations to the right and left of the plane z_k, respectively. The effect of spontaneous and piezoelectric polarization can be incorporated in to the Poisson equation as a term of immobile polarization charges. As a result of polarization, the electric field over the well and barrier in a QW can be written as:

$$F_w = \frac{(P_b - P_w)L_b}{e_0(L_b e_w + L_w e_b)} \text{ and } F_b = \frac{(P_w - P_b)L_w}{e_0(L_b e_w + L_w e_b)} \tag{B-3}$$

where F are built-in electric fields, L are layer thicknesses, e_0 is the permittivity of free space, and e are dielectric constants of materials. The subscript w and b denote the well and barrier, GaN and AlN, respectively.

B.2 Schrödinger Equation

In physics, specifically quantum mechanics, the Schrödinger equation is an equation that describes how the quantum state of a physical system changes in time. It is as central to quantum mechanics as Newton's laws are to classical mechanics. In the standard interpretation of quantum mechanics, the quantum state, also called a wave function or state vector, is the most complete description that can be given to a physical system. The Schrödinger equation takes several different forms, depending on the physical situation. The Schrödinger equation for a particle of mass m in a potential well (one-dimensional potential) aligned along the z-axis is:

$$-\frac{\mathbf{h}^2}{2m}\frac{\partial^2}{\partial z^2}y(z) + V(z)y(z) = Ey(z) \tag{B-4}$$

For an electron in a crystal structure (in semiconductor), the Schrödinger equation can be derived from eq. B-4 by substituting m with an empirical fitting parameter called the effective mass m^* where:

$$E = \frac{\mathbf{h}^2 k^2}{2m^*} \tag{B-5}$$

Equation B-5 is known as the effective mass approximation where k is a wave vector. The eq. B-4 can now be written as:

$$-\frac{\mathbf{h}^2}{2m^*}\frac{\partial^2}{\partial z^2}y(z) + [V(z) - E]y(z) = 0 \tag{B-6}$$

The problem now is to find the solution of both the energy eigenvalues E and the eigenfunction $y(z)$ for any $V(z)$. Hence, the shooting method using 3-point finite difference method (FDM) for numerical solution has been introduced [133] by expanding the second-order derivative in terms of finite differences. The Eq. B-6, then, can be derived as:

$$y(z+dz) = \left[\frac{2m^*}{\mathbf{h}^2}(dz)^2(V(z)-E)+2 \right] y(z)-y(z-dz) \qquad \text{(B-7)}$$

Equation B-9 implies that if the wave function is known at the two points $(z-dz)$ and z, then the value of the wave function at $(z+dz)$ can be calculated for any energy E. This iterative equation forms the basis of a standard method of solving differential equations numerically, and is known as the shooting method [133].

Using two known values of the wave function $y(z-dz)$ and $y(z)$, a third value, i.e. $y(z+dz)$, can be predicted. Using this new point $y(z+dz)$, together with $y(z)$ and by making the transformation $z+dz \rightarrow z$, a fourth point, $y(z+2dz)$, can be calculated, and so on. Hence, the complete wave function can be deduced for any particular energy. The solutions for stationary states have wave functions which satisfy the standard boundary conditions, i.e.

$$y(z) \rightarrow 0 \text{ and } \frac{dy(z)}{dz} \rightarrow 0, \text{ as } z \rightarrow \infty \qquad \text{(B-8)}$$

The first two values of the wave function necessary to start off the procedure can be generally chosen as:

$$y(0) = 0 \text{ and } y(dz) = 1 \qquad \text{(B-9)}$$

B.3 Band Non-parabolicity Implement

For semiconductor heterostructures with relatively low barrier heights and low carrier densities, the electrons cluster around the subband minima and their energy is in turn reasonably close to the bulk conduction band minima, i.e. within a couple of hundred meV, compared to a bandgap of the order of 1.5 eV. In this region, the band minima, both the bulk conduction band and the in-plane subband, can be described by a parabolic $E-\mathbf{k}$ curve, recalled from eq. B-5:

$$E = \frac{\mathbf{h}^2|\mathbf{k}|^2}{2m^*} \qquad \text{(B-10)}$$

where $\mathbf{k}$ can be read as a three-dimensional vector for the bulk, or as a two-dimensional in-plane vector $|\mathbf{k}_{x,y}|$ for a subband.

However, in situations where the electrons are forced up to higher energies, by either large barrier heights or narrow wells, or in the case of very high carrier densities, eq. B-10

becomes more approximate [99,100]. This is even more important for holes in the valence band. The approximation can be improved upon by adding addition terms into the polynomial expansion for the energy. For example, no matter how complex the band structure along a particular direction, it clearly has inversion symmetry and hence can always be represented by an expansion in even powers of k, if sufficient terms are included, i.e. the energy E can always be described by:

$$E = a_0 k^0 + a_2 k^2 + a_4 k^4 + a_6 k^6 + \mathbf{K} = \sum_{i=0}^{\infty} a_{2i} k^{2i} \qquad \text{(B-11)}$$

Usually when discussing single band models, as has been focused on entirely so far, the energy origin is set at the bottom of the band of interest, and thus $a_0 = 0$. In addition, truncating the series at k^2, gives $a_2 = \mathbf{h}^2/(2m^*)$.
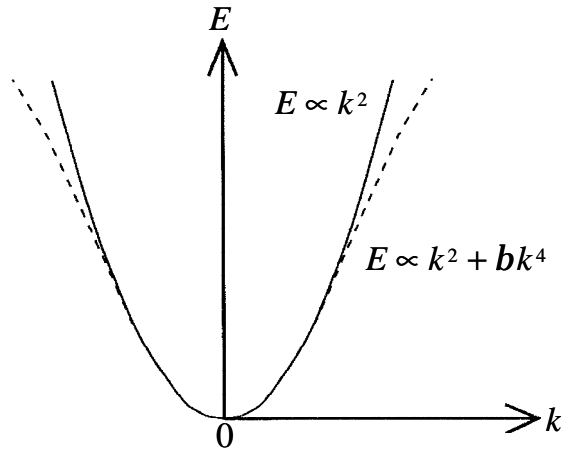
Fig. B.2 Non-parabolicity of the bulk and subband structure

The next best approximation is to include terms in k^4, hence accounting for band non-parabolicity, as displayed in Fig. B.2, with:

$$E = a_2 k^2 + a_4 k^4 = \frac{\mathbf{h}^2}{2m^*} \left(k^2 + b k^4 \right) \qquad \text{(B-12)}$$

where

$$b = a_2 \frac{2m^*}{\mathbf{h}^2} \qquad \text{(B-13)}$$

According to the basic definition of effective mass [134], i.e.

135

$$m^* = \mathbf{h}^2 \left(\frac{\partial^2 E}{\partial k^2} \right)^{-1} \tag{B-14}$$

then clearly m^* remains a function of k, unlike the case of parabolic bands where it is a constant. As it is a function of k, then it is also a function of energy, and indeed band non-parabolicity is accounted for by allowing the effective mass to have an energy dependence [135]:

$$m^*(E) = m^*(0) \left[1 + a(E - V) \right] \tag{B-15}$$

where V is the barrier height and the parameter a is given by [136,137]:

$$a = \left[1 - \frac{m^*(0)}{m_0} \right]^2 \Big/ E_g \tag{B-16}$$

where E_g is the semiconductor bandgap. With this new form of the effective mass, the Schrödinger equation (eq. B-4) then becomes:

$$-\frac{\mathbf{h}^2}{2} \frac{\partial}{\partial z} \frac{1}{m^*(z, E)} \frac{\partial}{\partial z} y(z) + V(z) y(z) = E y(z) \tag{B-17}$$

which can be solved by adapting the iterative shooting equation (eq. B-7). From eq. B-17, using 3-ponit finite different method, one can write as:

$$\frac{y(z + dz)}{m^*(z + \frac{dz}{2}, E)} = \left\{ \frac{2(dz)^2}{\mathbf{h}^2} [V(z) - E] + \frac{1}{m^*(z + \frac{dz}{2}, E)} + \frac{1}{m^*(z - \frac{dz}{2}, E)} \right\} y(z)$$
$$- \frac{y(z - dz)}{m^*(z - \frac{dz}{2}, E)} \tag{B-18}$$

which is the variable effective mass shooting equation, and is solved according to the boundary condition. The effective mass m^* can be found at the intermediate points, $z \pm dz/2$, by taking the mean of the two neighboring points at z and $\pm dz$. Clearly, eq. B-18 collapses back to the original form in eq. B-7 when m^* is constant.

B.4 Non-abrupt Interface Implement

In addition to the band non-parabolicity implement, the effect of non-abrupt interface between layers has also to be included to the calculation model. The non-abrupt region is

represented by step-shape graded layer. To simplify the model, the built-in electric field across the step-shape graded layer was neglected. The thickness of non-abrupt interfaces was varied so that the simulation fits with the experiment result. The Al-content in AlGaN non-abrupt layers was 0.5 by considering that the center of non-abrupt region was centered at the junction of AlN and GaN.

B.5 A Self-Consistent of Schrödinger-Poisson Equation

At this point, the Schrodinger equation for any heterostructure for which the band-edge potential profile defining the structure is known has been solved. However, all of the theoretical methods and examples described so far have concentrated solely on solving systems for a single charge carrier. In many devices such models would be inadequate as large numbers of charge carriers, e.g. electrons, can be present in the conduction band. In order to decide whether or not typical carrier densities would give rise to a significant additional potential on top of the usual band-edge potential terms, it then becomes necessary to solve the electrostatics describing the system.

When considering the case of an n-type material, then (although obvious) it is worth starting that the number of 'free' electrons in the conduction band is equal to the number of positively charged ionized donors in the heterostructure. The additional potential term $V_r(z)$ arising from charge distribution r, can be expressed by using Poisson's equation:

$$\nabla^2 V_r = -\frac{r}{e} \tag{B-19}$$

The solution is generally obtained via the electric field strength E; recalling that:

$$\mathbf{E} = \nabla V \tag{B-20}$$

the potential then would follow in the usual way [138]:

$$V(\mathbf{r}) = -\int_{-\infty}^{\mathbf{r}} \mathbf{E} \bullet d\mathbf{r} \tag{B-21}$$

Given that the potential profiles, $V_{CB}(z)$ for example, are one-dimensional, then they will also produce a one-dimensional charge distribution. In addition, remembering that the quantum

wells are assumed infinite in the *x-y* plane then any charge density $r(z)$ can be thought of as an infinite plane, i.e. a sheet, with areal charge density $s(z)$ and thickness dz, as shown in Fig. B.3(a). Such an infinite plane of charge produces an electric field perpendicular to it, and with a strength:

$$\mathbf{E} = \frac{s}{2e} \tag{B-22}$$
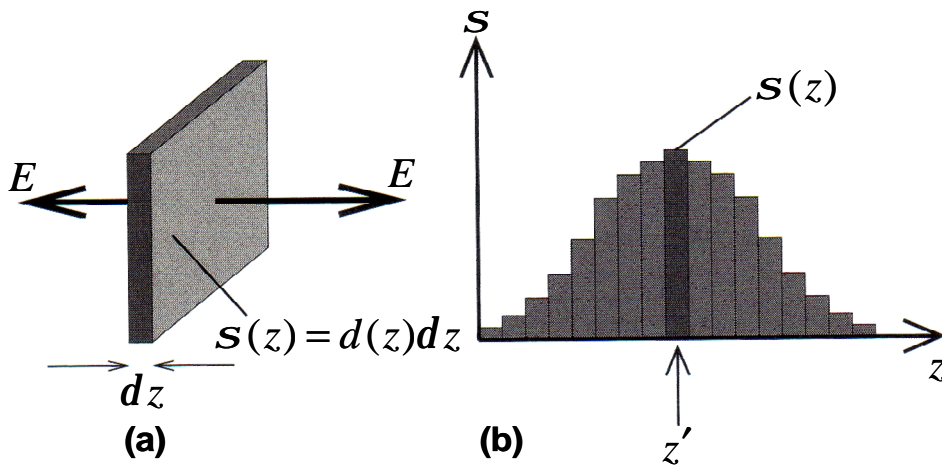
Fig. B.3 Electric field strength from an infinite plane of charge of volume density $d(z)$ and the thickness dz

Note that as the sheet is infinite in the plane, then the field strength is constant for all distances from the plane. The total electric field strength due to many of these planes of charge, as shown in Fig. B.3(b), is then just the sum of the individual contributions as follows:

$$\mathbf{E} = \sum_{z'=-\infty}^{\infty} \frac{s(z')}{2e} \operatorname{sign}(z-z') \tag{B-23}$$

where the function sign is defined as

$$\operatorname{sign}(z) = +1, \ z \geq 0 \ \text{ and } \ \operatorname{sign}(z) = -1, \ z < 0 \tag{B-24}$$

and has been introduced to account for the vector nature of $\mathbf{E}$, i.e. if a single sheet of charge is at a position z', then for $z \geq z'$, $\mathbf{E}(z) = +s/(2e)$, whereas for $z < z'$, $\mathbf{E}(z) = -s/(2e)$. Note further that it is only the charge neutrality, i.e. there are as many ionized donors (or acceptors) in the system as there are electrons (or holes), or expressed mathematically:

138

$$\sum_{z=-\infty}^{\infty} s(z) = 0 \qquad \text{(B-25)}$$

which ensures that the electric field, and hence the potential, go to zero at large distances from the charge distribution. For the case of a doped semiconductor, there would be two contributions to the charge density $s(z)$, where the first would be the ionized impurities and the second the free charge carriers themselves. While the former would be known from the doping density in each semiconductor layer, as defined at growth time, the latter would be calculated from the probability distributions of the carriers in the heterostructure. Thus if $d(z)$ defines the volume density of the dopants at position z, where the planes are separated by the usual step length dz, then the total number of carriers, per unit cross-sectional area, introduced into the heterostructure is given by:

$$N = -\int_{-\infty}^{\infty} d(z)dz \qquad \text{(B-26)}$$

The net charge density in any of the planes follows as

$$s(z) = q\left[N y^*(z) y(z) - d(z) \right] dz \qquad \text{(B-27)}$$

where q is the charge on the extrinsic carriers. The step length dz selects the proportion of the carriers that are within that 'slab' and converts the volume density of dopant, $d(z)$ into an areal density.

If the charge carriers are distributed over more than one subband, then the contribution to the charge density $s(z)$ would have to be summed over the relevant subbands, i.e.

$$s(z) = q\left(\sum_{i=1}^{n} N_i y_i^*(z) y_i(z) - d(z) \right) dz \qquad \text{(B-28)}$$

where $\sum_{i=1}^{n} N_i = N$.

The energy eigenvalues are calculated by considering the introduction of a further test electron into the system and incorporating the potential due to the carrier density already present into the standard Schrödinger equation, i.e. the potential term $V(z)$ in eq. B-6 becomes:

$$V(z) \rightarrow V_{CB}(z) + V_r(z) \qquad \text{(B-29)}$$

where V_{CB} represents the band edge potential at zero doping and the potential due to the non-zero number of carriers, i.e. the charge density r, is represented by the function V_r.

139

The numerical shooting method, described in detail earlier in this chapter, can be used without alteration to solve for this new potential, which will thus yield new energies and wave functions. The latter is an important point since the potential due to the charge distribution is itself dependent on the wave functions. Therefore, it is necessary to form a closed loop solving Schrödinger equation, calculating the potential due to the resulting charge distribution, adding it to the original band-edge potential, solving Schrödinger equation again, and so on—a process which is illustrated schematically in Fig. B.4.

The process is repeated until the energy eigenvalues converge; at this point the wave functions are simultaneously solutions to both Schrödinger and Poisson equations—the solutions are described as self-consistent, rather like Hartree's approach to solving many electron atoms [139].
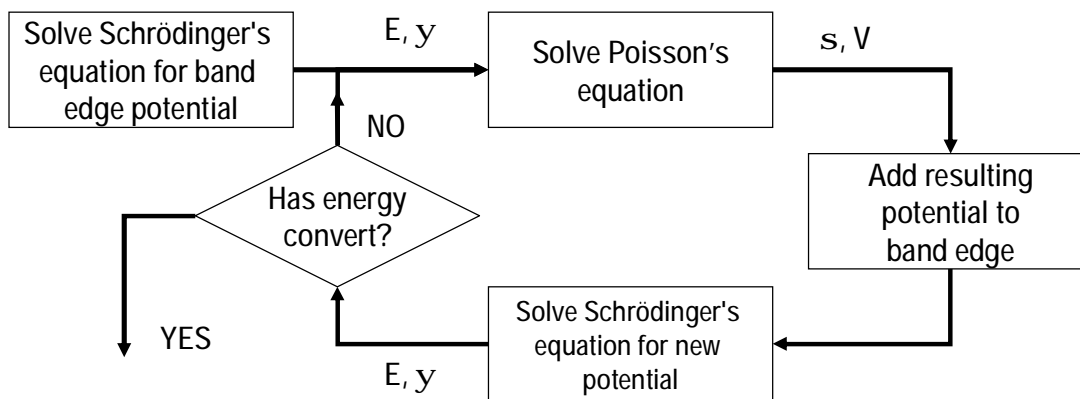
Fig. B.4 Block diagram illustrating the process of self-consistent iteration

Appendex C Suggestions on Further Investigation

This section is offered for one who would like to investigate the intersubband optical devices related to the intersubband absorption in MOVPE grown GaN/AlN MQWs and/or the AlN-based optical waveguide. This section is divided into two parts: the growth of GaN/AlN MQWs aspect and the fabrication of AlN-base optical waveguide aspects.

In the viewpoint of the growth of GaN/AlN MQWs by pulse injection MOVPE, though the optimization of growth parameters has been carried out in this dissertation, the intersubband transition characteristics in GaN/AlN MQWs can be possibly improved. In term of shorter transition wavelength < 1.5-μm range, the most important factor is considerably the abruptness of GaN/AlN interface. Several growth methods can be employed implementing with the current pulse injection growth method; for example, the growth of AlN barrier by pulse injection method [82-84] and the indium surfactant [48,50]. J. S. yang et al. has report the tremendous improvement of crystal quality and surface morphology of AlN layer deposited by pulse injection method at 800 °C which is comparable to that of high quality AlN layer grown at high temperature. However, in order to adopt this propose to the growth of GaN/AlN MQWs, one should consider and adjust the growth condition and gas flow sequence. The full-width at half-maximum of an absorption peak should be most likely improved with the abrupt interface of MQWs since the sharpness of absorption peak corresponds to the surfactant of GaN/AlN interface. In the view point of intersubband absorption intensity, it is possible to enhance the electron concentration by increasing the amount of Si atoms incorporating into GaN layers. This includes the increasing of partial pressure of SiH_4. Nevertheless, the issue of 3-D island growth of GaN layer induced by large amount of Si should be kept in mind as a factor that can dramatically degrade the crystal quality of GaN layer as well as roughen the interface between GaN and AlN.

For the aspect of the AlN-based optical waveguide fabrication, one can challenge the issue of high non-saturated propagation loss by careful fabrication and revising the waveguide

structure. As indicated in chapter 5 that, the AlN-based waveguides in this work were suffered from an immaturity fabrication resulting in an imperfect waveguide shape and rough sidewall particularly the high-mesa structure. It is very promising that the unnecessary propagation loss can be marvelously decreased just by the careful and optimized fabrication. The suggestion method is optimizing the ICP dry etching of nitride layers since the step-like sidewall of high-mesa waveguide is considerably occurred during ICP dry etching process. In the viewpoint of spot-size converter, one can employ the vertical spot-size converting by some additional etching processes in order to form a stair-like spot-size converter [47,86]. One should also concern about the damages of sidewall of the GaN/AlN MQWs and of surface AlN buffer layer during the core removal process by ICP-RIE. These damages induce additional non-saturated loss in TM-polarization and increase the saturation energy. This propose should counter the issue of high required pumping pulse energy by enhancing the coupling efficiency, confining more light into the MQWs core and decrease excess TM-polarization loss. The number of GaN/AlN MQWs should also be optimized for the best absorption saturation per unit area of MQWs core.

References

[1] A. V. Gopal, H. Yoshida, A. Neogi, N. Georgiev, T. Mozume, T. Simoyama, O. Wada, and H. Ishikawa, "Intersubband absorption saturation in InGaAs-AlAsSb quantum wells ," IEEE J. Quantum Electron. **38**, 1515 (2002).

[2] R. Akimoto, B. S. Li, K. Akita, and T. Hasama, "Subpicosecond saturation of intersubband absorption in (CdS/ZnSe)/BeTe quantum-well waveguides at telecommunication wavelength," Appl. Phys. Lett. **87**, 181104 (2005).

[3] B. S. Ma, W. J. Fan, Y. X. Dang, W. K. Cheah, W. K. Loke, W. Liu, D. S. Li, S. F. Yoon, D. H. Zhang, H. Wang, and C. H. Tung, "GaInNAs double-barrier quantum well infrared photodetector with the photodetection at 1.24 µm," Appl. Phys. Lett. **91**, 051102 (2007).

[4] C. Gmachl, H. M. Ng, S. N. G. Chu, and A. Y. Cho, "Intersubband absorption at lambda~1.55 µm in well- and modulation-doped GaN/AlGaN multiple quantum wells with superlattice barriers," Appl. Phys. Lett. **77**, 3722 (2000).

[5] C. Gmachl, H. M. Ng, and A. Y. Cho, "Intersubband absorption in degenerately doped GaN/Al$_x$Ga$_{1-x}$N coupled double quantum wells," Appl. Phys. Lett. **79**, 1590 (2001).

[6] K. Kishino, A. Kikuchi, H. Kanazawa, and T. Tachibana, "Intersubband transition in (GaN)$_m$/(AlN)$_n$ superlattices in the wavelength range from 1.08 to 1.61 µm," Appl. Phys. Lett. **81**, 1234 (2002).

[7] A. Helman, M. Tchernycheva, A. Lusson, E. Warde, F. H. Julien, Kh. Moumanis, G. Fishman, E. Monroy, B. Daudin, L. S. Dang, E. Bellet-Amalric, and D. Jalabert, "Intersubband spectroscopy of doped and undoped GaN/AlN quantum wells grown by molecular-beam epitaxy," Appl. Phys. Lett. **83**, 5196 (2003).

[8] N. Suzuki and N. Iizuka, "Effect of Polarization Field on Intersubband Transition in AlGaN/GaN Quantum Wells," Jpn. J. Appl. Phys. **38**, L363 (1999).

[9] S. Nicolay, J. F. Carlin, E. Feltin, R. Butte, M. Mosca, N. Grandjean, M. Ilegems, M. Tchernycheva, L. Nevou, and F. H. Julien, "Midinfrared intersubband absorption in lattice-matched AlInN/GaN multiple quantum wells," Appl. Phys. Lett. **87**, 111106 (2005).

[10] M. Tchernycheva, L. Nevou, L. Doyennette, F. H. Julien, E. Warde, F Guillot, E. Monroy, E. Bellet-Amalric, T. Remmele, and M. Albrecht, "Systematic experimental and theoretical

investigation of intersubband absorption in GaN/AlN quantum wells," Phys. Rev. B **73**, 125347 (2006).

[11] N. Iizuka, K. Kaneko, and N. Suzuki, "Near-infrared intersubband absorption in GaN/AlN quantum wells grown by molecular beam epitaxy," Appl. Phys Lett. **81**, 1803 (2002).

[12] N. Iizuka, K. Kaneko, and N. Suzuki, "Sub-picosecond all-optical gate utilizing GaN intersubband transition," Opt. Express **13**, 3835 (2005).

[13] A. Rubio, J. L. Corkill, M. L. Cohen, E. L. Shirley, and S. G. Louie, "Quasiparticle band structure of AlN and GaN," Phys. Rev. B **48**, 11810 (1993).

[14] W. R. L. Lambrecht and B. Segall, *Properties of Group III Nitrides*, Inspec, London, 1994.

[15] Kh. Moumanis, A. Helman, F. Fossard, M. chernycheva, A. Lusson, F. H. Julien, B. Damilano, N. Grandjean, and J. Massies, "Intraband absorptions in GaN/AlN quantum dots in the wavelength range of 1.27–2.4 µm," Appl. Phys. Lett. **82**, 868 (2003).

[16] F. Guillot, E. Bellet-Amalric, E. Monroy, M. Tchernycheva, L. Nevou, L. Doyennette, F. H. Julien, L. S. Dang, T. Remmele, M. Albrecht, T. Shibata, and M. Tanaka, "Si-doped GaN/AlN quantum dot superlattices for optoelectronics at telecommunication wavelengths," J. Appl. Phys. **100**, 044326 (2006).

[17] D. Hofstetter, S.-S. Schad, H. Wu, W. J. Schaff, and L. F. Eastman, "GaN/AlN-based quantum-well infrared photodetector for 1.55 µm," Appl. Phys. Lett. **83**, 572 (2003).

[18] E. Baumann, F. R. Giorgetta, D. Hofstetter, H. Lu, X. Chen, W. J. Schaff, L. F Eastman, S. Golka, W. Schrenk, and G. Strasser, "Intersubband photoconductivity at 1.6 µm using a strain-compensated AlN/GaN superlattice," Appl. Phys. Lett. **87**, 191102 (2005).

[19] D. Hofstetter, E. Baumann, F. Giorgetta, J. Dawlaty, P. George, F. Rana, F. Guillot, and E. Monroy, "High frequency measurements on an AlN/GaN-based intersubband detector at 1550 and 780 nm," Appl. Phys. Lett. **92**, 231104 (2008).

[20] L. Doyennette, L. Nevou, M. Tchernycheva, A. Lupu, F. Guillot, E. Mon¬roy, R. Colombelli, and F H. Julien, "GaN-based quantum dot infrared photodetector operating at 1.38 µm," Electron. Lett. **41**, 1077 (2005).

[21] A. Vardi, N. Akopian, G. Bahir, L. Doyennette, M. Tchernycheva, L. Nevou, F H. Julien, F Guillot, and E. Monroy, "Room temperature demonstration of GaN/AlN quantum dot intraband infrared photodetector at fiber-optics communication wavelength," Appl. Phys. Lett. **88**, 143101 (2006).

[22] A. Vardi, G. Bahir, F Guillot, C. Bougerol, E. Monroy, S. E. Schacham, M. Tchernycheva, and F H. Julien, "Near infrared quantum cascade detector in GaN/AlGaN/AlN heterostructures," Appl. Phys. Lett. **92**, 011112 (2008).

[23] N. Iizuka, K. Kaneko, and N. Suzuki, "Sub-picosecond modulation by intersubband transition in ridge waveguide with GaN/AlN quantum wells," Electron. Lett. **40**, 962 (2004).

[24] N. Iizuka, K. Kaneko, and N. Suzuki, "Polarization dependent loss in III-nitride optical waveguides for telecommunication devices," J. Appl. Phys. **99**, 093107 (2006).

[25] Y. Li, A. Bhattacharyya, C. Thomidis, T. D. Moustakas, and R. Paiella, "Ultrafast all-optical switching with low saturation energy via intersubband transitions in GaN/AlN quantum-well waveguides," Opt. Express **15**, 17922 (2007).

[26] M. Tchernycheva, L. Nevou, L. Doyennette, F H. Julien, F Guillot, E. Monroy, T. Remmele, and M. Albrecht, "Electron confinement in strongly coupled GaN/AlN quantum wells," Appl. Phys. Lett. **88**, 153113 (2006).

[27] K. Driscoll, A. Bhattacharyya, T. D. Moustakas, R. Paiella, L. Zhou, and D. J. Smith, "Intersubband absorption in AlN/GaN/AlGaN coupled quantum wells," Appl. Phys. Lett. **91**, 141104 (2007).

[28] E. Baumann, F. R. Giorgetta, D. Hofstetter, S. Leconte, F. Guillot, E. Bellet-Amalric, and E. Monroy, "Electrically adjustable intersubband absorption of a GaN/AlN superlattice grown on a transistorlike structure," Appl. Phys. Lett. **89**, 101121 (2006).

[29] N. Kheirodin, L. Nevoum, H. Machhadani, P. Crozat, L. Vivien, M. Tchernycheva, A. Lupu, F H. Julien, G. Pozzovivo, S. Golka, G. Strasser, F Guillot, and E. Monroy, "Electrooptical Modulator at Telecommunication Wavelengths Based on GaN–AlN Coupled Quantum Wells," IEEE Photonics Technol. Lett. **20**, 724 (2008).

[30] L. Nevou, M. Tchernycheva, F H. Julien, F Guillot, and E. Monroy, "Short wavelength (λ=2.13 µm) intersubband luminescence from GaN/AlN quantum wells at room temperature" Appl. Phys. Lett. **90**, 121106 (2007).

[31] L. Nevou, F H. Julien, M. Tchernycheva, F Guillot, E. Monroy, and E. Sarigiannidou, "Intraband emission at λ~1.48 µm from GaN/AlN quantum dots at room temperature," Appl. Phys. Lett. **92**, 161105 (2008).

[32] Y. Inoue, H. Nagasawa, N. Stone, K. Ishino, A. Ishida, H. Fujiyasu, J. J. Kim, H. Makino, T. Yao, S. Sakakibara, and M. Kuwabara, "Fabrication and characterization of short period AlN/GaN quantum cascade laser structures," J. Cryst. Growth **265**, 65 (2004).

[33] V. D. Jovanovic, D. Indjin, Z. Ikonic, and P. Harrison, "Simulation and design of GaN/AlGaN far-infrared (λ~34 µm) quantum-cascade laser," Appl. Phys. Lett. **84**, 2995 (2004).

[34] D. Indjin, Z. Ikonic, V. D. Jovanovic, N. Vukmirovic, P. Harrison, and R. W. Kelsall, "Relationship between carrier dynamics and temperature in terahertz quantum cascade structures: simulation of GaAs/AlGaAs, SiGe/Si and GaN/AlGaN devices," Semicond. Sci. Technol. **20**, S237 (2005).

[35] A. Ishida, K. Matsue, Y. Inoue, H. Fujiyasu, H. J. Ko, A. Setiawan, J. J. Kim, H. Makino, and T. Yao, "Design and Preparation of AlN/GaN Quantum Wells for Quantum Cascade Laser Applications," Jpn. J. Appl. Phys. **44**, 5918 (2005).

[36] N. Vukmirovic, V. D. Jovanovic, D. Indjin, Z. Ikonic, P. Harrison, and V Milanovic, "Optically pumped terahertz laser based on intersubband transitions in a GaN/AlGaN double quantum well," J. Appl. Phys. **97**, 103106 (2005).

[37] G. Sun, J. B. Khurgin, and R. A. Soref, "Design of a GaN/AlGaN intersubband Raman laser electrically tunable over the 3-5 µm atmospheric transmission window," J. Appl. Phys. **99**, 033103 (2006).

[38] N. Suzuki, N. Iizuka, "Electron Scattering Rates in AlGaN/GaN Quantum Wells for 1.55-µm Inter-Subband Transition," Jpn. J. Appl. Phys. **37**, L369 (1998).

[39] B. K. Ridley, "Electron scattering by confined LO polar phonons in a quantum well," Phys. Rev. B **39**, 5282 (1989).

[40] A. Seilmeier, H. J. Hübner, M. Wörner, G. Abstreiter, G. Weimann, and W. Schlapp, "Direct observation of intersubband relaxation in narrow multiple quantum well structures," Solid State Elec. **31**, 767 (1988).

[41] T. Asano, M. Tamura, S. Yoshizawa, and S. Noda, "Pump-probe measurement of ultrafast all-optical modulation based on intersubband transition in n-doped quantum wells," Appl. Phys. Lett. **77**, 19 (2000).

[42] S. Noda, T. Uemura, T. Yamashita, and A. Sasaki, "All-optical modulation using an n-doped quantum-well structure," J. Appl. Phys. **68**, 6529 (1990).

[43] N. Susuki and N. Iizuka, "Feasibility Study on Ultrafast Nonlinear Optical Properties of 1.55-µm Intersubband transition in AlGaN/GaN Quantum Wells," Jpn. J. Appl. Phys. **36**, L1006 (1997).

[44] N. Iizuka, K. Kaneko, and N. Suzuki, "All-Optical Switch Utilizing Intersubband Transition in GaN Quantum Wells," IEEE J. of Quantum Elec. **42**, 765 (2006).

[45] C. Kumtornkuttikul, T. Shimizu, N. Iizuka, N. Suzuki, M. Sugiyama, and Y. Nakano, "AlN Waveguide with GaN/AlN Quantum Wells for All-Optical Switch Utilizing Intersubband Transition," Jpn. J. Appl. Phys. **46**, L352 (2007).

[46] T. Shimizu, C. Kumtornkuttikul, N. Iizuka, N. Suzuki, M. Sugiyama, and Y. Nakano, "Fabrication and Measurement of AlN Cladding AlN/GaN Multiple-Quantum-Well Waveguide for All-Optical Switching Devices Using Intersubband Transition," Jpn. J. Appl. Phys. **46**, 6639 (2007).

[47] N. Iizuka, H. Yoshida, N. Managaki, T. Shimizu, H. Sodabanlu, C. Kumtornkittikul, M. Sugiyama, and Y. Nakano, "Integration of GaN/AlN all-optical switch with SiN/AlN waveguide utilizing spot-size conversion," Opt. Express **17**, 23247 (2009).

[48] S. Nicolay, E. Feltin, J. F. Carlin, M. Mosca, L. Nevou, M. Tchernycheva, F. H. Julien, M. Ilegems, and N. Grandjean, "Indium surfactant effect on AlN/GaN heterostructures grown by metal-organic vapor-phase epitaxy: Applications to intersubband transitions," Appl. Phys. Lett. **88**, 151902 (2006).

[49] S. Nicolay, E. Feltin, J. F. Carlin, N. Grandjean, L. Nevou and F. H. Julien, M. Schmidbauer, T. Remmele, and M. Albrecht, "Strain-induced interface instability in GaN/AlN multiple quantum wells," Appl. Phys. Lett. **91**, 061927 (2007).

[50] C. Bayram, N. Péré-laperne, R. McClintock, B. Fain, and M. Razeghi, "Pulsed metal-organic chemical vapor deposition of high-quality AlN/GaN superlattices for near-infrared intersubband transitions," Appl. Phys. Lett. **94**, 121902 (2009).

[51] S. Sekiguchi, T. Shimoyama, H. Yoshida, J. Kasai, T. Mozume, and H. Ishikawa, Technical Digest of 2005 Optical Fiber Communication Conference, Anaheim, CA, 6-11 March 2005 Paper No. OFE4.

[52] R. Akimoto, B. S. Li, K. Akita, and T. Hasama, "Ultrafast intersubband optical switching in II-VI-based quantum well for optical fiber communications," Phys. stat. sol. (B). **243**, 805 (2006).

[53] K. Akita, R. Akimoto, T. Hasama, H. Ishikawa, and R. Takanashi, "Intersubband all-optical switching in sub-µm high-mesa SCH waveguide structure with wide-gap II-VI-based quantum wells", Electron. Lett., **42**, 1352 (2006).

[54] K. Akita, R. Akimoto, B.S. Li, T. Hasama, and H. Ishikawa, "Fabrication of High-Mesa Waveguides Based on Wide Band Gap II-VI Semiconductors for Telecom Wavelength Applications," Jpn. J. Appl. Phys. **46**, 200 (2007).

[55] A. C. Jones and P. O'Brien, *CVD of Compound Semiconductors: Precursor Synthesis, Development and Applications,* VCH, Weinheim,1997.

[56] S. Nakamura, M. Senoh, N. Iwasa, S. Nagahama, T. Yamada, and T. Mukai, "Superbright Green InGaN Single-Quantum-Well-Structure Light-Emitting Diodes," Jpn. J. Appl. Phys. **34**, L1332 (1995).

[57] S. D. Lester, F. A. Ponce, M. G. Craford, and D. A. Steigerwald, "High dislocation densities in high efficiency GaN-based light-emitting diodes," Appl. Phys. Lett. **66**, 1249 (1995).

[58] T. Mukai, H. Narimatsu, and S. Nakamura, "Amber InGaN-Based Light-Emitting Diodes Operable at High Ambient Temperatures," Jpn. J. Appl. Phys. **37**, L479 (1998).

[59] S. Nakamura, S. Pearton, and G. Fasol, *The Blue Laser Diode: The Complete Story*, 2nd ed., Springer, Berlin, 2000.

[60] S. Nakamura, M. Senoh, S. Nagahama, N. Iwasa, T. Matsushita, and T. Mukai, "Blue InGaN-based laser diodes with an emission wavelength of 450 nm," Appl. Phys. Lett. **76**, 22 (2000).

[61] S. Yagi, M. Shimizu, H. Okumura, H. Ohashi, Y. Yano, and N. Akutsu, "High Breakdown Voltage AlGaN/GaN Metal–Insulator–Semiconductor High-Electron-Mobility Transistor with TiO2/SiN Gate Insulator," Jpn. J. Appl. Phys. **46**, 2309 (2007).

[62] M. H. Wong, Y. Pei, J. S. Speck, and U. K. Mishra, "High power N-face GaN high electron mobility transistors grown by molecular beam epitaxy with optimization of AlN nucleation," Appl. Phys. Lett. **94**, 182103 (2009).

[63] B. Butun, T. Tutgut, E. Ulker, T. Yelboga, and E. Ozbay, "High-performance visible-blind GaN-based *p-i-n* photodetectors," Appl. Phys. Lett. **92**, 033507 (2008).

[64] Y. Zhang, S. C. Shen, H. J. Kim, S. Choi, J. H. Ryou, R. D. Dupuis, and B. Narayan, "Low-noise GaN ultraviolet *p-i-n* photodiodes on GaN substrates," Appl. Phys. Lett. **94**, 221109 (2009).

[65] S. Arulkumaran, G. I. Ng, Z. H. Liu, and C. H. Lee, "High temperature power performance of AlGaN/GaN high-electron-mobility transistors on high-resistivity silicon," Appl. Phys. Lett. **91** , 083516 (2007).

[66] B. S. Kang, H. T. Wang, F. Ren, and S. J. Pearton, "Electrical detection of biomaterials using AlGaN/GaN high electron mobility transistors," J. Appl. Phys. **104**, 031101 (2008).

[67] X. L. Liu, D.-C. Lu, L. S. Wang, X. H. Wang, D. Wang, and L. Y. Lin, "The dependence of growth rate of GaN buffer layer on growth parameters by metalorganic vapor-phase epitaxy ," J. of Cryst. Growth **193**, 23 (1998).

[68] D. G. Zhao, J. J. Zhu, D. S. Jiang, Hui Yang, J. W. Liang, X. Y. Li, and H. M. Gong, "Parasitic reaction and its effect on the growth rate of AlN by metalorganic chemical vapor deposition," J. of Cryst. Growth **289**, 72 (2006).

[69] N. Fujimoto, T. Kitano, G. Narita, N. Okada, K. Balakrishnan, M. Iwaya, S. Kamiyama, H. Amano, I. Akasaki, K. Shimono, T. Noro, T. Takagi, ans A. Bandoh, "Growth of high-quality AlN at high growth rate by high-temperature MOVPE," Phys. stat. sol. (C) **3**, 1617 (2006).

[70] H. M. Ng, C. Gmachl, S. N. G. Chu, and A. Y. Cho, "Molecular beam epitaxy of GaN/Al$_x$Ga$_{1-x}$N superlattices for 1.52-4.2 μm intersubband transitions," J. Crystal Growth **220**, 432 (2000).

[71] N. Suzuki, N. Iizuka, and K. Kaneko, "Calculation of Near-Infrared Intersubband Absorption Spectra in GaN/AlN Quantum Wells," Jpn. J. Appl. Phys. **42**, 132 (2003).

[72] J. M. Li, Y. W. Lu, X. X. Han, J. J. Wu, X. L. Liu, Q. S. Zhu, and Z. G. Wang, "Theoretical investigation of intersubband transition in Al$_x$Ga$_{1-x}$N/GaN/Al$_y$Ga$_{1-y}$N step quantum well," Physica E **28**, 453 (2005).

[73] N. A. Fichtenbaum, T. E. Mates, S. Keller, S. P. DenBaars, U. K. Mishra, "Impurity incorporation in heteroepitaxial N-face and Ga-face GaN films grown by metalorganic chemical vapor deposition," J. Cryst. Growth **310**, 1124 (2008).

[74] C. H. Seager, A. F. Wright, J. Yu, and W. Götz, "Role of carbon in GaN," J. Appl. Phys. **92**, 6553 (2002).

[75] I. Waki, C. Kumtornkittikul, Y. Shimogaki, and Y. Nakano, "Shortest intersubband transition wavelength (1.68 μm) achieved in AlN/GaN multiple quantum wells by

metalorganic vapor phase epitaxy", Appl. Phys. Lett. **82**, 4465 (2003) [Errata, **84**, 3703 (2004)]

[76] J. S. Yang, H. Sodabanlu，M. Sugiyama, Y. Nakano, and Y. Shimogaki，"Fabrication of abrupt AlN/GaN MQWs by Low Temperature-MOVPE," 69th Japanese Society of Applied Physics (Chubu Univ., Japan), Sep., 2008.

[77] J. S. Yang, H. Sodabanlu, M. Sugiyama, Y. Nakano, and Y. Shimogaki, "Fabrication of Abrupt AlN/GaN Multi Quantum Wells by Low Temperature Metal Organic Vapor Phase Epitaxy," Appl. Phys. Express **2**, 051004-1 (2009).

[78] J. S. Yang, H. Sodabanlu, M. Sugiyama, Y. Nakano, and Y. Shimogaki, "Blueshift of intersubband transition wavelength in AlN/GaN multiple quantum wells by low temperature metal organic vapor phase epitaxy using pulse injection method," Appl. Phys. Lett. **95**, 162111 (2009).

[79] J. S. Yang, H. Sodabanlu，M. Sugiyama, Y. Nakano, and Y. Shimogaki，"Low Temperature MOVPE Growth of high quality GaN Layer by Pulse Injection Method," 39th The Society of Chemical Engineers, Japan (Hokkaido Univ., Japan), Sep., 2007.

[80] J. S. Yang, H. Sodabanlu，M. Sugiyama, Y. Nakano, and Y. Shimogaki，"Low Temperature MOVPE Growth of n-type GaN by Pulse Injection Method," 68th Japanese Society of Applied Physics (Hokkaido institute of technology, Japan), Sep., 2007.

[81] J. S. Yang, H. Sodabanlu，M. Sugiyama, Y. Nakano, and Y. Shimogaki，"Effect of 1st H2 purge time and TMGa supply time in GaN growth by pulse injection method"，55th Japanese Society of Applied Physics (Nihon Univ., Japan), Mar., 2008.

[82] J. S. Yang, H. Sodabanlu, I. Waki, M. Sugiyama, Y. Nakano, and Y. Shimogaki, "Low Temperature MOVPE Growth of AlN by Pulse Injection Method at 800 ℃," Jpn. J. Appl. Phys. **46**, L927 (2007).

[83] J. S. Yang, H. Sodabanlu, I. Waki, M. Sugiyama, Y. Nakano, and Y. Shimogaki, "Process Design of Pulse Injection Method for Low-Temperature Metal Organic Vapor Phase Epitaxial Growth of AlN at 800 ℃," J. Cryst. Growth **311**, 383 (2009).

[84] J. S. Yang, M. Sugiyama, Y. Nakano, and Y. Shimogaki, "Low Temperature MOVPE Growth of AlN by Pulse Injection Method for Improvement of Crystal Quality," 25th Electronic Materials Symposium (Izu, Japan), Jun., 2006 .

[85] N. Iizuka, T. Shimizu, C. Kumtornkittikul, M. Sugiyama, and Y. Nakano, "Absorption saturation of AlN-based waveguide utilizing intersubband transition in GaN/AlN quantum wells," OECC2008, Sydney, Australia, 2008.

[86] N. Iizuka, H. Yoshida, N. Managaki, T. Shimizu, H. Sodabanlu, M. Sugiyama, and Y. Nakano, "Saturation of intersubband absorption in GaN/AlN-based waveguide integrated with spot-size converter," LEOS2008, California, USA, 2008.

[87] P. F. Fewster, "Interface roughness and period variations in MQW structures determined by X-ray diffraction," J. Appl. Crystallogr. **21**, 524 (1988).

[88] P. F. Fewster, N. L. Andrew, and C. T. Foxon, "Microstructure and composition analysis of group III nitrides by X-ray scattering," J. Crystal Growth **230**, 398 (2001).

[89] T. Detchprohm, N. K. Hiramatsu, K. Itoh, and I. Akasaki, "Relaxation Process of the Thermal Strain in the GaN/α-Al$_2$O$_3$ Heterostructure and Determination of the Intrinsic Lattice Constants of GaN Free from the Strain," Jpn. J. Appl. Phys. **31**, L1454 (1992).

[90] K. Tsubouchi, and N. Mikoshiba, "Zero-Temperature-Coefficient SAW Devices on AlN Epitaxial Films," IEEE Trans. Son. Ultrason. **32**, 634 (1985).

[91] C. M. Krowne, "Semiconducotr heterostructure nonlinear Poisson eqaution," J. Appl. Phys. **65**, 1602 (1989).

[92] I-H. Tan, G. L. Snider, L. D. Chang, and E. L. Hu, "A self-consistent solution of Schrödinger-Poisson equations uisng a non-nuniform mesh," J. Appl. Phys. **68**, 4071 (1990).

[93] G. L. Snider, I-H. Tan, L. D. Chang, and E. L. Hu, "Electron states in mesa-etched one-dimensional quantum well wires," J. Appl. Phys. **68**, 2849 (1990).

[94] S. H. Park, and S. L. Chung, "Spontaneous polarization effects in wurtzite GaN/AlGaN quantum wells and comparison with experiment," Appl. Phys. Lett. **76**, 1981 (2000).

[95] F. Bernardini, and V. Fiorentini, "Polarization fields in nitride nanostructures: 10 points to think about," Appl. Surf. Sci. **166**, 33 (2000).

[96] J. Sanchez-Rojas, J.A. Garrido, and E. Muñoz, "Tailoring of internal fields in AlGaN/GaN and InGaN/GaN heterostructure devices," Phys. Rev. B **61**, 2773 (2000).

[97] J. Wang, J. B. Jeon, Y. M. Sirenko, and K. W. Kim, "Piezoelectric Effect on Optical Properties of Pseudomorphically Strained Wurtzite GaN Quantum Wells," IEEE Photon. Technol. Lett. **9**, 728 (1997).

[98] O. Ambacher, R. Dimitrov, M. Stutzmann, B. E. Foutz, M. J. Murphy, J. A. Smart, J. R. Shealy, N. G. Weimann, K. Chu, M. Chumbes, B. Green, A. J. Sierakowski, W. J. Schaff, and L. F. Eastman, "Role of Spontaneous and Piezoelectric Polarization Induced Effects in Group-III Nitride Based Heterostructures and Devices," Phys. Stat. Sol. (B) **216**, 381 (1999).

[99] V. Fiorentini, F. Bernardini, F. D. Sala, A. D. Carlo, and P. Lugli, "Nonparabolicity and a sum rule associated with bound-to-bound and bound-to-continuum intersubband transitions in quantum wells," Phys. Rev. B **50**, 8663 (1994).

[100] S. Syed, J. B. Heroux, Y. J. Wang, M. J. Manfra, R. J. Molnar, and H. L. Stormer, "Nonparabolicity of the conduction band of wurtzite GaN," Appli. Phys. Lett. 83, 4553 (2003).

[101] S. Wolf, R.N. Tauber, *Silicon Processing for the VLSI Era, Vol. 1, Process Technology*, Sunset Beach Lattice Press, CA, USA, 1986.

[102] E. Y. Chang, G. T. Cibuzar, J. M. Vanhove, R. M. Nagarajan, and K. P. Pande, "GaAs device passivation using sputtered silicon nitride," Appl. Phys. Lett. **53**, 1638 (1988).

[103] M. Zhu, H.C. Chin, G. S. Samudra, and Y.C. Yeo, "Fabrication of gate stack with high gate work function for implantless enhancement-mode GaAs n-channel metal-oxide-semiconductor field effect transistor applications," Appl. Phys. Lett. **92**, 123513 (2008).

[104] M. L. Green, E. P. Gusev, R. Degraeve, and E. L. Garfunkel, "Ultrathin (<4 nm) SiO2 and Si-O-N gate dielectric layers for silicon microelectronics: Understanding the processing, structure, and physical and electrical limits," J. Appl. Phys. **90**, 2057 (2001).

[105] E. Dehan, P. Temple-Boyer, R. Henda, J. J. Pedroviejo, and E. Scheid, "Optical and structural properties of SiO_x and SiN_x materials," Thin Solid Films **266**, 14 (1995).

[106] C. Savall, J. C. Bruyère, and J. P. Stoquert, "Chemical bonds and microstructure in nearly stoichiometric PECVD $aSi_xN_yH_z$," Thin Solid Films **260**, 174 (1995).

[107] K. Matsuzaki, A. Hirabayashi, and M. Saga, "Characterization of Reactively Sputtered Silicon Nitride," J. Electrochem Soc. **139**, 3259 (1992).

[108] T. Serikawa, A. Okamoto, "Properties of Magnetron-Sputtered Silicon Nitride Films," J. Electrochem. Soc. **131**, 2928 (1984).

[109] R. Banerjee, A.K. Bandyopadhyay, J.K. Rath, A.K. Batabyad, and A.K. Barua, "Properties of hydrogenated amorphous Si---N films prepared by r.f. magnetron sputtering with emphasis on the non-stoichiometric region," Thin Solid Films **192**, 295 (1990).

[110] S.K. Gosh, T.K. Hatwar, "Preparation and characterization of reactively sputtered silicon nitride thin films," Thin Solid Films **166**, 359 (1988).

[111] T. Shimizu, Improvement of Waveguide Structure for Low-Power Operation of AlN/GaN Quantum-Wells Intersubband-Transition All-Optical Switch, Master Thesis, Department of Electronics Engineering, School of Engineering, The University of Tokyo, 2007.

[112] R. Hui, S. Taherion, Y. Wan, J. Li, S. X. Jin, J. Y. Lin, and H. X. Jiang, "GaN-based waveguide devices for long-wavelength optical communications," Appl. Phys. Lett. **82**, 1326 (2003).

[113] P. K. Kandaswamy, F. Guillot, E. Bellet-Amalric, E. Monroy, L. Nevou, M. Tchernycheva, A. Michon, F. H. Julien, E. Baumann, F. R. Giorgetta, D. Hofstetter, T. Remmele, M. Albrecht, S. Birner, and Le Si Dang, "GaN/AlN short-period superlattices for intersubband optoelectronics: A systematic study of their epitaxial growth, design, and performance," J. Appl. Phys. **104**, 093501 (2008).

[114] A. V. Lobanova, E. V. Yakovlev, R. A. Talalaev, S. B. Thapa, and F. Scholz, "Growth conditions and surface morphology of AlN MOVPE," J. Crystal Growth **310**, 4935 (2008).

[115] Y. Ohba, and R. Sato, "Growth of AlN on sapphire substrates by using a thin AlN buffer layer grown two-dimensionally at a very low V/III ratio," J. Crystal Growth **221**, 258 (2000).

[116] A. V. Lobanova, K. M. Mazaev, R. A. Talalaev, M. Leys, S. Boeykens, K. Cheng, and S. Degroote, "Effect of V/III ratio in AlN and AlGaN MOVPE," J. Crystal Growth **287**, 601 (2006).

[117] A. Dadgara, A. Krosta, J. Christen, B. Bastek, F. Bertram, A. Krtschil, T. Hempel, J. Bläsing, U. Haboeck, and A. Hoffmann, "MOVPE growth of high-quality AlN," J. Crystal Growth **297**, 306 (2006).

[118] S. B. Thapaa, C. Kirchnera, F. Scholz, G. M. Prinz, K. Thonke, R. Sauer, A. Chuvilin, J. Biskupek, U. Kaiser, and D. Hofstetter, "Structural and spectroscopic properties of AlN layers grown by MOVPE," J. Crystal Growth **298**, 383 (2007).

[119] A. Nakajima, Y. Furukawa, S. Koga, and H. Yonezu, "Growth of high-quality AlN with low pit density on SiC substrates," J. Crystal Growth **265**, 351 (2004).

[120] C. Kumtornkittikul, GaN/AlN Multiple Quantum Wells and Nitride-Based Waveguide Structures for Ultrafast All-Optical Switch Utilizing Intersubband Transition, Ph.D.

dissertation, Department of Electronics Engineering, School of Engineering, The University of Tokyo, 2006.

[121] N. Nishizawa and T. Goto, "Widely Broadened Super Continuum Generation Using Highly Nonlinear Dispersion Shifted Fibers and Femtosecond Fiber Laser," Jpn. J. Appl. Phys. **40**, L365 (2001).

[122] C. Gmachl, D. L. Sivco, R. Colombelli, F. Capasso, and A. Y. Cho, "Ultra-broadband semiconductor laser," Nature **415**, 883 (2002).

[123] Y. Ozeki, K. Taira, K. Aiso, Y. Takushima and K. Kikuchi, "Highly flat super-continuum generation from 2 ps pulses using 1 km-long erbium-doped fibre amplifier," Electron. Lett. **38**, 1642 (2002).

[124] F. O. Ilday, F. W. Wise, and T. Sosnowski, "High-energy femtosecond stretched-pulse fiber laser with a nonlinear optical loop mirror," Opt. Lett. **27**, 1531 (2002).

[125] J. W. Nicholson, M. F. Yan, P. Wisk, J. Fleming, F. DiMarcello, E. Monberg, A. Yablon, C. Jørgensen, and T. Veng, "All-fiber, octave-spanning supercontinuum," Opt. Lett. **28**, 643 (2003).

[126] Y. Takushima, K. Yasunaka, Y. Ozeki and K. Kikuchi, "87 nm bandwidth noise-like pulse generation from erbium-doped fibre laser", Electron. Lett. **41**, 399 (2005).

[127] J. Heber, C. Gmachl, H. Ng, and A. Cho, "Comparative study of ultrafast intersubband electron scattering times at ~1.55 µm wavelength in GaN/AlGaN heterostructures," Appl. Phys. Lett. **81**, 1237 (2002).

[128] J. Hamazaki, S. Matsui, H. Kunugida, K. Ema, H. Kanazawa, T. Tachibana, A. Kikuchi, and K. Kishino, "Ultrafast intersubband relaxation and nonlinear susceptibility at 1.55 µm in GaN/AlN multiple-quantum wells," Appl. Phys. Lett. **84**, 1102 (2004).

[129] N. Kalonji and J. Semo, "High efficiency, long working distance laser diode to single mode fiber coupling," Electron. Lett. 30, 892 (1994).

[130] H. M. Presby and C. A. Edwards, "Near 100% efficient fiber microlenses," Electron. Lett. 28, 582 (1992).

[131] I. Moerman, P. P. Van Daele, and P. M. Demeester, "A Review on Fabrication Technologies for the Monolithic Integration of Tapers with III–V Semiconductor Devices," IEEE J. Selec. Topics in Quan. Elec. 3, 1308 (1997).

[132] F. Bernardini, V. Fiorentini, and D. Vanderbilt, "Spontaneous polarization and piezoelectric constants of III-V nitrides," Phys. Rev. B **56**, R10024 (1997).

[133] J. P. Killingbeck, *Microcomputer Algorithms*, Hilger, Bristol, 1992.

[134] S.M. Sze, *Semiconductor Devices*, Wiley, New York, 2006.

[135] Y. Hirayama, J. H. Smet, L. H. Peng, C. G. Fonstad, and E. P. Ippen, "Feasibility of 1.55 μm Intersubband Photonic Devices Using InGaAs/AlAs Pseudomorphic Quantum Well Structures," Jpn. J. Appl. Phys. **33**, 890 (1994).

[136] H. Asai and Y. Kawamura, "Intersubband absorption in $In_{0.53}Ga_{0.47}As/In_{0.52}Al_{0.48}As$ multiple quantum wells," Phys. Rev. B **43**, 4748 (1991).

[137] A. Raymond, J. L. Robert, and C. Bernard, "The electron effective mass in heavily doped GaAs," J. Phys. C **12**, 2289 (1979).

[138] W. J. Duffin, *Electricity and Magnetism*, McGraw-Hill, Third edition, 1980.

[139] R. M. Eisberg, *Fundamentals of Modern Physics*, Wiley, New York, 1961.

[140] N. M. Pearsall, T. J. Coutts, R. Hill, G. J. Russell, and K. J. Lawson, "Surface Damage to InP substrates during R.F. Sputtering," Thin Solid Films **80**, 177 (1981).

[141] K. Mitani and T. Kawano, "Damage in a GaAs Surface Caused by RF-Sputter Deposition of SiO_2," Jpn. J. Appl. Phys. **34**, 4649 (1995).

[142] B. Y. Yu, W. C. Lin, Y. Y. Chen, Y. C. Lin, K. T. Wong, J. J. Shyue, "Sputter damage in Si (0 0 1) surface by combination of $C60^+$ and Ar^+ ion beams," Appl. Surf. Science **255**, 2490 (2008).

[143] S. Arulkumaran, T. Egawa, H. Ishikawa, T. Jimbo, and M. Umeno, "Investigations of SiO_2/n-GaN and Si_3N_4/n-GaN insulator–semiconductor interfaces with low interface state density," Appl. Phys. Lett. **73**, 809 (1998).

[144] X. Z. Dang, E. T. Yu, E. J. Piner and B. T. McDermott, "Influence of surface processing and passivation on carrier concentrations and transport properties in AlGaN/GaN heterostructures," J. Appl. Phys. **90**, 1357 (2001).

[145] A. V. Vertiatchikh, L. F. Eastman, W. J. Schaff, and T. Prunty, "Effect of surface passivation of AlGaN/GaN heterostructure field-effect transistor," Electron Lett. **38**, 388 (2002).

[146] M. Köhler, *Etching in Microsystem Technology*, Wiley-VCH, New York, 1999.

[147] C. M. Jeon and J. L. Lee, "Effects of tensile stress induced by silicon nitride passivation on electrical characteristics of AlGaN/GaN heterostructure field-effect transistors," Appl. Phys. Lett. **86**, 172101 (2005).

[148] B. M. Green, K. K. Chu, E. M. Chumbes, J. A. Smart, J. R. Shealy, and L. F. Eastman, "The role of surface passivation on the microwave characteristics of AlGaN/GaN HEMT's," IEEE Electron Device Lett. **21**, 268 (2000).

[149] S. Arulkumaran, T. Egawa, H. Ishikawa, T. Jimbo, and Y. Sano, "Surface passivation effects on AlGaN/GaN high-electron-mobility transistors with SiO_2, Si_3N_4, and silicon oxynitride," Appl. Phys. Lett. **84**, 613 (2004).

[150] S. Arulkumaran, G. I. Ng, and Z. H. Liu, "Effect of gate-source and gate-drain Si_3N_4 passivation on current collapse in AlGaN/GaN high-electron-mobility transistors on silicon," Appl. Phys. Lett. **90**, 173504 (2007).

[151] N. Suzuki, N. Iizuka, and K. Kaneko, "FDTD Simulation of Femtosecond Optical Gating in Nonlinear Optical Waveguide Utilizing Intersubband Transition in AlGaN/GaN Quantum Wells," IEICE Trans. Electron **E83-C**, 981 (2000).

[152] W. T. Reed Jr., "Theory of dislocation in Germanium," Phil. Mag. **45**, 775 (1954).

[153] A. Kikuchi, T. Yamada, S. Nakamura, K. Kusakabe, D. Sugihara, and K. Kishino, "Improvement of crystal quality of RF-plasma-assisted molecular beam epitaxy grown Ga-polarity GaN by high-temperature grown AlN multiple intermediate layers, Jpn. J. Appl. Phys. **39**, L330–L333 (2000).

[154] E. Ozturk, and I. Sokmenl, "The electric field effects on intersubband optical absorption of Si δ-doped GaAs layer," Solid state communication **126**, 605 (2003).

List of Publications

Related Technical Journals

[1] J. S. Yang, <u>H. Sodabanlu</u>, I. Waki, M. Sugiyama, Y. Nakano, and Y. Shimogaki, "Low Temperature MOVPE Growth of AlN by Pulse Injection Method at 800 ℃," Jpn. J. Appl. Phys., Vol 46, No 38, pp L927-L929, 2007

[2] J. S. Yang, <u>H. Sodabanlu</u>, I. Waki, M. Sugiyama, Y. Nakano, and Y. Shimogaki, "Process Design of Pulse Injection Method for Low-Temperature Metal Organic Vapor Phase Epitaxial Growth of AlN at 800 ℃," J. Cryst. Growth, Vol 311, No 2, pp 383-388, 2009

[3] J. S. Yang, <u>H. Sodabanlu</u>, M. Sugiyama, Y. Nakano, and Y. Shimogaki, "Fabrication of Abrupt AlN/GaN Multi Quantum Wells by Low Temperture Metal Organic Vapor Phase Epitaxy," Appl. Phys. Express, Vol 2, pp 051004, 2009

[4] <u>H. Sodabanlu</u>, J. S. Yang, Y. Shimogaki, M. Sugiyama, and Y. Nakano, "Intersubband Transition at 1.52 μm in GaN/AlN Multiple Quantum Wells Grown by Metal Organic Vapor Phase Epitaxy," Appl. Phys. Express. Vol 2, pp 061002, 2009

[5] <u>H. Sodabanlu</u>, J. S. Yang, Y. Shimogaki, M. Sugiyama, and Y. Nakano, "Strain effects on the intersubband transitions in GaN/AlN MQWs grown by low-temperature MOVPE with AlGaN interlayer," Appl. Phys. Lett., Vol 95, pp 161908-~ 161910, 2009

[6] J. S. Yang, <u>H. Sodabanlu</u>, M. Sugiyama, Y. Nakano, and Y. Shimogaki, "Blue Shift of Intersubband Transition Wavelength of AlN/GaN Multi Quantum Wells by Low Temperature Metal Organic Vapor Phase Epitaxy Using Pulse Injection Method," Appl. Phys. Lett., Vol 95, pp 162111- 162113, 2009

[7] N. Iizuka, H. Yoshida, N. Managaki, T. Shimizu, <u>H. Sodabanlu</u>, C. Kumtornkittikul, M. Sugiyama, and Y. Nakano, "Integration of GaN/AlN all-optical switch with SiN/AlN waveguide utilizing spot-size conversion," Opt. Express. Vol 17, No 25, pp 23247-23253, 2009

International Conference proceedings and presentations

[1] H. Sodabanlu, J. S. Yang, Y. Shimogaki, T. Tanemura, M. Sugiyama, and Y. Nakano, "Intersubband Absorption Saturation in AlN-based Waveguide with GaN/AlN Multiple Quantum Wells Fabricated by Metalorganic Vapor Phase Epitaxy," the 15th European Conference on Integrated Optics (Cambridge, England), April, 2010 (poster).

[2] J. S. Yang, H. Sodabanlu, M. Sugiyama, Y. Nakano, and Y. Shimogaki, "Intersubband Absorption at 1.55 µm in AlN/GaN multi quantum wells grown at 770 ˚C by metal organic vapor phase epitaxy using pulse injection method," the 15th International Conference on Metal Organic Vapor Phase Epitaxy (Warrendale, USA), May, 2010.

[3] J. S. Yang, H. Sodabanlu, M. Sugiyama, Y. Nakano, and Y. Shimogaki, "Blue-Shift of Intersubband Absorption Wavelength by Low Temperature Metal Organic Vapor Phase Epitaxy of AlN/GaN Multi Quantum Wells by Pulse Injection Method," International Conference on Nitride Simiconductor-8 (Jeju, Korea), Oct., 2009 (poster).

[4] H. Sodabanlu, J. S. Yang, Y. Shimogaki, M. Sugiyama, and Y. Nakano, "Improvement of 1.5-µm-Range Intersubband Transitions in MOVPE Grown GaN/AlN MQWs by AlGaN Interlayer," International Conference on Nitride Simiconductor-8 (Jeju, Korea), Oct., 2009 (poster).

[5] N. Iizuka, H. Yoshida, N. Managaki, T. Shimizu, H. Sodabanlu, M. Sugiyama, and Y. Nakano, "Saturation of intersubband absorption in GaN/AlN-based waveguide integrated with spot-size converter," The 21st Annual Meeting of The IEEE Lasers & Electro-Optics Society (California, USA) , Nov., 2008.

[6] J. S. Yang, H. Sodabanlu, M. Sugiyama, Y. Nakano, and Y. Shimogaki, "Fabrication of abrupt AlN/GaN MQWs by Low Temperature MOVPE," International Workshop on Nitride semiconductor 2008 (Montreux, Switzerland), p 436, Oct., 2008.

[7] J. S. Yang, H. Sodabanlu, M. Sugiyama, Y. Nakano, and Y. Shimogaki, "Impurity Incorporation and polarity of AlN Thin Films Layer Grown by Pulse Injection Method at 800 ℃," PRICM-6 (Jeju Island, Korea), Sep., 2007.

Domestic Conference proceedings and presentations

[1] J. S. Yang, <u>H. Sodabanlu</u>, M. Sugiyama, Y. Nakano, and Y. Shimogaki, "Fabrication of GaN and GaN/AlN MQWs at 800 ℃ by MOVPE using Pulse Injection Method," *26th Electronic Materials Symposium (EMS-22)*, pp. 185, Laforet Biwako, Japan, Jun., 2007.

[2] J. S. Yang, <u>H. Sodabanlu</u>, M. Sugiyama, Y. Nakano, and Y. Shimogaki, "Low Temperature MOVPE Growth of high quality GaN Layer by Pulse Injection Method," *39th The Society of Chemical Engineers, Japan*, Hokkaido Univ., Japan, Sep., 2007.

[3] 梁正承、<u>H. Sodabanlu</u>, 杉山正和, 霜垣幸浩, 中野義昭, "パルスインジェクション方式による n 型 GaN の低温 MOVPE 成長 (Low Temperature MOVPE Growth of n-type GaN by Pulse Injection Method)," 第 68 回応用物理学会学術講演会(北海道工業大学), 4a-ZR-4, 2007 年 9 月.

[4] 梁正承、<u>H. Sodabanlu</u>, 杉山正和, 霜垣幸浩, 中野義昭, "パルスインジェクション方式を用いた GaN 成長における水素パージ時間と TMGa 供給時間の効果 (Effect of 1st H2 purge time and TMGa supply time in GaN growth by pulse injection method)," 第 55 回応用物理学関係連合講演会(日本大学理工学部), 28a-B-10, 2008 年 3 月.

[5] <u>H. Sodabanlu</u>, 梁正承、杉山正和, 霜垣幸浩, 中野義昭, "MOVPE で作製した GaN/AlN MQW 導波路の吸収測定 (Absorption measurement of the waveguide with GaN/AlN MQWs grown by MOVPE)," 第 69 回応用物理学会学術講演会(中部大学), 4a-ZN-11, 2008 年 9 月.

[6] 梁正承、<u>H. Sodabanlu</u>, 杉山正和, 霜垣幸浩, 中野義昭, "低温 MOVPE 方式による急峻な AlN/GaN 多重量子井戸の作製(Fabrication of abrupt AlN/GaN MQWs by Low Temperature-MOVPE)," 第 69 回応用物理学会学術講演会(中部大学), 2a-CA-11, 2008 年 9 月.

[7] 梁正承、<u>H. Sodabanlu</u>, 杉山正和, 霜垣幸浩, 中野義昭, "パルスインジェクション方式で作製した AlN/GaN 多重量子井戸のサブバンド間吸収特性 (Intersubband Absorption property of AlN/GaN MQWs grown by Pulse Injection Method)," 第 56 回応用物理学関係連合講演会(筑波大学), 1a-ZJ-18, 2009 年 3 月.

[8] H. Sodabanlu, 梁正承、杉山正和, 霜垣幸浩, 中野義昭, "MOVPE 成長 GaN/AlN 量子井戸を用いた 1.5 µm 帯サブバンド間遷移の実現," 第 1 回窒化物半導体結晶成長講演会(東京農工大学), 2009 年 5 月.

[9] H. Sodabanlu, 梁正承、杉山正和, 霜垣幸浩, 中野義昭, "MOVPE で成長した GaN/AlN MQW コア導波路による 1.5 µm 帯サブバンド間吸収 (Intersubband absorption at 1.5-µm-range in MOVPE-grown optical waveguide with GaN/AlN MQWs core)," 第 70 回応用物理学会学術講演会(富山大学),11a-P8-23, 2009 年 9 月.

[10] 梁正承、H. Sodabanlu, 杉山正和, 霜垣幸浩, 中野義昭, "パルスインジェクション方式で作製した AlN/GaN 多重量子井戸のサブバンド間遷移特性に与える成長温度の効果 (Effect of growth temperature of ALN/GaN Multi Quantum Wells grown by Pulse Injection Method on their Intersubband Transition Property)," 第 70 回応用物理学会学術講演会(富山大学),10p-X-20, 2009 年 9 月.

[11] H. Sodabanlu, 梁正承、杉山正和, 霜垣幸浩, 中野義昭, "The Growth of GaN/AlN Multiple Quantum Wells by Metalorganic Vapor Phase Epitaxy for Optical Devices Utilizing Intersubband Transition at 1.55-µm," 応用物理学会学結晶工学分科会主催 2009 年・年末講演会(学習院創立百周年記念会館), 2009 年 12 月.

[12] 梁正承、H. Sodabanlu, 杉山正和, 霜垣幸浩, 中野義昭, "パルスインジェクション法を用いた MOVPE による AlN/GaN 多重量子井戸の 770℃ での作製と 1.55 µm でのサブバンド間遷移観測(Fabrication of AlN/GaN Multi Quantum Wells at 770℃ by Metal Organic Vapor Phase Epitaxy Using Pulse Injection Method and Observation of Intersubband Transition at 1.55 µm)," 第 57 回応用物理学関係連合講演会(東海大学), 18p-TA-5, 2010 年 3 月.

[13] H. Sodabanlu, 梁正承、種村拓夫、杉山正和, 霜垣幸浩, 中野義昭, "MOVPE 成長 GaN/AlN 量子井戸導波路におけるサブバンド間遷移吸収飽和の観測 (Observation of intersubband absorption saturation in MOVPE-grown GaN/AlN MQWs waveguide)," 第 57 回応用物理学関係連合講演会(東海大学), 17a-N-6, 2010 年 3 月.